The role
of marine biota
in the climate system
– an Earth system
model approach

RÉMY ASSELOT

The role of marine biota in the climate system - an Earth system model approach

DISSERTATION

WITH THE AIM OF ACHIEVING A DOCTORAL DEGREE AT THE FACULTY OF

MATHEMATICS, INFORMATICS AND NATURAL SCIENCES

DEPARTMENT OF EARTH SCIENCES

AT UNIVERSITÄT HAMBURG

SUBMITTED BY RÉMY ASSELOT

FROM BORDEAUX, FRANCE

HAMBURG, 2021

I used to think that top environmental problems were biodiversity loss,
ecosystem collapse and climate change.
I thought that thirty years of good science could address these problems.
I was wrong.
The top environmental problems are selfishness, greed and apathy,
and to deal with these we need a cultural and spiritual transformation.
And we scientists don't know how to do that.

Quote attributed to
- James Gustave Speth
Environmental lawyer and advocate

Abstract

Marine phytoplankton are unicellular algae that are the first link of the marine food chain. They can influence the climate system via biogeochemical and biogeophysical mechanisms, especially during large blooms. Phytoplankton can absorb light at the surface of the ocean, modifying the distribution of radiative heat along the water column. These changes in heat budget alter the oceanic properties, the atmospheric properties and finally the overall climate system. In this thesis, I investigate the role of the marine biota in the climate system by using an Earth system model of intermediate complexity called EcoGENIE. I modified the oceanic and ecosystem model components to consider phytoplankton light absorption.

Over the past years, the number of plankton functional types in models has increased but the relative importance of biological processes such as phytoplankton light absorption is still unclear. As a logical extension, I compared the relative importance of phytoplankton light absorption with an increase in marine ecosystem complexity. I show that phytoplankton light absorption increases the atmospheric CO_2 concentration and the overall heat budget of the planet. In contrast, increasing ecosystem complexity only slightly affects the carbon cycle and thus the heat budget. In conclusion, phytoplankton light absorption has a higher impact on the climate system than an increase in marine ecosystem complexity.

After demonstrating that phytoplankton light absorption has an impact on the climate system, I focus on the climate pathways behind the atmospheric warming due to this biogeophysical mechanism. Phytoplankton light absorption increases the oceanic temperature with consequences on the air-sea heat and CO_2 fluxes. I evidence that changes in air-sea CO_2 exchange due to phytoplankton light absorption have a larger contribution to the atmospheric heating than phytoplankton-induced changes in air-sea heat flux.

After demonstrating that phytoplankton light absorption increases the atmospheric temperature via an increase in atmospheric CO_2 concentration, I explore the effects of this biogeophysical mechanism would have in a warmer climate. To shed light on this question, I conduct simulations under RCPs and pre-industrial conditions. First, I evidence that the overall warming due to phytoplankton light absorption is smaller than the overall warming due to climate change. Secondly, chlorophyll biomass is expected to decrease under global warming and my results indicate that phytoplankton light absorption enhances the reduction of the chlorophyll biomass. As a consequence, less heat is trapped by chlorophyll and the effect of phytoplankton light absorption on the climate system is reduced. Thirdly I demonstrate that prescribing atmospheric CO_2 concentration in model simulations blur the real effect of phytoplankton light absorption on the climate system.

This thesis supports the idea that phytoplankton light absorption should be considered in climate studies as an internal constituent of the climate system for long-term climate adjustment.

Zusammenfassung

Marines Phytoplankton sind einzellige Algen, die Basis des marinen Nahrungsnetzes bilden. Sie können das Klima, insbesondere während ihrer Blüte über biogeochemische und biogeophysikalische Mechanismen beeinflussen. Phytoplankton kann Licht an der Oberfläche des Ozeans absorbieren und so die Verteilung der Strahlungswärme in der Wassersäule verändern. Diese Änderungen im Wärmehaushalt verändern die ozeanischen Eigenschaften, die atmosphärischen Eigenschaften und das gesamte Klima. In dieser Arbeit untersuche ich die Rolle der marinen Biota mit Hilfe eines Erdsystemmodells mittlerer Komplexität namens EcoGENIE. Ich habe die Ozean- und Ökosystem-Komponenten modifiziert, um die Lichtabsorption durch Phytoplankton (LAP) zu berücksichtigen.

In den letzten Jahren hat die Anzahl der Plankton-Funktionstypen in den Modellen zugenommen, aber eventuell ebenso bedeutende Prozesse, wie zum Beispiel LAP werden nicht berücksichtigt und ihre relative Bedeutung ist unklar. Daher have ich die konseqenzen von LAP und Prozessen komplexer Ökosysteme auf die Klimadynamik untersucht. Ich zeige, dass die Lichtabsorption durch Phytoplankton die atmosphärische CO_2-Konzentration und den Gesamtwärmehaushalt des Planeten erhöht. Im Gegensatz dazu beeinflusser komplexere Ökosysteme den Kohlenstoffkreislauf und damit die atmosphärische Temperatur nur geringfügig. Zusammenfassend lässt sich sagen, dass die LAP einen größeren Einfluss auf das Klima hat als eine Erhöhung der Komplexität des marinen Ökosystems.

Nachdem ich gezeigt habe, dass die LAP einen wichtigen Einfluss auf das Klima hat, untersuche ich, welche Klimapfade zu der biologisch induzierten atmosphärischen Erwärmung führen. Die LAP erhöht die ozeanische Temperatur mit Folgen für die Luft-Meer-Wärme- und CO_2-Flüsse. Ich zeige, dass Änderungen im Luft-Meer-CO_2-Austausch aufgrund von Phytoplankton-Lichtabsorption einen größeren Beitrag zur atmosphärischen Erwärmung haben als Änderungen im Luft-Meer-Wärmefluss.

Nachdem ich gezeigt habe, dass die LAP zu einem Anstieg der atmosphärischen CO_2-Konzentration und damit der atmosphärischen Temperatur führt, widme ich mich der Frage, welche Auswirkungen dieser biogeophysikalische Mechanismus in einem wärmeren Klima hat. Habe ich Simulationen unter vorindustriellen und RCP Szenarien durchgeführt. Meine Ergebnisse zeigen erstens, dass die Gesamterwärmung durch die LAP ist kleiner al Gesamterwärmung durch den Klimawandel. Zweitens zeige ich, dass die LAP die unter der globalen Erwärmung zu erwartende Abnahme der Chlorophyll-Biomasse verstärkt. Infolgedessen wird weniger Wärme durch Chlorophyll eingefangen und die Wirkung der LAP auf das Klima nimmt tendenziell ab. Drittens zeige ich, dass die Fixierung der atmosphärischen Konzentration von CO_2 in Klimasimulationen den tatsächlichen Effekt von LAP auf das Klima abschwächt.

Diese Arbeit untermauert die Idee, dass die LAP in Klimastudien als ein interner Bestandteil des Klima für die langfristige Klimaanpassung berücksichtigt werden sollte.

Résumé

Le phytoplancton est une algue unicellulaire constituant le premier maillon de la chaîne alimentaire dans les océans. Ces organismes peuvent influencer le climat par des mécanismes biogéophysiques, notamment lors de blooms phytoplanctoniques. Par exemple, le phytoplancton peut absorber la lumière à la surface de l'océan, modifiant la distribution de chaleur dans la colonne d'eau. Ces changements thermiques modifient les propriétés du climat dans son ensemble. Lors de cette thèse, j'étudie l'effet du phytoplancton sur le climat en utilisant un modèle climatique de complexité intermédiaire appelé EcoGENIE. J'ai modifié les composantes océaniques et écologiques de ce modèle afin de pouvoir étudier l'absorption lumineuse par le phytoplancton (ALP).

Récemment, le nombre de planctons représentés dans les modèles a augmenté mais l'importance de mécanismes biogéophysiques tel que l'ALP reste encore inconnue. J'ai donc comparé l'importance de ces deux mechanismes dans le cadre d'études climatiques. Je démontre que l'ALP augmente la concentration atmosphérique en CO_2 et donc la température de la planète. Un écosystème marin plus complexe engendre une légère modification du cycle du carbone et abaisse légèrement la température atmosphérique. En conclusion, l'ALP a un impact plus important sur le climat qu'un écosystème marin plus complexe.

Maintenant que j'ai démontré que l'ALP a un effet important sur le climat, je me suis demandé comment le phytoplancton réchauffait l'atmosphère. L'ALP augmente la température de l'océan, influençant les flux de chaleur et de CO_2 entre l'océan et l'atmosphère. Je démontre que l'augmentation de la température atmosphérique provenant de l'ALP est principalement due aux modifications du flux de CO_2 par le phytoplancton à l'interface entre l'atmosphère et l'océan.

Une fois que j'ai demontré que le phytoplancton augmente la température atmosphérique via une augmentation de la concentration atmosphérique de CO_2, je me suis demandé quels sont les effets de ce mecanisme biogéophysique dans un climat plus chaud. Pour répondre à cette question, j'ai effectué des simulations suivant les scenarios climatiques du GIEC ainsi que des scenarios pré-industriels. Premièrement, je montre que le réchauffement dû à l'ALP est moindre que l'augmentation des températures dû au réchauffement climatique. Deuxièmement, avec le réchauffement climatique, la biomasse de chlorophylle est supposée diminuer et mes résultats indiquent que l'ALP accélère cette réduction de chlorophylle dans les océans. En conséquence, moins de chaleur est absorbée par la chlorophylle et l'effet de l'ALP sur le climat a tendance à diminuer. Troisièmement, je démontre que fixer la concentration atmosphérique de CO_2 dans les simulations climatiques atténue l'effet réel de l'ALP sur le climat.

Ce travail soutient l'idée que l'absorption de la chaleur par le phytoplancton doit être considérée comme un constituant à part entière du système climatique pour étudier le climat sur le long terme.

Resumen

El fitoplancton marino es un conjunto de algas unicelulares que constituyen el primer eslabón de la red trófica marina. Estos organismos pueden influir en el clima a través de mecanismos biogeoquímicos y biogeofísicos, especialmente durante las grandes proliferaciones. Por ejemplo, el fitoplancton puede absorber la luz en la superficie del océano, modificando la distribución del calentamiento radiativo a lo largo de la columna de agua. Estos cambios en el balance térmico alteran las propiedades oceánicas y atmosféricas. En esta tesis, investigo el papel de la biota marina utilizando un modelo climático de complejidad intermedia llamado EcoGENIE. He modificado los componentes oceánicos y ecológicos de este modelo para estudiar la absorción de la luz por el fitoplancton (ALF).

En los últimos años, el número de plancton representado en los modelos ha aumentado, pero la importancia de algunos procesos biológicos, como la ALF, sigue siendo desconocida. Como extensión lógica, he comparado la importancia de estos dos mecanismos para los estudios climáticos. Muestro que la ALF aumenta la concentración atmosférica de CO_2 y el balance térmico global del planeta. En cambio, el aumento de la complejidad del ecosistema afecta ligeramente el ciclo del carbono y la temperatura atmosférica. En conclusión, la absorción de luz del fitoplancton tiene un mayor impacto en el clima que un aumento en la complejidad del ecosistema marino.

Una vez demostrado que la ALF tiene un impacto importante en el clima, me pregunto cuáles son las vías climáticas que están detrás del calentamiento atmosférico inducido biológicamente. La ALF aumenta la temperatura oceánica con consecuencias en los flujos de calor aire-océano y de CO_2. Demuestro que los intercambios de CO_2 aire-océano debidos a la ALF tienen una mayor contribución en el calentamiento atmosférico que los cambios en el flujo de calor aire-océano.

Una vez que demuestro que la ALF aumenta la temperatura atmosférica a través de un aumento de la concentración atmosférica de CO_2, me pregunto cuáles son los efectos de este mecanismo biogeofísico en un clima más cálido. Para arrojar luz sobre esta cuestión, realicé simulaciones bajo escenarios de cambio global RCPs y los escenarios preindustriales. En primer lugar, muestro que el calentamiento global debido a la ALF es inferior al calentamiento global debido al cambio climático. En segundo lugar, se espera que la biomasa de clorofila disminuya bajo el calentamiento global y mis resultados indican que la ALF aumenta la reducción de la biomasa de clorofila. Como consecuencia, la clorofila atrapa menos calor y el efecto de la ALF en el clima tiende a disminuir. En tercer lugar, demuestro que fijar la concentración atmosférica de CO_2 en las simulaciones climáticas mitiga el efecto real de ALF en el clima

Esta tesis apoya la idea de que la absorción de luz del fitoplancton debe ser considerada en los estudios climáticos como un componente interno del sistema climático para el ajuste climático a largo plazo.

Acknowledgments

I would like to thank everyone who supported, helped, and advised me through my PhD project.

First I would like to thank my supervisor **Inga Hense** for the opportunity she gave me to accomplish a PhD. I want to thank her for the time, support, advice, corrections, and for being there when I needed it. Thank you for revising my thesis, manuscripts, conference abstracts, and posters. Finally, thank you for helping me to broaden my scientific knowledge.

I would like to thank my co-supervisor **Frank Lunkeit** for the time and scientific discussions we had. I would also like to thank you for the time you took to solve my numerical issues and change the code of the model. I would like to thank you for the revision of my work.

I am thankful to **Matthias Hort** for being my panel chair, for the interesting talks we had during our meetings and for giving me advice on the chosen path of research during this project.

I would like to thank **Philip Holden** for welcoming me to London and showing me how to run the model. Thank you for the time you took to answer my large number of emails to help me with my numerical issues. Thank you for revising my manuscripts and posters.

I am grateful to **Andy Ridgwell** for answering my questions regarding the model and for introducing me to the cGENIE community.

I would like to thank the SICSS graduate school, specifically **Berit**, **Ingo** and **Sebastian** for organizing the different courses, retreats and parties. A big shoutout to all PhD students, it was great to meet so many people from so many different countries and cultures. It was a pleasure to be a PhD representative for more than 2 years and I would like to thank the people with whom I shared this task, namely, **Ina**, **Patrick**, **Elena** and **Maike**.

I want to express my grateful thanks to all the people of the IMF who welcomed me and helped me to feel comfortable when I arrived in Hamburg. A special thought for the French community there, specifically **Xo**, **Aurélie**, **Louise**, **Romain**, **Fabien** and **Félix**. Thank you for the French dinners (raclette, tartiflette, galettes bretonnes...), the game nights (belotte, jeu des animaux...) and the evenings watching rugby. Furthermore, I would like to thank the ecosystem modeling-geeks group, **Jana**, **Maike**, **Harshal**, **Félix** and **Laurin** for their insightful comments and discussions on my work. I will miss our group meetings!

Contents

INTRODUCTION

Motivation

The name given to our planet, Earth, comes from Proto-Germanic language and is a synonym for dry land [Stevenson, 2010]. It is a misnomer because it does not describe the dominant feature of the planet, which is a vast expanse of water. The oceans occupy about 71% of the planet's surface, with the deepest part of the seafloor is ∼11.000 m from the surface of the ocean. The total volume of the marine environment provides approximately 300 times more space for life than that provided by land and freshwater combined [Lalli and Parsons, 1997]. All the biological activities in the marine environment are based on the activity of microorganisms that use light, carbon and other essential elements to produce organic matter. These microorganisms are unicellular algae, collectively called phytoplankton. They are the most abundant plant in the ocean, therefore their role in the food chain is important and essential. They contribute to a staggering 95% of the oceanic primary production [Nielsen, 1975], converting inorganic matter into new organic matter by the process of photosynthesis. More than 4,000 species of phytoplankton have been described [Lalli and Parsons, 1997] and new species are continually being added to this total.

The dynamics and distribution of phytoplankton in the ocean are influenced by light penetration, along with physical and biogeochemical properties of the ocean. These properties are predicted to change due to ongoing global warming, occurring since the beginning of the industrial era. Global warming affects the structure, distribution, seasonal dynamics and taxonomic composition of phytoplankton communities. Today, the vast majority of scientific attention is focused on the effect of climate change on marine biota. However, the opposite, the effect of marine biota on the climate system is less considered. The goal of this thesis is to better understand the interactions between phytoplankton and the climate system and to understand the role of these microorganisms in the future climate system. I focus on one particular biogeophysical mechanism - phytoplankton light absorption and apply an Earth system model of intermediate complexity to study its role on the climate system. I chose this mechanism because it is the most widely considered biogeophysical mechanism in climate science [Hense et al., 2017], and because of its immediate and significant impact on the climate system. In this thesis, I investigate: (1) the relative importance of phytoplankton light absorption compared to an increased number of phytoplankton groups represented in climate models, (2) the importance of diverse climate pathways behind the phytoplankton-induced atmospheric warming, and (3) the effect of phytoplankton light absorption under future climate scenarios.

Role of phytoplankton in the marine ecosystem

Due to their diversity and abundance in the ocean, phytoplanktonic organisms have an important influence on the marine ecosystem. Via the process of photosynthesis, these microorganisms take up dissolved CO_2 from the surrounding seawater. They also release O_2 due to photolysis of H_2O and produce organic matter. Phytoplankton is part of the biological pump and contributes to 48% of the global carbon fixation [Käse and Geuer, 2018]. In addition to carbon, phytoplankton necessitates certain elements such as nitrogen (N), phosphorus (P) and iron (Fe) to produce biomass. These microorganisms can therefore influence the biogeochemical cycles [Benitez-Nelson, 2000; Zehr and Kudela, 2011; Tréguer and De La Rocha, 2013].

Since phytoplankton are the basis of the marine food web, a portion of these microorganisms serve as prey for zooplankton, fish larvae, fish and other higher trophic levels (Figure 1.1). These bigger organisms, via grazing and food consumption, release fecal pellets that are stored in the form of particulate organic matter (POM). Another part of phytoplankton biomass is transformed into particulate and dissolved organic matter (DOM) via viral attacks and cell death. The remaining organic matter is taken up by bacteria and archaea which are in turn a food source for zooplankton; these interactions represent the microbial loop [Worden et al., 2015].
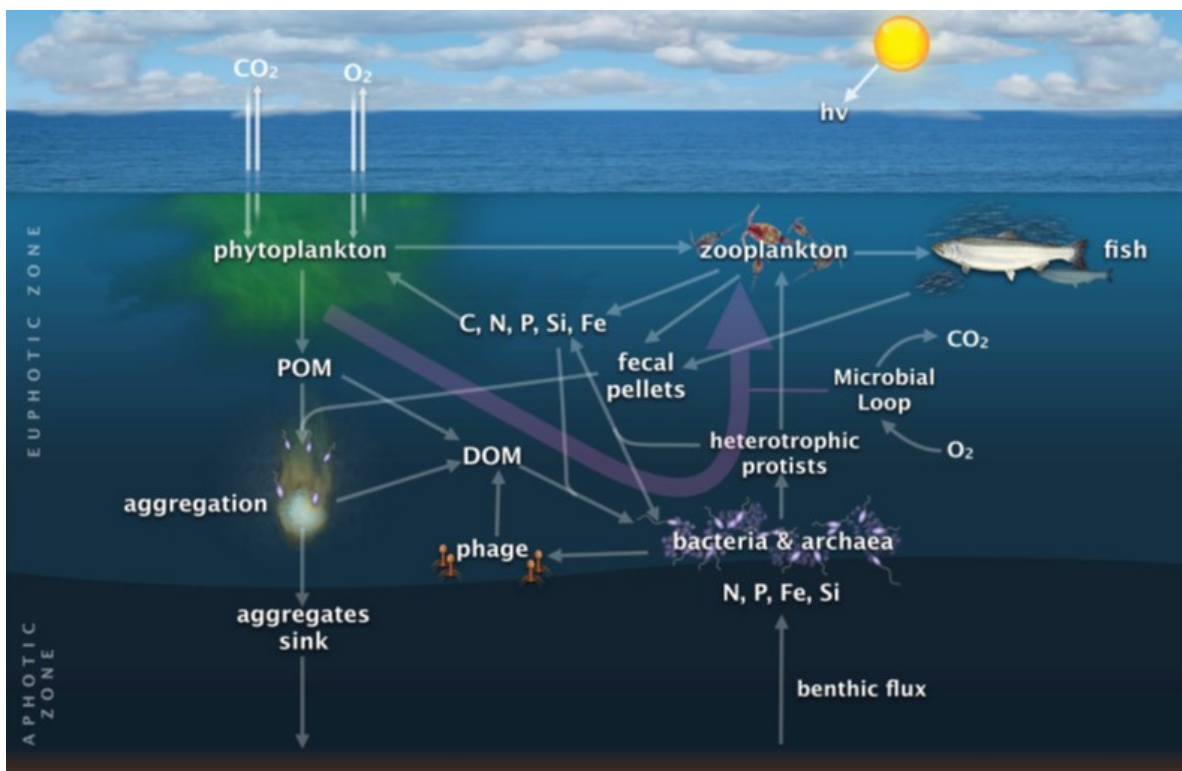
Figure 1.1: Schematic representation of the marine food web. Phytoplankton grows via the take up of light, nutrients and CO_2. These microorganisms are transferred to higher trophic levels such as zooplankton or fish, or released into the water as particulate or dissolved organic matter (POM and DOM). A fraction of the organic matter aggregates and sinks in the deep ocean where it is stored for hundreds or thousands of years. The purple arrow represents the microbial loop where POM and DOM are taken up by bacteria and archaea, which are in turn food for zooplankton. Figure from Worden et al. [2015].

Phytoplankton organisms are integral in the marine food web because they are primary producers, meaning that they are the first link of the food chain. Moreover, they influence the distribution of nutrients and oceanic biogeochemical cycles of the ocean. As such, phytoplankton influences its surrounding environment and, by extension, the global climate system via diverse mechanisms.

Role of marine biota in the climate system

According to Hense et al. [2017], marine biota can influence the climate system via three classes of mechanisms (Figure 1.2). The first class of mechanisms comprises the biogeochemical pumps, which control the distribution of ocean nutrients and have the potential to impact the marine carbon cycle. The second class of mechanisms is the biological gas and particle shuttles, which can play a role in the distribution of atmospheric greenhouse gases and alters the formation of clouds. Finally, the third class of mechanisms includes the biogeophysical mechanisms which have an impact on the optical and physical properties of the ocean. This last class of mechanisms is divided into three sub-mechanisms: (1) the light absorption mechanism, impacting the distribution of heat in the water column, (2) the albedo mechanism, affecting the shortwave radiation reflected by the ocean surface, and (3) the turbulent mixing mechanism that reduces the vertical mixing in the mixed layer of the ocean.
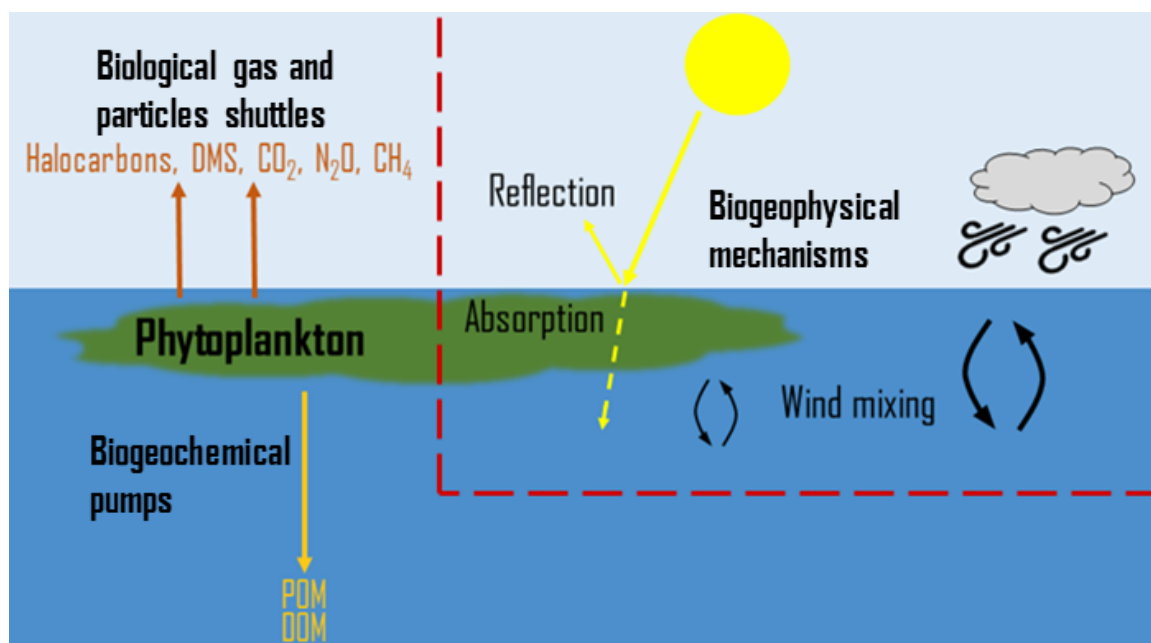
Figure 1.2: Schematic representation of the climate-relevant biological mechanisms. The biogeochemical pumps represent the uptake of carbon in the upper ocean and the sinking of this carbon in the deep ocean (POM = Particulate Organic Matter; DOM = Dissolved Organic Matter). The biological gas and particle shuttles consider the impact of the marine biosphere on the atmosphere due to the emission of gases and particles. The biogeophysical mechanisms address the changes in thermal, optical and mechanical properties of the ocean. These mechanisms are comprised in the red rectangle and are divided into three sub-mechanisms, namely reflection, light absorption and wind mixing.

Biogeochemical pumps

The biogeochemical pumps comprise the marine part of the carbon cycle. This class of mechanisms includes the biological pump, defined as the uptake of CO_2 in the upper ocean by marine biota and the sinking of this carbon in the abyssal ocean. The biological pump is part of a major process that brings down carbon from the atmosphere into the ocean surface, where carbon is dissolved, converted into particles through primary production, consumed by the marine biota and finally exported into the deep ocean [Turner, 2015]. A previous estimate suggests that the biological pump annually removes approximately 10 billion tons of carbon from the surface of the ocean [Buesseler and Boyd, 2009]. Phytoplankton is not the only important group in the biological pump process. Zooplankton contributes as well to the sinking of carbon via fecal pellets. Zooplankton fecal pellets represent ∼40% of the overall sinking particulate carbon flux [Ducklow et al., 2001; Dubischar and Bathmann, 2002; Turner, 2015] although their contribution to the export of particulate organic carbon (POC) is highly variable. The biological pump has changed on geological timescales and has shaped the past and present climate systems and biogeochemical cycles [Meyer et al., 2016]. Evidence of CO_2 draw-down during the Last Glacial Maximum led Sigman and Boyle [2000] to propose a hypothesis in which reduced atmospheric CO_2 was due to a stronger oceanic biological pump. This hypothesis was later supported by model simulations [LeGrand and Alverson, 2001]. The biological pump is often considered as the most important marine biological mechanism for the climate system.

The biogeochemical pumps include the microbial carbon pump, described as the transformation of easily degradable organic carbon into refractory organic carbon by microbes. The refractory organic carbon is not easily degradable and therefore can be stored in the ocean for several thousands of years. This long-time storage means that the microbial carbon pump will have little effect on the climate system on centennial timescales [Hense et al., 2017]. Although few studies exist on the microbial carbon pump, Benner and Herndl [2011] estimate that 8-23 TgC/year of refractory organic carbon is produced in the upper 200 m of the ocean by microbes. In a changing climate, the role of the microbial carbon pump in long-term carbon storage might become more significant [Polimene et al., 2017], thus warranting new strategies to better quantify this mechanism [Robinson et al., 2018].

Finally, the biogeochemical pumps comprise the alkalinity pump. This mechanism alters the oceanic carbonate chemistry via organisms developing calcite or aragonite shells. These organisms release CO_2 during the calcification process (formation of their shells), causing a decrease in oceanic alkalinity at the surface but the sinking dissolved material increases alkalinity in the deep ocean. Therefore, the alkalinity pump has consequences on oceanic CO_2 uptake and CO_2 storage in the ocean. Zhang and Cao [2016] evidence that the alkalinity pump plays a significant role in the oceanic CO_2 uptake, ocean pH and atmospheric CO_2 concentrations. The authors conclude that the effect of the alkalinity pump is comparable or even larger than the effect of global warming due to anthropogenic CO_2 emissions.

Biological gas and particle shuttles

The biological gas and particle shuttle mechanisms describe the impact of the marine biota on the atmosphere due to emissions of gases and particles. This process was first introduced by Shaw [1983], who studied the size of aerosol particles as they entered central Alaska from the Pacific marine environment. Despite their short lifetime, these emissions of gases and particles act as aerosols and influence cloud formation and/or atmospheric greenhouse

gas concentrations. Diverse recent studies show that cloud formation can be impacted by whole phytoplankton cells or by substances secreted by these organisms [Burrows et al., 2013; Wilson et al., 2015]. For instance, on a regional scale during summer, high oceanic chlorophyll concentrations can enhance the number of cloud droplets, therefore increasing cloud albedo. In turn, increased cloud albedo has been shown to enhance summertime reflected solar radiation by 10 W/m^2 over parts of the Southern Ocean, which is comparable to the expected effect of anthropogenic aerosols over polluted regions in the Northern Hemisphere [McCoy et al., 2015]. The most abundant gases produced by the marine biota are dimethyl sulfite (DMS) and short-lived halocarbons [Hense et al., 2017].

DMS produced by the marine biota is oxidized in the atmosphere to form a sulphate aerosol. This atmospheric gas is involved in the albedo feedback. DMS emissions by the marine biota have been estimated larger than the combined fluxes of DMS due to volcanoes, land biosphere and biomass burning [Liss et al., 1997]. The contribution of marine biota in the production of DMS is larger than the production from other natural sources such as volcanic sulfate and sea salt. The direct and indirect cooling effects induced by marine biota DMS emissions have been estimated to be -0.23 W/m^2 and -0.76 W/m^2, respectively [Rap et al., 2013].

Both warm and cold water species of marine biota produce halocarbons, the magnitude of their production rates being dependent on their growth stage [Tait and Moore, 1995]. Short-lived halocarbons destroy the ozone and significantly change the radiative budget and the climate system [Lim et al., 2017]. Moreover, halocarbon such as bromine plays a role in the Antarctic ozone hole formation. Fernandez et al. [2017] use a coupled chemistry-climate model to demonstrate that the Antarctic ozone hole increased by 14% when bromine from marine biota is considered in their simulations, which is in line with ozone observational data (NIWA-BS observations, [Bodeker et al., 2005]). Furthermore, according to a study using a chemical-radiative transport model, the short-lived halocarbons emitted by marine biota have contributed to -0.02 W/m^2 to global radiative forcing since the pre-industrial period [Hossaini et al., 2015].

Several other greenhouse gases are emitted by marine biota. The most important one is CO_2, which is emitted in the atmosphere via respiration by marine organisms. Additionally, N_2O has an essential warming potential and about 20% of the global production of N_2O is from the marine biota [Menon et al., 2007]. N_2O is mainly produced during the nitrification process of the nitrogen cycle. Marine sources of CH_4 are related to microorganisms but are negligible compared to terrestrial or anthropogenic sources [Hense et al., 2017]. The research area of marine biogenic gases is relatively new and their effects on the future climate system are still poorly constrained [Hopkins et al., 2020].

Biogeophysical mechansisms

The biogeophysical mechanisms affect the thermal, optical and mechanical properties of the ocean. Indeed, marine organisms can influence the upper ocean and alter the light absorption, the ocean surface albedo and the turbulent mixing by wind. These three processes may induce changes that have an impact on the climate system. This section focuses on surface albedo and turbulent mixing processes, while phytoplankton light absorption is described in a separate section because it is the most relevant and most studied biogeophysical mechanism.

Role of marine biota on the ocean albedo

The ocean surface albedo is defined as the ratio between the upward and downward shortwave radiation above the oceanic surface. It is influenced by the solar zenith angle, wind speed, transmission by atmospheric cloud/aerosols and oceanic chlorophyll concentration [Jin et al., 2004]. Marine organisms floating at the surface of the ocean such as phytoplankton can reduce the amount of light penetrating the ocean and therefore reduce the temperature of the ocean. Moreover, the quantity of light entering the ocean depends on the species, the color and the structure of the marine organisms [Jin et al., 2004]. For instance, Gondwe et al. [2001] use satellite data to study the influence of coccolithophore blooms on the direct radiative forcing. The authors show that the impact of these organisms is negligible on ocean albedo. In contrast, a previous modeling study estimates that coccolithophore blooms can change the oceanic albedo, by driving a 0.22 W/m^2 cooling of the global ocean [Tyrrell et al., 1999]. Additionally, the authors estimate that coccolithophores contribute to $\sim0.13\%$ of the global annually averaged albedo. On a local scale, coccolithophores can have an important effect on surface ocean optics with values for subsurface reflectance of $\sim38\%$ compared to 3-5% in the absence of these marine organisms [Balch et al., 1991]. Furthermore, positively buoyant species such as cyanobacteria play an essential role on the ocean albedo [Kahru et al., 1993; Sonntag and Hense, 2011]. A recent and idealized modeling study finds that cyanobacteria increase the oceanic albedo and locally reduce the seasonal sea surface temperature (SST) by a maximum of 0.2°C [Jung and Moon, 2019].

Role of marine biota on the turbulent wind mixing

Turbulent mixing in the upper part of the ocean is influenced by wind at the air-sea interface. Phytoplankton floating at the surface of the ocean change the viscosity of the water dampening surface waves and inhibit surface mixing by wind [Hutchinson and Webster, 1994]. The ocean stratification and heat distribution in the water column are therefore altered. A previous study shows that this biogeophysical process is dominant in the reduction of wind stress over a shallow coral reef area [Deacon, 1979]. Cyanobacteria play an important role in this climate-relevant process. These organisms modify the oceanic viscosity and therefore affect ocean circulation and SST [Sonntag, 2013]. The seasonal equatorial SST can be increased to a maximum of 0.8°C due to wind stress changes by marine biota [Jung and Moon, 2019].

Albedo mechanism versus turbulent mixing mechanism

Relatively few studies have compared the effect of marine biota on the turbulent mixing and albedo. Sonntag [2013] compare these two mechanisms with a 3-D coupled biological-physical model, neglecting the effect of these mechanisms on the atmosphere. Then, Jung and Moon [2019] used a global coupled ocean-biogeochemistry model to study these two biogeophysical mechanisms but do not include ocean-atmosphere interactions. Both Sonntag [2013] and Jung and Moon [2019] conclude that changes of oceanic turbulent mixing due to phytoplankton have a higher impact on the climate system than changes of oceanic albedo due to marine biota. However, the impact of a third mechanism, phytoplankton light absorption, on the climate system is even higher than the effect of the two aforementioned biogeophysical mechanisms.

Phytoplankton light absorption

To this day, phytoplankton light absorption is the most studied biogeophysical mechanism in climate studies. Half of today's Earth system models include the light absorption mechanism involved in the feedback between the marine biota and the temperature of the ocean [Hense et al., 2017]. Given that phytoplankton light absorption is the main biogeophysical mechanism included in climate studies, I focus on this mechanism in particular. Furthermore, I concentrate my research on this particular biogeophysical mechanism because its impact on the climate system is immediate and significant (see below). For instance, phytoplankton light absorption has pronounced effects on the heat budget, oceanic circulation, sea-ice cover and atmospheric properties. It also triggers a strong climate response resulting in multiple feedback loops [Sonntag and Hense, 2011]. Several observational and modeling studies have shown that phytoplankton light absorption affects the climate system; however the importance of this biogeophysical mechanism compared to a higher number of plankton groups represented in climate models is still unknown (Research Question 1; Chapter 3). In this section, I summarize the current state of knowledge on phytoplankton light absorption and introduce the remaining research gaps from previous studies.

Observations

During large blooms, phytoplankton are known to absorb light and therefore modify the vertical light distribution of radiative heating in the ocean (Figure 1.3). This interaction between light penetration and chlorophyll concentrations has been known for several decades [Smith and Baker, 1978]. Observations between 1972 and 2006 reveal that during large spring blooms in coastal mid-latitude regions, 31-42% of the light can be absorbed by phytoplankton [Fleming-Lehtinen and Laamanen, 2012]. This heating process has been observed and studied on a local scale with different methods. A series of satellite images and simultaneous ship transects show that the accumulation of phytoplankton can locally increase the SST by up to 1.5°C [Kahru et al., 1993]. Furthermore, remotely sensed data on ocean color show that phytoplankton distribution influences seasonal SST with a local maximum heating of 4°C [Sathyendranath et al., 1991]. In situ optical, physical and biological observations evidence a heating rate of 0.13°C in the mixed layer of the western equatorial Pacific Ocean due to phytoplankton blooms [Siegel et al., 1995]. Moreover, field data based on sensor measurement of SST record a maximum temperature difference of 4.7°C between the ocean surface and 2 m depth. This difference of temperature in the water column is attributed to high surface phytoplankton concentrations [Ramp et al., 1991]. Recent high-resolution in situ observations in the Indo-West Pacific reveal that in the presence of large phytoplankton blooms, the temperature of the ocean can increase by 0.95°C [Wurl et al., 2018]. All observations report local heating of the ocean surface but the magnitude of this warming varies. To study phytoplankton light absorption on a larger scale we, therefore, use models.
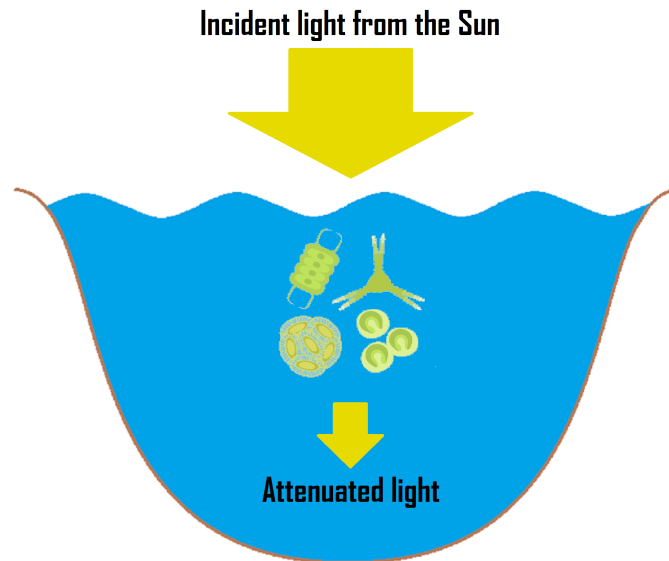
Figure 1.3: Schematic representation of the phytoplankton light absorption mechanism. Phytoplankton cell at the surface of the ocean alter the penetration of light in the water column. As a consequence, the heat distribution is altered and the oceanic temperature is affected.

Modeling studies

The effect of phytoplankton light absorption on the climate system has been investigated with a broad range of models. In this section, I introduce the simulated effect of phytoplankton on ocean properties, sea-ice dynamics and atmospheric properties.

Effects on the ocean

As demonstrated by observations, most of the model studies indicate a warming of the SST with phytoplankton light absorption. For instance, an idealized study with a water column coupled biological-physical model shows that the warming of the ocean surface can be as high as 2°C [Sonntag and Hense, 2011]. Moreover, the results evidence a seasonal variation of the warming and a positive feedback loop, favoring the growth of surface buoyant phytoplankton. Ocean General Circulation Models (OGCMs) and Coupled General Circulation Models (CGCMs) have attempted to demonstrate the effect of phytoplankton on the surface oceanic temperature. The surface oceanic heating reported for these modeling studies varies between 0.5-2°C [Murtugudde et al., 2002; Wetzel et al., 2006; Patara et al., 2012]. Furthermore, several studies show that phytoplankton light absorption can alter the seasonal cycle of SST [Lengaigne et al., 2007, 2009; Manizza et al., 2005].

Not all modeling studies indicate an ocean surface heating, several show a global surface cooling effect. Indeed, the presence of phytoplankton at the surface blocks the penetration of heat and cools the subsurface of the ocean, this phenomenon is called the shading effect. The colder subsurface water is then transported to the surface via shallow vertical mixing. This shading effect has been shown to act on seasonal [Manizza et al., 2005] or annual [Paulsen et al., 2018] time scales and decreases the SST by 0.1-0.5°C.

In turn, these changes of the surface oceanic temperature affect ocean circulation. For instance, in the tropical regions, phytoplankton light absorption can increase the surface

currents from the tropics to the subtropics [Manizza et al., 2008]. The changes in ocean dynamics can therefore cause a general shoaling effect by ∼5 m of the mixed layer depth (MLD), producing an upward movement of the Equatorial Undercurrent [Manizza et al., 2005, 2008]. The modifications of the physical properties of the ocean have consequences for surface nutrient contents and primary production. Manizza et al. [2008] show that surface nutrient concentrations increase but subsurface nutrient concentrations decrease, leading to a small increase of the global water integrated primary production. The authors indicate that these biogeochemical changes have consequences on biogenic calcification processes, POC export and $CaCO_3$ export. Furthermore, changes in ocean physics due to phytoplankton light absorption can lead to feedbacks on the climate. For instance, Manizza et al. [2005] show that the presence of phytoplankton changes the oceanic heat distribution, the ocean stratification and the sea-ice cover, increasing therefore the phytoplankton biomass by up to 12%, thus amplifying the initial physical perturbation.

Effects on the sea-ice dynamics

Changes in the oceanic properties can impact sea-ice dynamics. Using an uncoupled ocean-atmosphere model, Manizza et al. [2005] suggest that phytoplankton light absorption reduces sea-ice cover by 2-6% in summer in the Southern Hemisphere while there is almost no impact on the Arctic Ocean sea-ice cover. The decrease in sea-ice cover indicated by Manizza et al. [2005] in the Southern Ocean are in agreement with a one-dimensional thermodynamic sea-ice model coupled to a bio-optical model [Zeebe et al., 1996]. This idealized study evidences that an algal layer located in the top of the ice sheet increases sea-ice temperature of 0.3K for snow depth <5 cm. Lengaigne et al. [2009] use a coupled atmosphere-ocean model with an interactive biogeochemical component and focus on the Arctic Ocean to study the effect on phytoplankton light absorption. The authors find that the maximum increase of SST is ∼0.5°C along the continental shelves in late summer, leading to an annual reduction of 24% of the sea-ice thickness in the Arctic Ocean. This seasonal heating increases melting, precipitation and river runoff provoking an input of freshwater in the northern Atlantic, slowing down the overturning circulation.

Effects on the atmosphere

Phytoplankton light absorption does not only affect the ocean and sea-ice properties but also affects the atmospheric properties. Indeed, the ocean and the atmosphere are not two different climate compartments but they communicate via heat, water or gas transfers. Shell et al. [2003] were the first to question the effect of phytoplankton light absorption on the atmospheric temperatures. The authors used an uncoupled ocean-atmosphere model and evidence an amplification of the seasonal cycle of temperature in the lowest atmospheric layer. This seasonal amplification has an average of 0.3K but can locally reach 1K. The effect of phytoplankton light absorption in the mid-latitudes can even extend throughout the troposphere, where temperature changes are small but still visible [Shell et al., 2003]. In turn, changes in the atmospheric temperatures affect the atmospheric dynamics and several modeling studies report a modification of the Hadley and Walker circulation [Shell et al., 2003; Wetzel et al., 2006; Gnanadesikan and Anderson, 2009; Patara et al., 2012; Paulsen et al., 2018].

Several studies try to understand how phytoplankton light absorption warms the atmosphere. For instance, Patara et al. [2012] show that phytoplankton light absorption increases the specific atmospheric humidity, enhancing the Earth's greenhouse effect. As a

consequence, the authors show that global and annual atmospheric temperature averages increase by 0.5°C. Moreover, Manizza et al. [2008] show that phytoplankton light absorption causes a shift in the ecosystem community and changes the biogeochemical properties of the ocean. Consequently, on a global scale, the air-sea O_2 flux slightly decreases while the air-sea CO_2 flux slightly increases but these fluxes can highly vary regionally [Manizza et al., 2008]. These studies demonstrate that phytoplankton light absorption influences the climate pathways at the atmosphere-ocean interface. However, the importance of the air-sea heat and CO_2 fluxes behind the phytoplankton-induced atmospheric warming is still unknown (Research Question 2; Chapter 4).

Moreover, several modeling studies considering phytoplankton light absorption indicate that this biogeophysical mechanism plays a role in large climate oscillations such as El Niño-Southern Oscillation (ENSO). However, the conclusions of these studies and the reasons behind changes in ENSO dynamics diverge. Indeed, a strengthening [Marzeion et al., 2005; Löptien et al., 2009] or weakening [Anderson et al., 2007; Jochum et al., 2010] of ENSO are reported as well as changes in its oscillation period [Zhang et al., 2009]. Changes in ENSO dynamics are either attributed to the presence of chlorophyll at the Equator [Timmermann and Jin, 2002; Jochum et al., 2010] or off-Equator [Anderson et al., 2009; Paulsen et al., 2018]. These contradictory conclusions might be due to the rather short time-scale of the studies. Indeed, Jochum et al. [2010] indicate that several centuries-long simulations might not be sufficiently long to assess the relation between ENSO and an interactive chlorophyll.

Effects under global warming

Under global warming, the distribution and abundance of phytoplankton biomass are expected to decrease. For instance, remote-sensed ocean color data shows that between 1998 and 2006, an expansion of 15% of low surface chlorophyll areas occurs on a global scale [Polovina et al., 2008]. This reduction in chlorophyll biomass is directly linked to a warming of the ocean surface [Gregg et al., 2005]. These observations are supported by most climate model predictions. For instance, an intercomparison of four fully coupled atmosphere-ocean models indicates a global decrease in net primary production of 2-20% under a low greenhouse gas emissions scenario [Steinacher et al., 2010]. With the predicted damping of phytoplankton biomass, several studies investigate the effect of phytoplankton in a warmer world. Sonntag [2013] runs simulations with a homogeneous increase of 3°C in SST and compares these simulations with a present-day SST forcing. The author indicates that phytoplankton light absorption leads to a local increase of SST of 0.2°C in the warmer scenario. Park et al. [2015] focus on the Arctic region and runs simulations where atmospheric CO_2 concentration increases by 1% each year from 1990, doubling its initial concentration. The authors indicate that phytoplankton light absorption amplifies future Arctic warming by 20%. Finally, Paulsen [2018] performs simulations under a warming scenario with a 1% transient increase in atmospheric CO_2 concentration each year. The author reports that phytoplankton light absorption locally increases the SST by up to 0.7K. These studies demonstrate that phytoplankton light absorption plays a role in the future climate but none of them investigate the effect of phytoplankton light absorption under global warming scenarios taking into account future socio-economics aspects. Furthermore, the effect of phytoplankton light absorption under global warming has been studied with idealized [Sonntag, 2013; Park et al., 2015] or complex climate models [Paulsen, 2018] but never with climate models of intermediate complexity. Thus I wonder if climate models of intermediate complexity are sufficient to capture the patterns and magnitude of changes evidence with complex climate models (Research Question 3; Chapter 5).

Objectives and thesis structure

This thesis is one step to better understand how phytoplankton affects the current and future climate system. I focus on a particular biogeophysical mechanism, phytoplankton light absorption, and its role in the physical and biogeochemical environment. To study this biogeophysical mechanism, I used an Earth system model of intermediate complexity (EMIC).

In the second chapter, I give an introduction on EMICs and present the model I used during my thesis. I detail the implementation of phytoplankton light absorption in the model. I also introduce the calibration, the shortcomings and finally the climate sensitivity of the model.

In the introduction section, I demonstrate that phytoplankton light absorption affects the climate system. However, the importance of this biogeophysical mechanism is still unclear. To shed light on this research gap, in the third chapter of this thesis, I compare the importance of phytoplankton light absorption versus the importance of a higher number of plankton functional types on the climate system. I conduct several simulations with and without phytoplankton light absorption as well as with a high or low number of zooplankton and phytoplankton species. The main research question in the third chapter is:

1. **Does phytoplankton light absorption have a higher impact on the climate system than an increase in marine ecosystem complexity?**

I show that phytoplankton light absorption increases the atmospheric temperature. As a logical follow-up, I explore how phytoplankton light absorption warms the atmosphere and investigate the climate pathways behind the phytoplankton-induced atmospheric heating. I isolated four different climate pathways related to air-sea heat and CO_2 fluxes. In the fourth chapter, I address the question:

2. **How does phytoplankton light absorption increase the atmosphere temperature?**

Answering the second question, I demonstrate that phytoplankton light absorption warms the atmosphere mainly via an increase in air-sea CO_2 flux. With human-induced global warming affecting also the climate system via CO_2 emissions, I speculate on the effect of phytoplankton light absorption in a high CO_2 world. I study this biogeophysical mechanism under the four Representative Concentration Pathways (RCPs) and their extensions used by the fifth IPCC Assessment Report. In the fifth chapter, I state the following research question:

3. **How does phytoplankton light absorption alter the climate system under global warming scenarios?**

Finally, the last chapter summarizes the main conclusions of this thesis and speculates on the perspectives for future work on the topic.

Technical remarks

The three main chapters (Chapters 3, 4 and 5) of this thesis are written in the style of journal publications, containing their own introduction, model description and conclusions. These individual chapters can thus be read independently from each other. Chapter 3 has been submitted to the *Journal of Advances Modeling Earth Systems* and is in the hands of the reviewers. Chapter 4 is ready for submission to *Biogeosciences*.

The introduction, model description and conclusion sections are written in the first person singular while Chapters 3, 4 and 5 are written in the first person plural.

EARTH SYSTEM MODELS OF INTERMEDIATE COMPLEXITY

General statements

To explore and better understand the climate system, models have been developed. The representation of the climate mechanisms depends on various parameters that can be modified, altering the quality of the climate simulations [Shi et al., 2019]. Therefore several sensitivity analyses must be conducted in order to tune the climate models to recreate the natural patterns observed. These climate models are divided into three different classes depending on their complexity. The coupled general circulation models (CGCMs) are the most complex models and include biological, physical, biogeochemical and geochemical processes. They describe in detail individual weather patterns and regional current systems but their main limitation is their high computational time for long-term simulations. On the other side of the complexity spectrum are the conceptual and tutorial models. These models are rather simple mechanistic models and often designed to study the plausibility of climate processes.

Earth system models of intermediate complexity (EMICs) were created to address the gap between complex and rather simple climate models. The development of EMICs in climate research centers started in the 1980s [Petoukhov, 1980; Chalikov and Verbitsky, 1984; Gallée et al., 1991] and several dozens of EMICs have been established to date. They are developed to describe the Earth system excluding the interactions between humans and nature, humans are only an external forcing [Claussen et al., 2002]. EMICs are designed for different objectives: most are designed for simulations over several millennia while some are designed to simulate the interactions of as many climate components as possible. These models combine most of the climate mechanisms included in complex CGCMs but in a more condensed way. These simplifications of mechanisms allow therefore for long-term simulations without the need for supercomputers. EMICs are used for a broad range of purposes, from general studies [e.g. Holden et al., 2018; Ödalen et al., 2018] to more specific studies [e.g. Goes et al., 2019]. These models can be successfully employed as a highly efficient tool for the assessment of the long-term climate under various future and past climate scenarios, as well as for testing different parametrization schemes for climate mechanisms and feedbacks [Petoukhov et al., 2005; Zickfeld et al., 2013].

The motivation of this thesis is to study the interactions of marine biota, biogeophysics, biogeochemistry and the climate system. These interactions are computationally expensive in high-resolution models. Therefore I chose to use an EMIC called EcoGENIE to study the role of marine biota on the climate system.

EcoGENIE

During my PhD, I used the Grid-ENabled Integrated Earth system model (GENIE) framework [Lenton et al., 2007] consisting of several modules describing the dynamics of the Earth system (Figure 2.1). This model is suitable for this thesis because it considers the key feedbacks and interactions between the marine ecosystem, the marine carbon cycle, atmospheric CO_2 and the climate system. I used the version with the new ecosystem component (ECOGEM) that explicitly accounts for the growth and interaction of an arbitrary number of plankton species [Ward et al., 2018]. The new ecosystem component and GENIE form the recent EcoGENIE Earth system model. The efficient numerical terrestrial scheme and associated atmospheric changes [Williamson et al., 2006] is not used in this thesis, so the land surface is essentially passive. EcoGENIE has been recently used to study the relationship between marine biota and past climate. For instance, this model is used to assess and understand the interactions between the marine ecosystem and the warm climate of the early Eocene [Wilson et al., 2018]. EcoGENIE is also used to explore the relationships between plankton size, trophic complexity and the availability of nutrient phosphorus during the late Cryogenian [Reinhard et al., 2020b]. Moreover, the model contains the simplified atmosphere and carbon-centric version that has been previously applied to explore the interactions between marine biogeochemistry and climate for a broad range of timescales and past periods [Gibbs et al., 2016; Meyer et al., 2016; Tagliabue et al., 2016; Gutjahr et al., 2017; Fantle and Ridgwell, 2020]. The ocean physics, the sea-ice and the atmospheric components are run with 96 time-steps per year. The calculation for the ocean biogeochemistry component is operated 48 times per year. Finally, the marine ecosystem component takes 960 time-steps per year (or 20 time-steps for each ocean biogeochemistry component time-step).
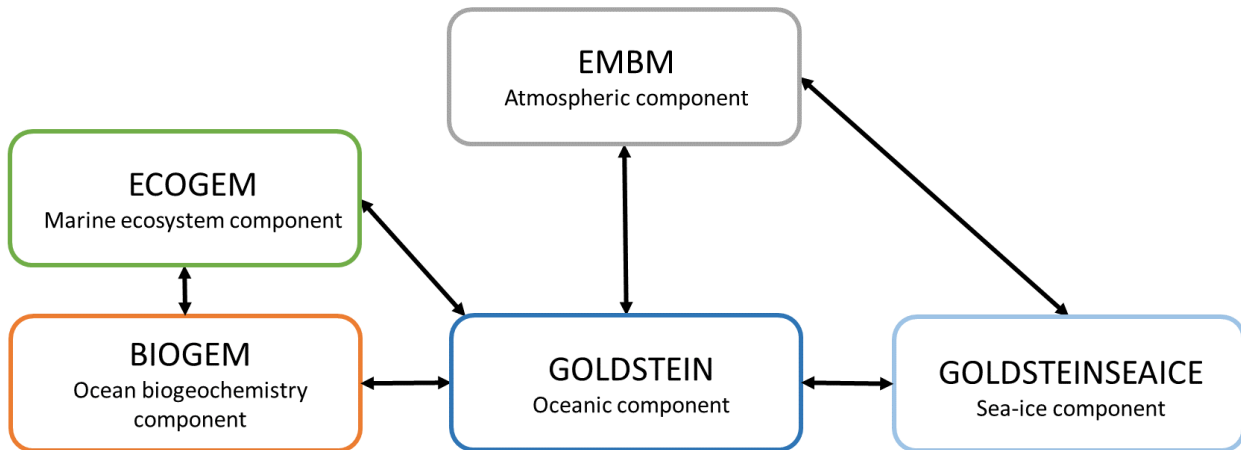
Figure 2.1: Schematic representation of EcoGENIE modules. Black arrows represent the links between the different components. The addition of ECOGEM to the previous GENIE components forms the EcoGENIE Earth system model.

Ocean physics component

The Global Ocean Linear Drag Salt & Temperature Equation Integrator (GOLDSTEIN) is a fast, 3D frictional geostrophic model with linear drag [Edwards and Marsh, 2005; Lenton et al., 2007; Marsh et al., 2011]. The model is based on the reduced physics of the thermocline equations, described for a single-basin configuration in Edwards et al. [1998]. It incorporates eddy-induced and isopycnal mixing following Griffies [1998]. The prognostic variables of this

model component are temperature, salinity and the three-dimensional velocity field. Heat, salinity and biogeochemical tracers are transported horizontally and vertically through advection, convection and mixing. Surface exchange of heat and moisture with the atmosphere and the sea-ice is applied as a surface boundary condition.

The horizontal oceanic grid (36 x 36) is constructed to be uniform in longitude and uniform in sine latitude, giving ~3.2° latitudinal increments at the equator increasing to 19.2° in the polar regions. The horizontal mesh has been widely used for very large ensembles [Marsh et al., 2004] and biogeochemical simulations [Cameron et al., 2005] with focus on the carbon cycle [Colbourn, 2011]. Usually, the ocean component is either divided into 8 or 16 vertical layers [Ridgwell et al., 2007; Marsh et al., 2011] but we increased the vertical resolution to 32 layers. The thickness of the 32 vertical layers increases with depth. The height of the oceanic surface layer is 29.38 m while the deepest layer is 456.56 m high.

Sea-ice component

The GOLDSTEINSEAICE component is a 2D model and describes the sea-ice dynamics [Edwards and Marsh, 2005]. Dynamical equations are solved for the fraction of the ocean surface covered by sea-ice and for the average height of sea-ice. Moreover, a diagnostic equation is solved for the ice surface temperature. The prognostic variables are ice thickness, ice areal fraction, and ice concentration. The transport of sea-ice includes sources and sinks of these variables. Moreover, the thermodynamical growth or decay of sea-ice depends on the net heat flux going from the ocean and atmosphere into the sea-ice. Sea-ice dynamics consist of advection by surface currents and Laplacian diffusion. The sea-ice component acts as a coupling module between the ocean and the atmosphere where heat and freshwater are conserved between these three components.

Atmospheric component

The Energy Moisture Balance Model (EMBM) describes the atmospheric dynamics [Edwards and Marsh, 2005; Marsh et al., 2011]. It is based closely on the UVic Earth system model [Weaver et al., 2001]. This model is a vertically integrated 2D atmospheric model with surface air temperature and surface-specific humidity as prognostic variables. Heat and moisture are horizontally transported by winds and mixing. Moreover, precipitation instantaneously removes all moisture corresponding to the excess above a relative humidity threshold. Atmosphere, ocean and sea-ice exchange moisture and heat. Heat fluxes depend on incoming shortwave radiation, sensible and latent heat fluxes, re-emitted longwave radiation and outgoing planetary longwave radiation. The outgoing planetary longwave radiation is a function of different greenhouse gases selected in the model setup (CO_2, water vapor, CH_4, N_2O). Moisture fluxes depend on precipitation, evaporation and sublimation. The incoming shortwave radiation can vary seasonally in the model.

Land scheme

The model has no dynamical land surface scheme, therefore the land surface temperature is assumed to be equal to the surface atmospheric temperature. Evaporation over land is set to zero, thus the atmospheric heat source over land is simplified with the outgoing longwave radiation. The sensible heat flux and the latent heat flux are equal to zero. Precipitation over land is added to appropriate coastal ocean grid cells according to a prescribed runoff map.

Ocean biogeochemistry component

The BIOGEochemical Model (BIOGEM) calculates the redistribution of biogeochemical tracers occurring other than by transport due to oceanic circulation and is based on the biogeochemical cycle of phosphorus [Ridgwell et al., 2007]. The biogeochemical redistribution happens through the removal of nutrients, dissolved inorganic carbon (DIC), and alkalinity by biological activity in the surface ocean layer. The biological activity is resolved by the marine ecosystem component of the model (see below). In BIOGEM, the resulting export of particulate organic matter to the ocean interior is subject to remineralization. More specifically, the remineralization of sinking POC with depth is predicted by a globally uniform fixed exponential function. Further redistribution of tracers occurs through gas exchange between the atmosphere and ocean as well as due to the formation and decay of dissolved organic matter (DOM). The state variables are the inorganic resources and the dead organic matter. Moreover, the biological pump is parameterized by an implicit biological community: biological uptake is limited by light, temperature and nutrient availability. Any uptake returns instantly to exported POM or DOM in the ocean interior. The formation of calcium carbonate ($CaCO_3$) is associated with the biological fixation of carbon and its dissolution follows a fixed remineralization profile. Moreover, this component calculates the air-sea CO_2 and O_2 exchange. The value of atmospheric CO_2 predicted by BIOGEM is used as input for the radiative scheme of the atmospheric component, thus providing climate feedback. The configuration of this component used during my thesis is capable of reproducing large-scale distribution of nutrients [Ridgwell et al., 2007] and the complete oceanic carbonate chemistry [Holden et al., 2013]. Furthermore, this configuration of BIOGEM can project anthropogenic CO_2 inventories consistent with data [Cao et al., 2009].

Recently, the nitrogen cycle has been updated to allow the global nitrogen fixation rate to fit more recent observations and to introduce a limitation of nitrification by oxygen in addition to ammonium [Naafs et al., 2019]. Moreover, an oceanic and atmospheric methane cycle [Reinhard et al., 2020a], and an anoxic iron and sulphur cycles [Van de Velde et al., 2020] have been implemented in the model. Even more recently, a temperature-dependent representation of the marine carbon cycle for both past and future climate simulations has been added in the model [Crichton et al., 2021]. These recent changes and implementations in biogeochemical cycles are not considered during this thesis.

Marine ecosystem component

The size-structured ecological component (ECOGEM) represents and describes the plankton populations and the ecological dynamics [Ward et al., 2018]. The new ECOGEM component replaces the biological uptake formulation of BIOGEM. With this marine ecosystem component, the biological uptake is limited by light, temperature as well as nutrient availability but passes through a dynamic plankton community before returning to organic or inorganic matter. The plankton community is subject to trophic interactions such as mortality, resource competition and predation. Predation is simply defined as the consumption of any living organism, including both herbivorous and carnivorous interactions. The mortality of the plankton community is reduced at very low biomass such that plankton cannot become extinct. Plankton mortality and grazing are the only two sources of organic matter, with partitioning between non-sinking dissolved and sinking particulate organic matter. The state variables represent the nutrient resources, the plankton biomass and the organic matter. Each plankton population is associated with biomass state variables for carbon, phosphorus and chlorophyll. In ECOGEM the stoichiometry is flexible, it depends on environmental conditions and the status of the food web. This flexible stoichiometry allows

phytoplankton to flexibly take up nutrients according to nutrient availability. ECOGEM is a plankton functional type (PFT) model meaning that plankton populations are defined by functional groups (zooplankton, phytoplankton, mixotroph, diatom...) with different traits. Furthermore, each functional group can be subdivided into size classes with specific size-dependent traits. For my PhD, I only incorporated two functional groups in the model, namely phytoplankton and zooplankton, except in Chapter 3 where I integrated six phytoplankton and six zooplankton groups.

Phytoplankton is characterized by nutrient uptake and photosynthesis traits. The uptake of nutrients by phytoplankton follows a Michaelis-Menten function [Franks, 2002] where small phytoplankton cells have a higher nutrient affinity than large phytoplankton cells. Temperature affects the growth of phytoplankton through an Arrhenius-like equation.

Zooplankton is characterized by predation and grazing traits. Zooplankton grazing is dependent on the available prey biomass, with zooplankton preferentially grazing on preys that are 10 times smaller than themselves.

Coupling methodology between BIOGEM and ECOGEM

At the beginning of each ECOGEM time-step, the inorganic resources such as nutrients (DIC, PO_4, Fe) and important physical properties are transferred from BIOGEM to ECOGEM (Figure 2.2). These inorganic resources are taken up by phytoplankton through photosynthesis. At the end of each ECOGEM time-step, the rates of change in inorganic resources and organic matter are passed back to BIOGEM. The rate of change in inorganic resources updates the DIC, PO_4, Fe, oxygen and alkalinity tracers. The rate of change in the dissolved organic matter is implemented in the dissolved organic matter pools while the rate of change in the particulate organic matter is instantly remineralised using the BIOGEM export function. Finally, the rate of change in the plankton biomass updates the living biomass concentrations in ECOGEM.
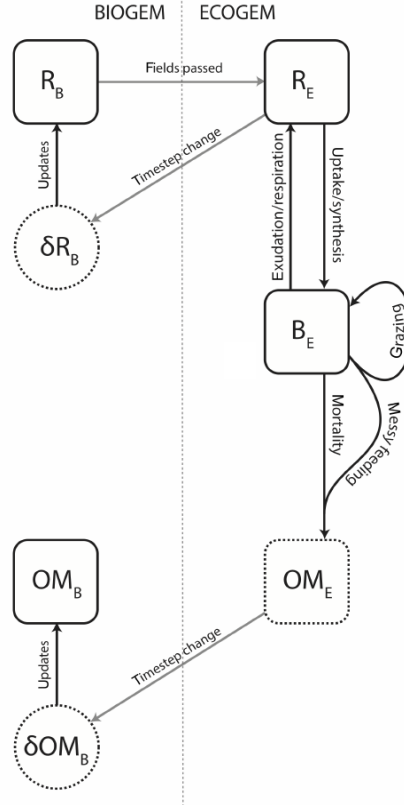
Figure 2.2: Schematic representation of the coupling between BIOGEM and ECOGEM. R indicates the dissolved inorganic resources such as nutrients: DIC, PO_4 and Fe. B represents the plankton biomass such as the carbon biomass or the chlorophyll biomass. OM indicates the dead organic matter such as POM and DOM. Subscripts B and E denote state variables from BIOGEM and ECOGEM respectively. Finally, δ represents the rate of change. Figure from Ward et al. [2018].

Implementation of phytoplankton light absorption

In ECOGEM the incoming shortwave radiation is absorbed by the particles and dissolved molecules. The light level is calculated as the mean photosynthetically available radiation within a variable mixed layer [Kraus and Turner, 1967]. The total light attenuation coefficient is given by Eq. 2.1:

$$k_{tot} = k_w + k_{Chl} \cdot Chl_{ML} \qquad (2.1)$$

Where k_{tot} is the total light absorption coefficient, k_w is light absorption by water (0.04 m^{-1}), k_{Chl} is the light absorption by chlorophyll (0.03 $m^{-1}(mg\ Chl)^{-1}$) and Chl_{ML} is the chlorophyll concentration distributed across the mixed layer. The values for k_w and k_{Chl} are taken from [Ward et al., 2018]. The vertical light absorption is described by the scheme Eq. 2.2:

$$I(z) = I_0 \cdot \exp[(-k_w - k_{Chl} \cdot Chl_{tot}) \cdot z] \qquad (2.2)$$

Where $I(z)$ is the radiation at depth z, I_0 is the radiation at the surface of the ocean, Chl_{tot} is the total chlorophyll concentration, k_w and k_{Chl} are the light absorption coefficients mentioned previously. Solar radiation in the ocean decreases exponentially with depth through

absorption. We allow primary production and light to penetrate until the sixth layer of the model (221.84 m deep), which is the lower limit of the euphotic zone [Tett, 1990]. In our model setup, maximum absorption occurs in the upper oceanic layer and minimum absorption occurs in the sixth layer. As seen and discussed previously, phytoplankton changes the optical properties of the ocean. We implemented the warming of water via phytoplankton light absorption into the model following the scheme proposed by Hense [2007] and Patara et al. [2012] Eq. 2.3

$$\frac{\partial T}{\partial t} = \frac{1}{\rho \cdot c_p} \frac{\partial I}{\partial z} \tag{2.3}$$

$\partial T/\partial t$ denotes the temperature changes, c_p is the specific heat capacity of water, ρ is the ocean density, I is the solar radiation incident at the ocean surface, and z is the depth. Part of the light absorbed by phytoplankton is released in form of fluorescence and heat, however the fluorescence form can be ignored [Lewis et al., 1983]. We therefore assume that the all light absorption leads to heating of the water.

Calibration and known shortcomings of EcoGENIE

Earth system models are only a representation of the climate system so their parameters must be tuned for a good depiction of the real world. As all climate models, several parameters of EcoGENIE have been tuned to suit climatological observations. The parameters of the oceanic component (GOLDSTEIN) were calibrated against annual mean climatological observations of temperature, salinity, surface air temperature and humidity using the ensemble Kalman filter (EnKF) methodology [Hargreaves et al., 2004; Annan et al., 2005]. Furthermore, the parameters of the ocean biogeochemistry component (BIOGEM) were optimized with respect to a 3D data fields of phosphate [Conkright et al., 2002] and alkalinity [Key et al., 2004] using the EnKF methodology [Annan et al., 2005]. After calibration, the global particulate organic carbon, inorganic carbon export and dissolved O_2 are consistent with recent data and computationally expensive 3D ocean circulation model estimates [Ridgwell et al., 2007].

Even if the model has been calibrated, several pitfalls and shortcomings happen in the climate representation. For instance, the model is known to underestimate the strength of upwelling, therefore underestimating surface nutrient concentrations [Ward et al., 2018]. Moreover, the model also underestimates sea-ice concentrations in polar regions, therefore the albedo is increased artificially in these regions and is rather unrealistic compared with observations [Lenton et al., 2006; Holden et al., 2010]. The horizontal oceanic grid in this work gives good estimates of climate variables in the low and mid-latitudes. However, in the polar regions, the sea-ice distribution and the regional ocean circulation can be improved by a higher horizontal resolution [Marsh et al., 2011]. The single-layer atmospheric component introduces significant weakness [Holden et al., 2016]. For instance, the diffusive moisture transport implies poor precipitation fields that cannot represent convective precipitation or monsoon dynamics. Furthermore, the atmospheric component applies prescribed surface wind fields, defined either from climatology or from outputs of more complex models, therefore dynamic ocean feedbacks are restricted to the thermohaline circulation. Clouds are represented through a prescribed albedo field [Lenton et al., 2006] and a spatially uniform adjustment to outgoing longwave radiation (OLR). Moreover, uncertain cloud feedbacks on the radiative balance in a changing climate are represented through a globally uniform temperature-dependent adjustment to OLR.

Ward et al. [2018] compare the model with (EcoGENIE) and without (cGENIE) the ecosystem component in terms of their correlation to observations (WOA09 for dissolved PO_4 and O_2 [Garcia et al., 2010] and GLODAPv2 for alkalinity and DIC [Olsen et al., 2016]). The authors show that cGENIE has a more realistic distribution of oxygen, alkalinity, phosphate and DIC than EcoGENIE. This is not surprising because cGENIE has been tuned on various occasions to match observations while EcoGENIE has not yet been optimized in this way.

Climate sensitivity of EcoGENIE

The climate sensitivity is the global averaged air temperature change in response to changes in radiative forcing, mostly due to increased level of atmospheric CO_2 concentration. Essentially, it dictates how much atmospheric temperature will rise in response to a doubling of pre-industrial CO_2 level. Due to climate inertia, climate sensitivity depends on the timescale chosen. Scientists agree on three different forms of climate sensitivity:

- The transient climate response (TCR) is defined as the atmospheric temperature response over a human timescale. In this case, the distribution of heat between the atmosphere and the ocean has not reached equilibrium yet.

- The equilibrium climate sensitivity (ECS) is defined as the atmospheric temperature response over centuries. In this case, the additional heat due to a higher atmospheric CO_2 concentration has time to disperse in the atmosphere and deep ocean.

- The Earth system sensitivity (ESS) is defined as the atmospheric temperature response over several millennia. It includes very long-term climate feedbacks such as changes in ice sheets or vegetation cover.

Hereafter, climate sensitivity will be referred as ECS.

Svante Arrhenius was the first to quantify global warming as a consequence of doubling atmospheric CO_2 and thus to study climate sensitivity. He used observations to estimate the amount of radiation absorbed by water vapor and atmospheric CO_2. In his first study on the matter, he found out that a twofold increase in atmospheric CO_2 concentration rises the air temperature by approximately 5-6°C [Arrhenius, 1896]. In a later work, he corrected these values to 4°C [Arrhenius, 1908; Lapenis, 1998]. Nowadays, climate sensitivity is used to determine the liability of climate models. A new consensus on climate sensitivity has emerged: it is very likely that climate sensitivity should be between 1.5-4.5°C for climate models [Charney et al., 1979; Collins et al., 2013; Knutti et al., 2017]. Moreover, climate models with a climate sensitivity slightly higher than 3°C perform better in climate variables than models with a climate sensitivity below 3°C [Caldwell et al., 2018].

[Holden et al., 2010] studied the climate sensitivity of GENIE in detail but with a different version of the model framework used for my PhD. They used a version of the model where the atmosphere, ocean, sea-ice and land vegetation (ENTS; [Williamson et al., 2006]) are represented. While I used a version of the framework where the atmosphere, ocean, sea-ice, ocean biogeochemistry and marine ecosystem are represented. They also used a lower vertical resolution for the oceanic component with 8 oceanic layers while there are 32 layers in my model setup. [Holden et al., 2010] find that the climate sensitivity for their version of the GENIE framework is 3.6°C, which is within the likely range defined previously. Moreover, a recent study using a version of the model with the ocean, sea-ice, ocean biogeochemistry,

dynamical atmospheric component (PLASIM; [Holden et al., 2016]) and with a land scheme (ENTS; [Williamson et al., 2006]) is associated with a climate sensitivity of 3.4°C for their version of GENIE [MacDougall et al., 2020].

To determine the climate sensitivity of EcoGENIE, I conducted two experiments (Table 2.1) with the same setup and the same spin-up as Chapters 3, 4 and 5. The spin-up is a model run of 10,000 years with only BIOGEM to allow for realistic nutrient distributions in the ocean. Then the experiments restart from the spin-up with a prescribed atmospheric CO_2 concentration for 1,000 years and with ECOGEM. The simulations are forced with the same constant flux of dissolved iron into the ocean surface [Mahowald et al., 2006]. Both experiments have the same ecosystem community, with one phytoplankton and one zooplankton species. The only difference between these two simulations is the value of the prescribed atmospheric CO_2.

Table 2.1: Name and description of the two simulations conducted to determine the climate sensitivity of the model

Simulation	Atm. CO_2 (ppm)	Size phytoplankton (μm)	Size zooplankton (μm)
1xCO2	278	46.25	146.15
2xCO2	556	46.25	146.15

For the experiment *1×CO2*, the atmospheric CO_2 concentration correspond to the pre-industrial concentration of 278 ppm. The second experiment, *2×CO2*, is parameterized with a double pre-industrial atmospheric CO_2 concentration of 556 ppm.

The pattern of the surface air temperature (SAT) for *1×CO2* (Figure 2.3a) is similar to the pattern of surface air temperature for *2×CO2* (Figure 2.3b). But the magnitude of SAT in *2×CO2* is higher than the magnitude of SAT in *1×CO2* (Figure 2.3c). Indeed the global average SAT for *2×CO2* is 15.5°C while for *1×CO2* it is 12.4°C. The global average difference of SAT between these two simulations, which represents the climate sensitivity of the model, is 3.1°C. A climate sensitivity of 3.1°C is in the likely range [Charney et al., 1979; Collins et al., 2013; Knutti et al., 2017] and is slightly higher than 3°C, indicating that the performance of the model is adequate to describe the climate variables of interest.
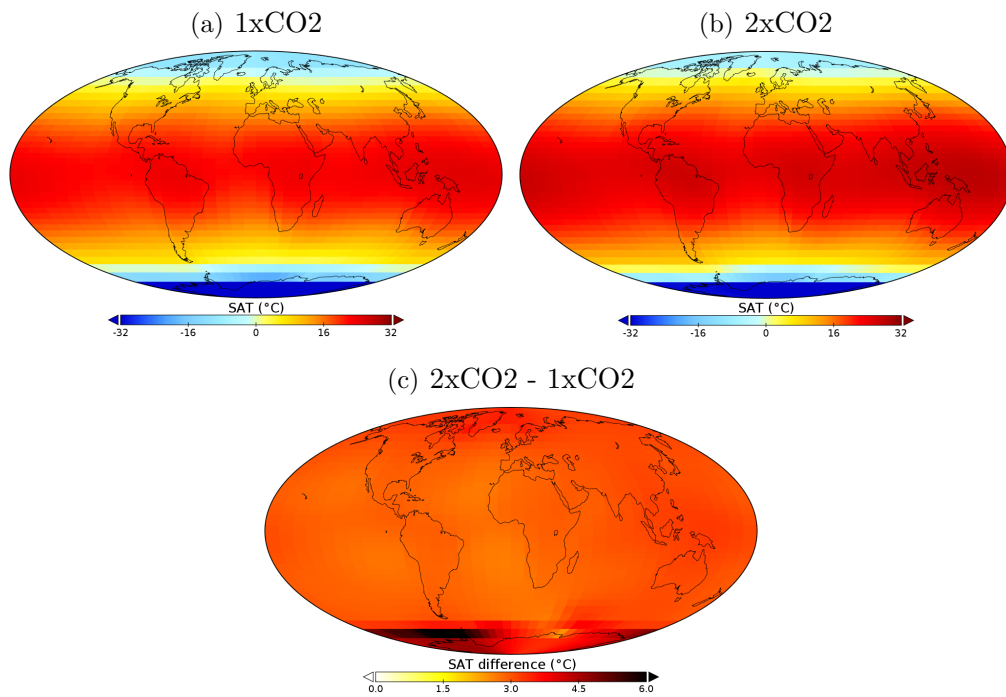
Figure 2.3: Surface air temperature (°C) for the experiments (a) 1xCO2 and (b) 2xCO2. Blue colors represent negative temperature while yellow/red colors represent positive temperature. (c) Surface atmospheric temperature difference (°C) between 2xCO2 - 1xCO2. Dark/brown colors indicate large differences while white/yellow colors represent no or small differences. Note that the differences between these two simulations are always positive.

THE IMPORTANCE OF PHYTOPLANKTON LIGHT ABSORPTION IN THE CLIMATE SYSTEM

We investigate the relative importance of ecosystem complexity and phytoplankton light absorption for climate studies. While the complexity of Earth system models with respect to marine biota has increased over the past years, the relative importance of biological processes in driving climate-relevant mechanisms such as the biological carbon pump and phytoplankton light absorption is still unknown. The climate effects of these mechanisms have been studied separately, but not together. To shed light on the role of biologically mediated feedbacks, we performed different model experiments with the EcoGENIE Earth system model. The model experiments have been conducted with and without phytoplankton light absorption and with two or twelve plankton functional types (PFTs). For a robust comparison, all simulations are tuned to have the same primary production. Our model experiments show that phytoplankton light absorption changes ocean physics and biogeochemistry. Higher sea surface temperature decreases the solubility of CO_2 which in turn increases the atmospheric CO_2 concentration, and finally the atmospheric temperature rises by 0.45°C. An increase in ecosystem complexity increases the export production of particulate organic carbon but decreases the amount of dissolved organic matter. These changes in the marine carbon cycling, however, hardly reduce the atmospheric CO_2 concentrations and slightly decrease the atmospheric temperature by 0.034°C. Overall we show that phytoplankton light absorption has a higher impact on the carbon cycle and on the climate system than a more detailed representation of the marine biota.

Introduction

Using an Earth system model (ESM), we focus on two climate-relevant feedbacks, the biological pump and the phytoplankton light absorption feedback to study their relative importance for the climate system. Increasingly more marine ecosystem processes, particularly related to the food web, are included in models, but it is unclear whether a higher degree of complexity has a greater impact on the climate system compared to other climate-relevant mechanisms that are often ignored, such as phytoplankton light absorption.

State-of-the-art marine ecosystem models include several nutrients and different plankton functional types (PFTs) such as diatoms, coccolithophores, picoeukaryotes and zooplankton [Laufkötter et al., 2015]. These PFT-models are embedded within Earth system models to study biogeochemical cycles [Le Quéré et al., 2005; Ilyina et al., 2013] with a focus on the carbon cycle. Indeed marine biota plays an essential role in the carbon cycle through the biological pump, defined as the uptake of carbon dioxide at the surface of the ocean and the sinking of the organic carbon to the abyssal ocean. Over geological time the biological pump has shaped ocean chemistry, biogeochemical cycling and ecosystem structure [Meyer et al., 2016]. Additionally, the biological pump has contributed to past variations of atmospheric CO_2, influencing the glacial/interglacial episodes during the ice ages of the Pleistocene period [Turner, 2015]. Watson and Liss [1998] used a simple model [Sarmiento and Toggweiler, 1984] to determine the importance of the biological pump on atmospheric CO_2. Their study suggests that if all marine life were to die, atmospheric CO_2 would increase by ∼450 ppm after a few hundred years.

Marine biota have not only an impact on the climate system through the carbon cycle but also affect, for example, the ocean's thermal, optical and mechanical properties via biogeophysical mechanisms [Hense et al., 2013]. Among these biogeophysical mechanisms, phytoplankton light absorption is particularly important. Previous observations between 1972 and 2006 reveal that during spring, when large blooms occur in coastal mid-latitude regions, 31-42% of the light can be absorbed by the phytoplankton [Fleming-Lehtinen and Laamanen, 2012]. The heat distribution in the upper ocean is then altered [Lewis et al., 1990; Sonntag and Hense, 2011], changing the sea surface temperature (SST) [Kahru et al., 1993; Patara et al., 2012], an important climate variable to understand interactions between the ocean and the atmosphere. Indeed, the SST affects atmospheric temperature, atmospheric humidity content, precipitation, as well as heat transfer between the ocean and the atmosphere [Jang et al., 2016; Lim et al., 2016]. These changes in atmospheric physics and chemistry can even alter the Walker and Hadley circulation [Gnanadesikan and Anderson, 2009; Paulsen et al., 2018]. A recent study [Patara et al., 2012] shows that phytoplankton light absorption increases the SST, enhancing evaporation and atmospheric humidity, and therefore the greenhouse effect. Changes in SST, in turn impact the oceanic circulation [Manizza et al., 2008]. These changes in ocean physics will cause feedbacks on the climate system. For instance, Manizza et al. [2005] used an Ocean General Circulation Model to show that phytoplankton light absorption intensifies the seasonal cycle of temperature, mixed layer depth and ice cover by roughly 10%, leading to an increase in phytoplankton biomass and thus to an amplification of the initial physical perturbations. But these feedbacks depend on the spatial and seasonal scale [Oschlies, 2004]. Finally, previous model studies focusing on phytoplankton light absorption report a strengthening [Marzeion et al., 2005; Paulsen et al., 2018] or weakening [Anderson et al., 2007; Jochum et al., 2010] of El Niño-Southern Oscillation as well as changes in its oscillation periods [Zhang et al., 2009].

None of these model studies have quantified the climate response to biologically-driven feedback mechanisms combined. In particular, the relative importance of ecosystem complexity and the effect on carbon export production compared to SST changes induced by phytoplankton light absorption has not been investigated. Additionally, the climate response has been only evaluated for a specific climate. The potential of marine biota in altering the climate system, in which atmospheric CO_2 is allowed to evolve freely, has not been demonstrated. To investigate these aspects we use an Earth system model of intermediate complexity (EMIC) [Claussen et al., 2002], called EcoGENIE [Ward et al., 2018]. For this purpose, we have modified the model by implementing phytoplankton light absorption.

Model description

We used the Grid-ENabled Integrated Earth system model (GENIE) [Lenton et al., 2007], consisting of several modules describing the dynamics of the individual Earth system components (Figure 3.1). GENIE is widely used for past climate and carbon-cycle studies [Gutjahr et al., 2017; Ödalen et al., 2018]. The new ecosystem component (ECOGEM) and GENIE form the recent EcoGENIE model [Ward et al., 2018]. We use the simplified atmosphere and carbon-centric version (cGENIE) that has been previously applied to analyze interactions between marine biological productivity, biogeochemistry and climate [Gibbs et al., 2016; Meyer et al., 2016; Tagliabue et al., 2016]. EcoGENIE contains different Earth system components and related processes including ocean circulation and marine biogeochemistry, atmospheric circulation, the marine ecosystem component and sea-ice dynamics. We modified the ecosystem (ECOGEM) and ocean component (GOLDSTEIN) to account for phytoplankton light absorption.
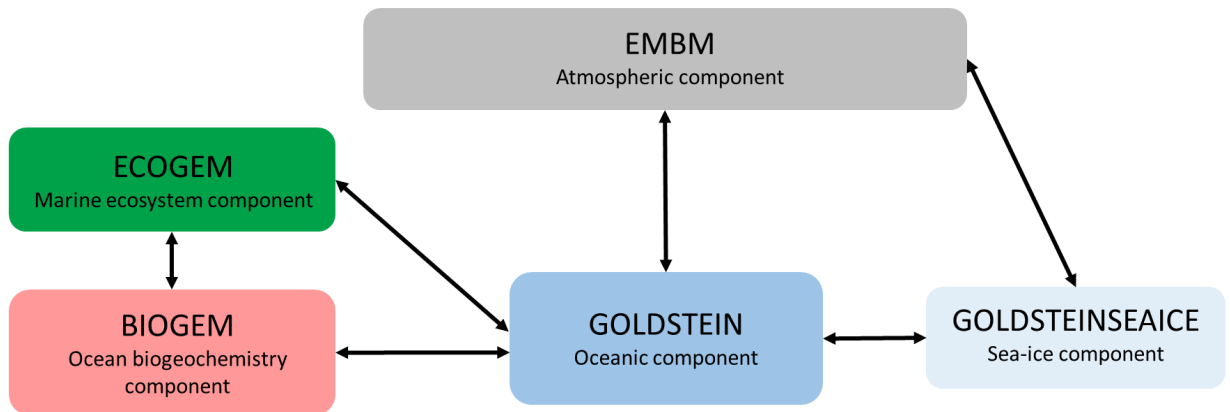
Figure 3.1: Schematic representation of EcoGENIE modules used for this study. Black arrows represent the links between the different components. The addition of ECOGEM to the previous GENIE components forms the EcoGENIE Earth system model.

Modules

Ocean physics component

The GOLDSTEIN component describes ocean physics. It is a 3D frictional-geostrophic ocean model [Edwards and Marsh, 2005; Marsh et al., 2011] based on the reduced physics of the thermocline equations, described for a single-basin configuration in Edwards et al.

[1998]. This model is similar to general circulation models, except that it neglects momentum advection and acceleration but incorporates eddy-induced and isopycnal mixing. This oceanic component includes a surface mixed layer scheme based on the scheme by Kraus and Turner [1967]. The parameters for GOLDSTEIN are calibrated against annual mean climatological observations of temperature, salinity, surface air temperature and humidity using the ensemble Kalman filter (EnKF) methodology [Hargreaves et al., 2004; Annan et al., 2005].

Sea-ice component

The GOLDSTEINSEAICE component describes the sea-ice dynamics. It is a 2D model and solves the equations for part of the ocean surface covered by ice [Edwards and Marsh, 2005]. A diagnostic equation is solved for the ice surface temperature. The sea-ice growth or decay depends on the net heat flux into the ice. The sea-ice dynamics consist of advection by surface currents and diffusion. The sea-ice component acts as a coupling module between the ocean and the atmosphere.

Atmospheric component

The Energy and Moisture Balance Model (EMBM) describes the atmospheric dynamics [Edwards and Marsh, 2005]. EMBM is based on the UVic Earth system model [Weaver et al., 2001]. It is a vertically integrated 2D atmospheric model with air temperature and specific humidity as prognostic variables. Heat and moisture are advected by winds and mixing. Precipitation instantaneously removes all moisture corresponding to the excess above a relative humidity. Atmosphere, ocean and sea-ice exchange moisture and heat fluxes.

Ocean biogeochemistry component

The BIOGEM module considers marine biogeochemical processes [Ridgwell et al., 2007]. This module calculates the transformations and spatial redistribution of biogeochemical quantities, plus the sea-air gas exchange of CO_2 and O_2. In this model, the state variables are the inorganic resources and the dead organic matter. The biological pump is parametrized by an implicit biological community: biological uptake is limited by light, temperature and nutrient availability. Any uptake returns instantly to exported particulate organic matter (POM) or dissolved organic matter (DOM) in the ocean interior. DOM is converted back to nutrients in the upper 12 oceanic layers (0-590m) while POM turns into nutrients in the deeper layers (590m-seafloor). Eventually, all organic matter is remineralized back to nutrients.

The model includes iron (Fe) and phosphate (PO_4) as limiting nutrients which is sufficient to realistically describe the distribution pattern of phytoplankton and zooplankton, nitrate (NO_3^-) is not considered here.

Ecosystem component

The ECOGEM component represents the marine plankton community and associated interactions within the ecosystem [Ward et al., 2018]. The state variables are not subject to physical transport, there are only local sources and sinks. Biological uptake is limited by light, temperature and nutrient availability replacing the BIOGEM formulation and ECOGEM also considers iron-light co-limitation. The ecosystem community is composed of different plankton populations, so-called plankton functional types (PFTs). They are described

by their size, their taxonomic position and thus by a set of specific and size-dependent traits. We consider different degrees of ecosystem complexity where the community is divided into two classes of PFTs: phytoplankton and zooplankton. The number of phytoplankton or zooplankton is not fixed and can be subdivided into different size classes with size-dependent traits. The phytoplankton populations are characterized by nutrient uptake and photosynthesis traits whereas the zooplankton populations by predation traits. Moreover, all populations are subject to respiration, mortality and internal trophic interactions. Plankton mortality and grazing are the two sources of organic matter, with partitioning between non-sinking dissolved and sinking particulate organic matter. According to Ward et al. [2018] the partitioning of organic matter is a size-based sigmoidal function following Eq.3.1:

$$\beta = \beta_a - \frac{\beta_a - \beta_b}{1 + \beta_c/[ESD]} \tag{3.1}$$

where, β is the parameter of partitioning between dissolved and particulate organic mater, ESD is the equivalent spherical diameter used to calculate the plankton cell volume, β_a is the maximum fraction to DOM as ESD approaches zero, β_b is the minimum fraction to DOM as ESD approaches infinity and β_c is the size at which the partitioning is 50:50 between DOM and POM. Please note that for the simulations with different numbers of PFTs, the average ESD for the entire population is the same but β will still be different, because of the nonlinear equation.

Coupling between BIOGEM and ECOGEM

The calculation in BIOGEM is performed 48 times per model year while the calculation in ECOGEM takes 20 time-steps for each BIOGEM time-step [Ward et al., 2018]. At the beginning of each ECOGEM time-step, the concentration of inorganic matters and important properties of the physical environment are imported from BIOGEM. The marine biota through photosynthesis transforms the inorganic compounds into living biomass. The rate of change in living biomass is used only to update the living biomass concentrations in ECOGEM. At the end of each ECOGEM time-step, the rates of change in inorganic and dead organic matter are passed back to BIOGEM and are used to update DIC, DOM, PO_4, Fe, oxygen and alkalinity. POM is instantly remineralised at depth using the standard export production functions.

Model modifications

Grid resolution

The horizontal grid (36 x 36) is constructed to be uniform in longitude and uniform in sine latitude, giving $\sim 3.2°$ latitudinal increments at the equator increasing to $19.2°$ in the highest latitude. This horizontal mesh has been widely used for very large ensembles [Marsh et al., 2004] and biogeochemical simulations [Cameron et al., 2005] with focus on the carbon cycle [Colbourn, 2011]. To better resolve the light absorption effect on ocean physics by biota, we use a higher vertical resolution than previous configurations with BIOGEM or EcoGENIE (e.g. Ward et al. [2018]). We consider 32 vertical layers that increase logarithmically from 29.38 m for the surface layer to 456.56 m for the deepest layer. All physical and biological parameters in the model are unchanged from the tuning of Ward et al. [2018] with exceptions of β_a in Eq.3.1 (see below for an explanation) and the Atlantic-Pacific moisture (APM) flux correction parameter. We increase the APM flux correction parameter from 0.8 Sv to 1.53 Sv in order to simulate a realistic Atlantic meridional overturning circulation

(AMOC) of 14.2 Sv. This flux correction is required because the atmospheric component is too simple to transport moisture across the American continent, and this parameter adjusts the salt balance between the different ocean basins. We need to validate the ocean circulation of our newly configured model against observations. We firstly focus our attention on the AMOC because it is the main driver of the worldwide oceanic circulation.

The increase in vertical resolution improves the representation of the AMOC (Figure 3.2). The AMOC is closer to observations (based on WOCE, Lumpkin and Speer [2007]) and model results of Atmosphere-Ocean General Circulation Models (AOGCMs) with a higher spatial resolution (e.g. Boulton et al. [2014]). In our new model setup the clockwise overturning cell in the upper ocean is more condensed and thus more realistic (Figure 3.2b, 3.2c). In addition, the model now reproduces a deeper counterclockwise overturning cell which was absent in the coarse resolution setup (Figure 3.2a). A change in AMOC and thus ocean circulation affects also the distribution and magnitude of the biogeochemical quantities. While in some regions, such as the subtropical ocean, the model representation is improved, there are other regions, e.g. the Arctic Ocean with less agreement between the model and observations. Overall, the biogeochemical fields are different between the model runs with a coarse and a finer vertical resolution. Note that we are mainly interested in resolving the effects of light absorption and the relative differences between our selected experiments (see below); therefore the absolute values are less relevant. The comparison of the biogeochemical quantities between the coarse, the finer vertical resolution, and observations are presented in the Appendix (Appendix 3.1 - 3.4).
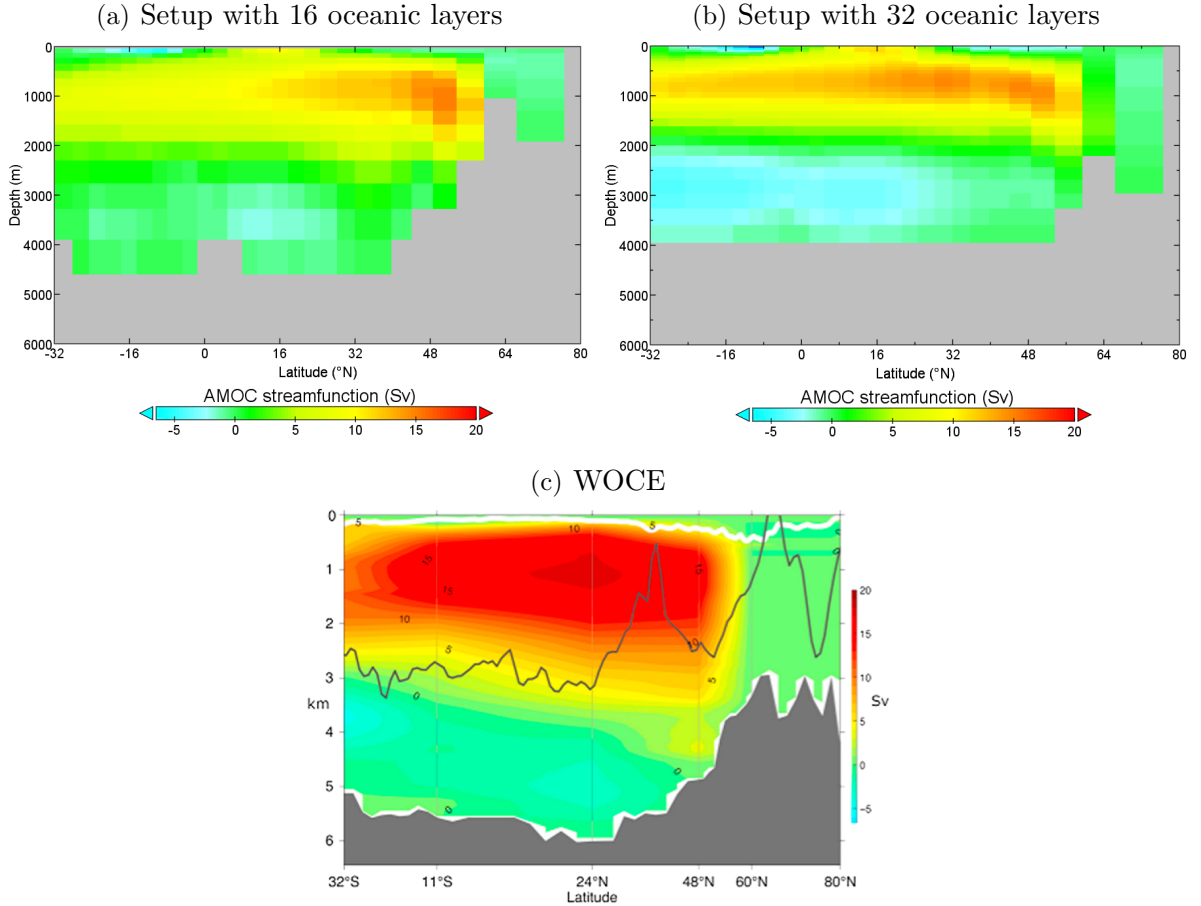
Figure 3.2: Modeled and observed AMOC streamfunction (Sv). Positive values represent clockwise overturning and negative values represent counter-clockwise overturning. Simulated AMOC for 1P1Z with: (a) the model configuration with 16 oceanic layers and (b) model configuration with 32 oceanic layers. (c) Mean AMOC estimated from hydrographic sections from the World Ocean Circulation Experiment (WOCE) [Lumpkin and Speer, 2007]. The grey line indicates the crest of the Mid-Atlantic Ridge and the white line represents the climatological mixed layer depth (Figure from Buckley and Marshall [2016]).

Light absorption in the ocean

The incoming short-wave radiation is taken from the climate component of the model and varies seasonally [Edwards and Marsh, 2005; Marsh et al., 2011]. The model takes into account the inhibition of light penetration due to the presence of organic and inorganic particles as well as dissolved molecules. The vertical light attenuation is described by the scheme Eq.3.2:

$$I(z) = I_0 \cdot \exp[(-k_w - k_{Chl} \cdot Chl_{tot}) \cdot z] \tag{3.2}$$

where $I(z)$ is the radiation at depth z, I_0 is the radiation at the surface of the ocean, k_w is the light absorption by water (0.04 m^{-1}), k_{Chl} is the light absorption by chlorophyll (0.03 m^{-1}(mg Chl)$^{-1}$) and Chl_{tot} is the total chlorophyll concentration. The values for k_w and k_{Chl} are adopted from Ward et al. [2018]. In our model, I_0 is always negative because it is a downward flux from the sun to the surface of the ocean. Solar radiation decreases exponentially with depth through attenuation; maximum absorption occurs in the upper ocean

layer and the minimum absorption takes place in the lowest ocean layer. In the standard model [Ward et al., 2018], all of this solar energy is absorbed in the surface layer while we allow light to penetrate until the sixth oceanic layer (221.84 m deep).

Phytoplankton changes the optical properties of the ocean [Sonntag and Hense, 2011] through phytoplankton light absorption. The absorption process can cause a radiative heating and change in ocean temperature. We implemented the warming of water by light absorption of phytoplankton into the model following, e.g. Hense [2007] and Patara et al. [2012] Eq.3.3:

$$\frac{\partial T}{\partial t} = \frac{1}{\rho \cdot c_p} \frac{\partial I}{\partial z} \tag{3.3}$$

$\partial T/\partial t$ denotes the temperature changes, c_p is the specific heat capacity of water, ρ is the ocean density, I is the solar radiation incident at the ocean surface, and z is the depth. We assume that the whole light absorption leads to heating of the water.

Model setup and experiments

We performed four different model experiments (Table 3.1) to study the impact of varying ecosystem complexity and phytoplankton light absorption on the climate. We performed a BIOGEM spin-up for 10,000 years to allow for a realistic nutrient distribution in the ocean. The spin-up is run with a constant atmospheric CO_2 concentration of 278 ppm. The experiments restart after this period for 1,000 years with ECOGEM, meaning that all experiments consider zooplankton and phytoplankton. Furthermore, in the simulations the atmospheric CO_2 is not fixed and can evolve freely over time. After 700 years of simulation, the model reaches a steady state but we analyze the outputs after model runs of 1,000 years. The model setup we used is very similar to the existing model setup used by Ward et al. [2018] to describe ECOGEM, but with five differences between the model setups:

First we use a different grid than Ward et al. [2018]. They used the "worlg4" topography, while we use the topography "ra32lv". In "worlg4" the Torres strait between Australia and Papua New Guinea is open, permitting an oceanic connection between the Pacific and Indian ocean, while in "ra32lv" the Torres strait is closed. The main difference between these two configurations, however, is the vertical resolution of the oceanic component. Indeed, in this study, the ocean has 32 layers with a surface layer of 29.38 m while Ward et al. [2018] have 16 oceanic layers with a surface layer of 80.84 m. For a comparison of the biogeochemical quantities between both configurations the reader is referred to the Appendix (Appendix 3.1 - 3.4).

Second, Ward et al. [2018] used 17 oceanic tracers while we only use 14 oceanic tracers relevant for the climate; we remove SO_4, H_2S, Mg and the atmospheric tracer pH_2S.

Third, we modify the ecosystem community to conduct our simulations. Our ecosystem community is based on the community used by Ward et al. [2018] to describe the ECOGEM model (Appendix 3.5). We run ECOGEM with different complexity of one and six phytoplankton and zooplankton species depending on the specific experiment. We additionally account for the phytoplankton light absorption for our selected simulations.

Fourth, we modify the vertical light attenuation scheme and apply Eq.3.2 and Eq.3.3 for all the experiments. With this change, the absorption of the solar radiation can occur in all the layers of the ocean and not only in the uppermost layer as in the standard setup used by Ward et al. [2018]. But for the experiments without phytoplankton light absorption $k_{Chl} = 0$ m^{-1}(mg Chl)$^{-1}$, so the light is attenuated only by k_w (see Eq.3.2).

Fifth and last, Ward et al. [2018] allow primary production only in their surface layer,

from the surface to 80.84 m deep while we allow primary production until the sixth oceanic layer, from the surface to 221.84 m deep.

Table 3.1: Name and description of the four simulations conducted

Experiment	Description
1P1Z	Simulation with 1 phyto- and 1 zooplankton species
1P1ZLA	Simulation with additional phytoplankton light absorption
6P6Z	Simulation with 6 phyto- and 6 zooplankton species
6P6ZLA	Simulation with additional phytoplankton light absorption

We assume a closed carbon cycle for all the model runs. Thus there is no input of carbon through volcanic fluxes or anthropogenic activities and only the relative size of the reservoirs (atmospheric CO_2, oceanic CO_2, POC, DIC...) can vary, not their total. We, therefore, allow that different climates can develop. Depending on the strength of the ecosystem response in the respective experiment more or less CO_2 might be emitted into the atmosphere leading to altered air temperature. Thus our setup allows changes in the atmospheric CO_2 concentrations and Earth's energy budget.

All experiments are forced with the same constant flux of dissolved iron into the ocean surface [Mahowald et al., 2006]. The incoming shortwave radiation varies seasonally but no trend is considered. The longwave radiation emitted by the surface of the planet is absorbed by the atmosphere and re-emitted upward and downward [Weaver et al., 2001]. The re-emission depends on the greenhouse gas concentrations in the atmosphere.

Comparable state of the experiments

In this study we are interested in the relative importance of the processes regarding phytoplankton light absorption and ecosystem complexity. Thus, a common basis is needed to compare our suite of experiments. In Earth system modeling this is often achieved by tuning the export production or the nutrients to obtain comparable model simulations. But since we are more interested in the climate impact, we make sure that the primary production (PP) is comparable.

We are aware that PP is much less constrained by observations than for example nutrients. However, first, we are more interested in the relative differences between the experiments and not in the absolute values. Second, adjusting the nutrients fields (e.g. DIC) would automatically adjust the carbon fluxes and will mask any change in carbon dynamics among the experiments.

For a robust comparison of the climate system between the different experiments, we adjusted the parameter β_a (see Eq.3.1) in the partitioning function to obtain the same values for primary production (Appendix 3.6). The parameter β_a is used to tune the model because it is not constrained by observation and has already been changed between different studies [Ward and Follows, 2016; Ward et al., 2018]. Primary production determines the two variables that drive the climate-relevant feedback mechanisms we are interested in. First, PP determines the amount of phytoplankton biomass, and this biomass affects phytoplankton light absorption and thus the sea and air surface temperature. Second, PP is directly and indirectly, the source of all different forms of organic biomass of which a part is sinking, leading to carbon export or carbon production and thus changes in atmospheric CO_2 concentrations and air temperature (Figure 3.3).
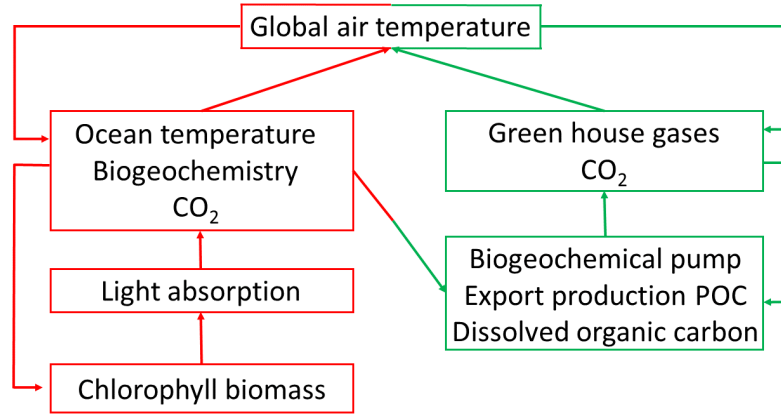
Figure 3.3: Schematic representation of the different links between the climate variables we analyze. The global atmospheric temperature is impacted by a biogeophysical mechanism (left, red color) and a biogeochemical mechanism (right, green color). Phytoplankton light absorption impacts directly SST, biogeochemical properties and atmospheric CO_2 concentration, leading indirectly to changes in chlorophyll biomass and global atmospheric temperature. Increasing ecosystem complexity affects directly the export production of particulate organic carbon (POC) and thus the biogeochemical pump. As a consequence, atmospheric CO_2 concentrations and therefore global atmospheric temperature can be altered.

After tuning the model, the values of our adjusted PP show only minor differences from an average value of 35.51±0.61 Gt/yr (Table 3.2). The standard deviation is only 0.61 Gt/yr. We consider this value small enough to compare the climate systems between the experiments.

Table 3.2: Global values of primary production (Gt/yr) for the four simulations.

Experiment	PP (Gt/yr)
1P1Z	35.97
1P1ZLA	35.39
6P6Z	34.46
6P6ZLA	36.22

Please note that we evaluate the total climate impact encompassing changes in the heat budget and in the carbon cycle due to the biogeophysical or biogeochemical feedbacks.

Biogeochemical properties

To compare the biogeochemical effects of phytoplankton light absorption and increasing ecosystem complexity on the climate system we look at changes in biogeochemical properties. We first present the changes in surface phytoplankton biomass due to phytoplankton light absorption. Second, we compare the changes in the downward flux of organic matter. Third, we look at changes in the atmospheric CO_2, which is allowed to evolve freely and is strongly determined by the environmental conditions at the air-sea interface (partial pressure of CO_2, sea surface temperature, the downward flux of organic matter and the air-sea flux of CO_2).

Surface phytoplankton biomass

We first compare phytoplankton concentration in chlorophyll units of the different simulations (Figures 3.4a and 3.4b) as this variable affects phytoplankton light absorption and thus heat distribution. Despite comparable primary production, the chlorophyll concentrations of the model runs with and without light absorption are different (*1P1ZLA* and *1P1Z*: Figure 3.4c, *6P6ZLA* and *6P6Z*: Appendix 3.7). The general patterns between the simulations with low and high ecosystem complexity are similar except in the equatorial region (Appendix 3.7) where chlorophyll is lower; globally chlorophyll concentration differences are slightly lower between the simulations *6P6ZLA-6P6Z* compared to *1P1ZLA-1P1Z*. Overall, the chlorophyll concentration is higher of 0.014 mgChl/m^3 in the model simulation *1P1ZLA* compared to *1P1Z*, similar to Manizza et al. [2005] but there are pronounced regional differences. The largest differences occur in the northern and southern polar regions where changes in sea-ice lead to a strong response in phytoplankton concentration. The presence or absence of sea-ice and thus light availability as well as the coarse resolution explain the rather sharp patterns of chlorophyll concentrations. In *1P1ZLA* the global averaged sea-ice thickness is reduced by ∼0.02 m and the sea-ice cover is diminished by 4.73% due to higher sea surface temperature (Figure 3.8c). As a consequence, light availability increases, stimulating the growth of phytoplankton. Moreover, the upwelling and mid-latitude regions show higher chlorophyll concentration in the simulation with phytoplankton light absorption in contrast to subtropical gyres where almost no differences occur. These regional patterns of higher chlorophyll concentration are controlled by the vertical velocity and the distribution of the nutrients. For instance, the upward vertical velocity in the upwelling regions along the western African coast and the south-western American coast are enhanced by 0.11 m/yr and by 0.54 m/yr, respectively (Appendix 3.8). These local increases of vertical velocity bring more nutrients to the surface and reduce the phosphate limitation in these regions (Appendix 3.9). The reduced phosphate limitation in *1P1ZLA* permits an increase of phytoplankton growth and therefore higher phytoplankton biomass.
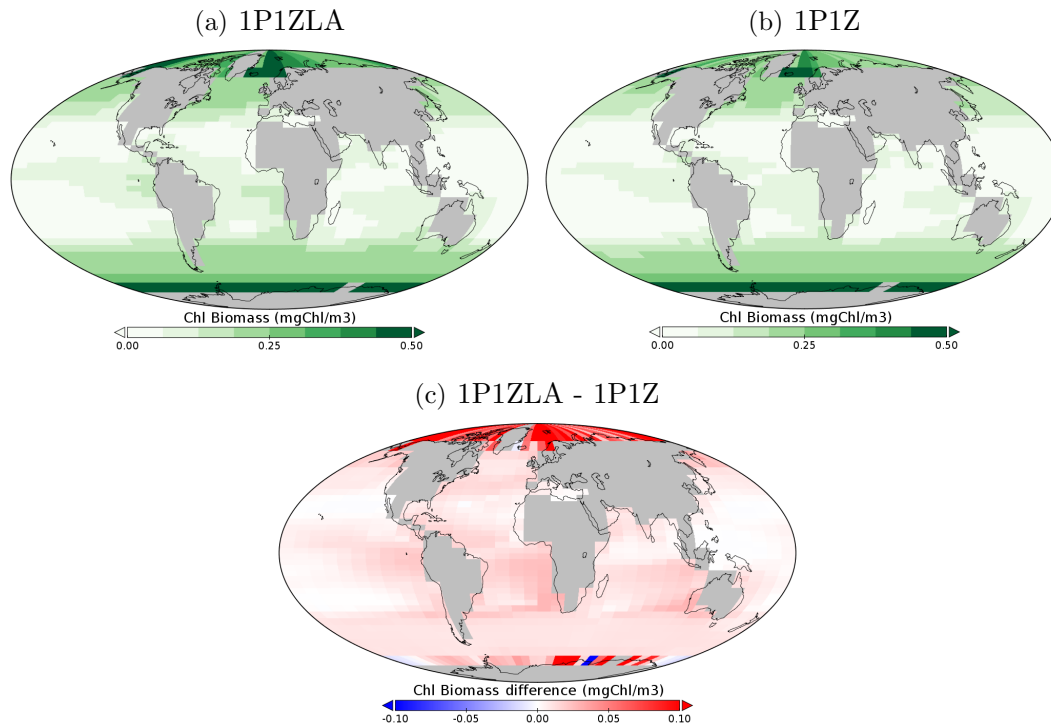
Figure 3.4: Chlorophyll biomass (mgChl/m^3) for the model runs (a) 1P1ZLA and (b) 1P1Z. (c) Chlorophyll biomass difference between the two simulations; blue colors indicate lower while red colors indicate higher chlorophyll concentrations in the model run with light absorption.

Downward flux of organic matter

Phytoplankton light absorption

To compare the downward flux of organic matter between our different simulations, we apply the approach by Toggweiler et al. [2003]. In their approach, the two water masses NADW and AABW are used as indicators for the nutrient "turnover" and thus the downward flux of organic matter. In models, this flux has upper and lower limits, constrained by the initial PO$_4$ concentrations in the deep water that is formed in the North Atlantic and Southern Ocean. The downward flux of organic matter can vary between these two limits via changes in deep water formation. The initial PO$_4$ concentration of the modeled AABW of 2.09 μmol/kg is slightly lower compared to average observed PO$_4$ concentrations in the deep water of 2.28 μmol/kg (World Ocean Atlas 2001; Conkright et al. [2002]) and we use the AABW as the lower limit. The initial PO$_4$ concentration of the modeled NADW of 1.78 μmol/kg is even lower and therefore the NADW represents the upper limit. Setting the "remineralization trajectories" for NADW and AABW (black diagonal lines) and plotting the DIC versus PO$_4$ concentrations of all grid point in the deep water (2,823 m) for the model runs *1P1ZLA* and *1P1Z* indicate the differences in depth of the downward flux of organic matter. Figure 3.5a shows that in *1P1ZLA* all points are significantly closer to the AABW remineralization trajectory, pointing towards a shallower downward flux of organic matter. On average, at 2,823 m depth, the PO$_4$ concentration decreases by 0.0318 μmol/kg, and the DIC concentration decreases by 11.75 μmol/kg in *1P1ZLA* compared to the reference simulation.

(a) Simulations 1P1ZLA and 1P1Z

(b) Simulations 6P6Z and 1P1Z
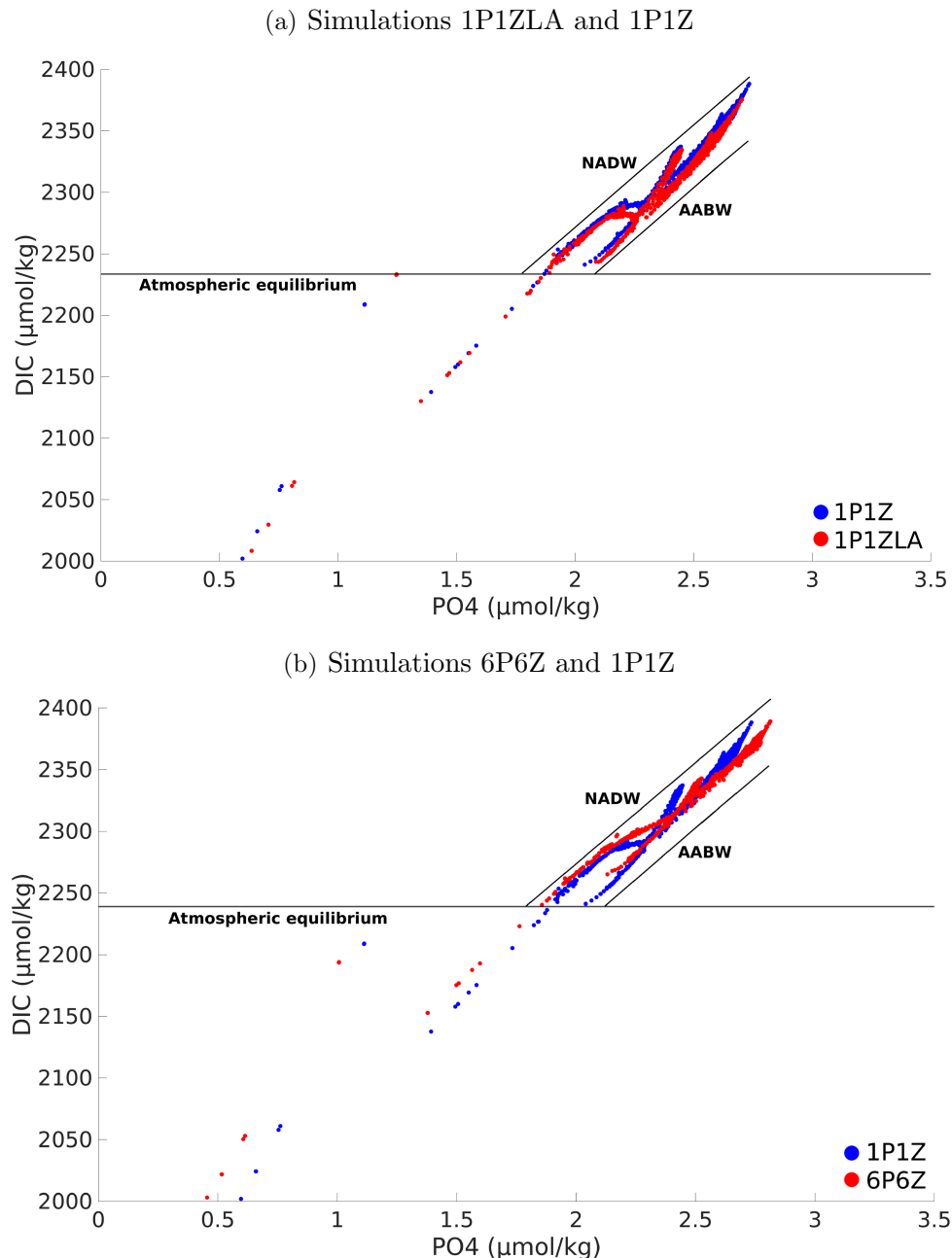
Figure 3.5: DIC vs PO$_4$ (μmol/kg) composition for all grid cells at the ocean depth level 26 (2,823 m depth) showing the influence of NADW and AABW on the composition of the deep water. The grey horizontal line gives the surface equilibrium of DIC for the simulations. The black diagonal lines show the phosphorus evolution of NADW and AABW. As such, they define the upper and lower limits of the downward flux of organic matter. The results shown here are exclusively for the oceanic depth level 26 (2,823 m depth) but same results can be shown from depth level 24 to 29. (a) Red points indicate the results for the simulation 1P1ZLA and blue points indicate results for the simulation *1P1Z*. (b) Red points indicate the results for the simulation 6P6Z and blue points indicate results for the simulation 1P1Z.

A closer look at the global DIC concentrations in the water column confirms a shallower downward flux of organic matter in the simulation with phytoplankton light absorption. The concentration of DIC is higher in the surface ocean and the DIC gradient between the surface and deep ocean is smaller in *1P1ZLA* compared to *1P1Z* (Table 3.3). While our parameter

changes (β_a) in Eq.3.1 calculating the partitioning between dissolved and particulate organic matter do not explain the differences in DIC (see Appendix 3.6), changes in the dynamics associated with phytoplankton light absorption are responsible for the higher DIC concentration at the surface. As a result of positive feedback, the atmospheric and oceanic CO_2 concentrations increase in *1P1ZLA* (see below). Additional effects contribute to the higher DIC concentration in *1P1ZLA*. The upward vertical velocity, specifically in the upwelling regions is enhanced which reduces the penetration depth of sinking material and "traps" organic matter closer to the surface. This process strengthens the "short" near-surface loop of carbon cycling ("microbial loop"). The deeper carbon cycling is weaker and less carbon is stored in the nonliving carbon pools and more in the living organic carbon pools. Not only phytoplankton but also zooplankton biomass is higher in the surface ocean; the latter is increased by ∼4%. Interestingly, higher zooplankton biomass does not result in higher (deeper) export production of fecal pellets which would lead to higher DIC concentrations in the deep ocean. Instead, zooplankton respiration is higher and together with the overall increase in atmospheric CO_2 concentrations, this leads to higher DIC concentrations in the surface ocean. In our steady state system with a closed carbon cycle, carbon that is higher in one pool is lower in another pool. Accounting for light absorption clearly accelerates carbon turnover.

Table 3.3: Concentration of DIC (mmol/kg) at the surface and benthic ocean. The third column represents surface-to-deep gradient of DIC.

Experiment	Surface DIC (mmol/kg)	Benthic DIC (mmol/kg)	ΔDIC (mmol/kg)
1P1Z	1.790	2.297	0.507
1P1ZLA	1.814	2.287	0.474
6P6Z	1.804	2.314	0.510

Increasing ecosystem complexity

Differences also occur in the distribution of the points between the model runs *1P1Z* and *6P6Z* on Figure 3.5b. For *6P6Z*, several points are closer to the NADW remineralization trajectory while others are closer to the AABW remineralization trajectory. We, therefore, calculate the average distance between all the points of *6P6Z* and the remineralization trajectories. The average distance between the AABW limit and the points is 0.1807 μmol/kg while the average distance between the NADW limit and the points is 0.1486 μmol/kg. Our results show that the points of *6P6Z* are slightly closer to the NADW remineralization trajectory, pointing towards a deeper downward flux of organic matter compared to *1P1Z*. Along with the higher export production of POC (see Table 3.4) and lower dissolved organic phosphorus (DOP, Appendix 3.10 and 3.11), the concentration of DIC increases by 0.0123 μmol/kg because all organic matter is eventually remineralized close to the seafloor (see also [Ward et al., 2018], [Ridgwell et al., 2007]). The higher export production of POC is due to the different number of plankton groups and the different surface-to-volume ratios between *1P1Z* and *6P6Z*. Although the average equivalent spherical diameter for the entire population is the same between both simulations, the fraction that goes into DOM is higher for smaller organisms and lower for larger organisms. Due to the nonlinearity of the system (see Eq.3.1), a higher proportion of organic matter ends up in POC in the model run *6P6Z* (Table 3.4). Again, our changes in the parameter β_a in Eq.3.1 that calculates the partitioning between dissolved and particulate organic matter do not explain the differences (see Appendix 3.6).

Table 3.4: Global export production of particulate organic carbon (Gt/yr) and dissolved organic carbon (μmolC/kg) after 1,000 years simulation. The values are vertically-integrated over the ocean. The third column is the partition of organic matter going into the dissolved phase.

Experiment	Export prod. POC (Gt/yr)	DOC (μmolC/kg)	Fraction to DOM (%)
1P1Z	4.02	1.05	63.3
1P1ZLA	3.97	1.02	63.2
6P6Z	4.50	0.98	62.6

Since the changes in ocean circulation are negligible in the simulations with different ecosystem complexity, we additionally compute the Apparent Oxygen Utilization (AOU) to further study the downward flux of organic matter on a global scale. AOU is a measure for biological activities of a water parcel since the last time it has been in contact with the atmosphere. It is computed as the oxygen saturation minus the oxygen concentration under the same temperature and salinity [Weiss, 1970]. The higher the AOU, the greater the amount of oxygen removed by heterotrophic biological processes (respiration and remineralization). Since there is no sediment layer in the model, all organic matter is eventually remineralized back to nutrients albeit at different depth levels depending on the organic matter form; DOM is remineralized in the upper ocean while POM is remineralized in the deeper ocean. We thus calculate the AOU in such a way that we take the difference between the oxygen saturation minus the oxygen concentration of the respective oceanic layer. At the surface, the AOU is similar between the simulations *1P1Z* and *6P6Z* but from 1,000 m depth the AOU distributions diverge (Figure 3.6). At depth, a higher ecosystem complexity increases the AOU, indicating a deeper downward flux and a greater amount of oxygen being removed by biological processes.
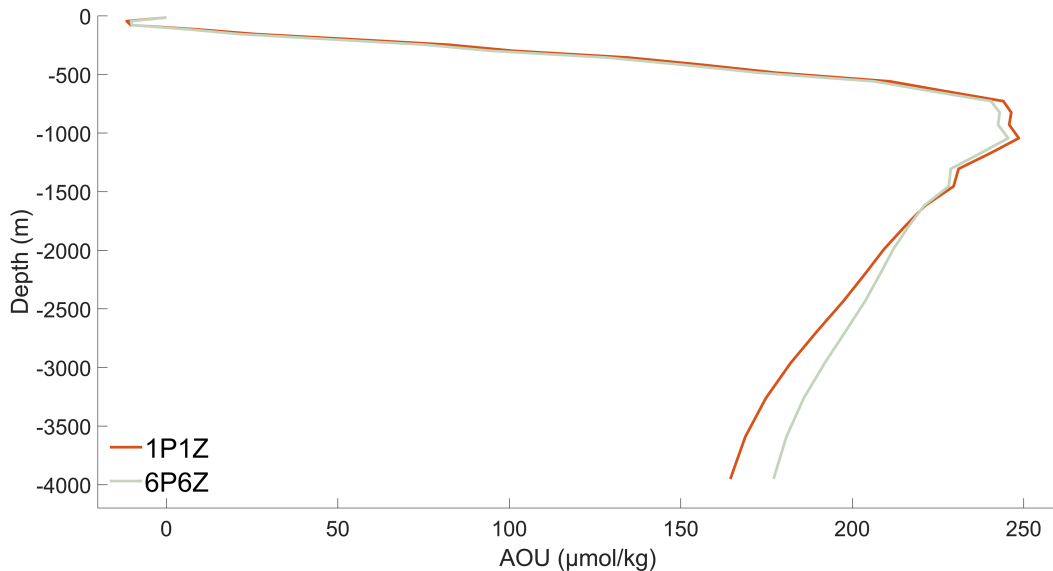
Figure 3.6: Vertical profile of AOU (μmol/kg) for the different simulations. The red curve represents the vertical profile of the simulation 1P1Z. The grey curve represents the vertical profile of the simulation 6P6Z.

Atmospheric CO_2 concentration

Atmospheric CO_2 concentration is significantly higher in *1P1ZLA* compared to *1P1Z* (Table 3.5). A closer look at the spin-up phase reveals the mechanisms behind. Phytoplankton light absorption immediately affects the stratification, increases SST, reduces the solubility of gases and therefore increases the air-sea CO_2 flux. To estimate the effect of the reduced CO_2 solubility on the air-sea CO_2 flux we used the values of *1P1Z* for our calculations. The CO_2 fluxes are a function of several factors including solubility, atmospheric CO_2, DIC and the proportion of sea ice cover. By adopting the values for these factors from *1P1Z* except for one, for which we take the value from *1P1ZLA*, we are able to separate the individual effects during the spin-up time. We find that by far the solubility has the largest effect on CO_2 fluxes and that the air-sea CO_2 flux increases from the beginning onwards with a roughly 10% increase already after 500 years. As a consequence, the atmospheric CO_2 concentration rises and thereby generates a positive feedback, leading to a global temperature rise (see below). The changes in solubility and hence CO_2 fluxes are the immediate response of light absorption that increases the stratification and SST; other second-order effects with changes in ocean physics arise during the course of the simulation. Yet, these changes such as a reduced sea-ice cover and enhanced upwelling only slightly modify the global CO_2 fluxes during the spin-up phase ($<1\%$ after 500 years). Finally, in steady state the difference in the atmospheric CO_2 concentrations between *1P1ZLA* and *1P1Z* is 18 ppm (Table 3.5), corresponding to 38 GtC. The largest contribution is due to the decreased CO_2 solubility but an altered biogeochemistry additionally contributes to changes in atmospheric CO_2 concentration. As shown above, the downward flux of organic matter is shallower with phytoplankton light absorption, affecting the carbon cycle. Together with a shallower remineralization and zooplankton respiration, the surface concentration of DIC increases (Table 3.3). Taking the difference of the vertically-integrated DIC between *1P1ZLA* and *1P1Z*, the DIC decreases by 35 GtC with phytoplankton light absorption. Compared to solubility changes, the changes in the downward flux of organic matter, however, may explain a smaller part of the climate system's response.

Table 3.5: Atmospheric CO_2 concentration (ppm) after 1,000 years-simulation for the four experiments with and without phytoplankton light absorption.

Experiment	Atm. CO_2 concentration (ppm)
1P1Z	165.87
1P1ZLA	183.75
6P6Z	165.43
6P6ZLA	173.69

In contrast, in the model runs with a higher ecosystem complexity changes in atmospheric concentrations are caused exclusively by biogeochemistry. Increasing the ecosystem complexity leads to a deeper downward flux of organic matter. Since all organic matter is remineralized at depth, the concentration of DIC increases at depth as well (see Figure 3.5b; Table 3.3). However, the changes are rather small and so the atmospheric CO_2 concentration only slightly decreases with a higher ecosystem complexity, as also suggested by the preformed PO_4 nutrients analysis (Appendix 3.12). The small decrease in atmospheric CO_2 concentration drives the small heat loss in the heat budget when ecosystem complexity increases (Table 3.6).

Temperature effects

Phytoplankton light absorption

The higher atmospheric CO_2 concentration significantly affects the system's heat budget (Table 3.6). The global surface atmospheric temperature is higher by 0.45°C in the model runs with phytoplankton light absorption (Figure 3.7d). Along with a higher surface atmospheric temperature (SAT), the ocean temperature increases globally in the model runs with phytoplankton light absorption as well (Figure 3.8d). Thus, the well-known effects of phytoplankton light absorption on ocean stratification [e.g. Manizza et al., 2008; Sonntag and Hense, 2011] are not visible as such. Yet, within the first 100 years of our simulations, we indeed find in the simulation with phytoplankton light absorption that the upper surface ocean is warmer and the deeper part cooler (Appendix 3.13), because phytoplankton absorbs light and shades the water column below. During the course of the model simulation into steady state, however, the decrease in the temperature-dependent solubility of CO_2 and changes in biogeochemistry (see above) lead to a rise of atmospheric CO_2 concentration in *1P1ZLA*. In steady state, we see the greenhouse effect with more longwave radiation being trapped in the atmosphere (Appendix 3.14). The higher greenhouse gas concentration alters the overall heat budget of the climate system leading to global warming of the atmosphere and ocean.

The maximum difference of SAT between *1P1ZLA-1P1Z* is 1.08°C in the Southern Ocean (Figure 3.7d). This value is slightly higher compared to previous model studies that show maximum values between 0.5-1°K in model runs with phytoplankton light absorption compared to those without [Shell et al., 2003; Patara et al., 2012]. However, in contrast to our model setup, Shell et al. [2003] use an ocean general circulation model with an uncoupled atmospheric model, thereby neglecting any interaction between the atmosphere and the ocean. Patara et al. [2012] use a coupled ocean-atmosphere general circulation model with a constant and prescribed atmospheric CO_2 concentration for their simulations. We argue that this strong response in SAT in our results is due to our experimental setup. We use a fully two-way coupled ocean-atmosphere model and assume a closed carbon cycle in which CO_2 is allowed to evolve freely.
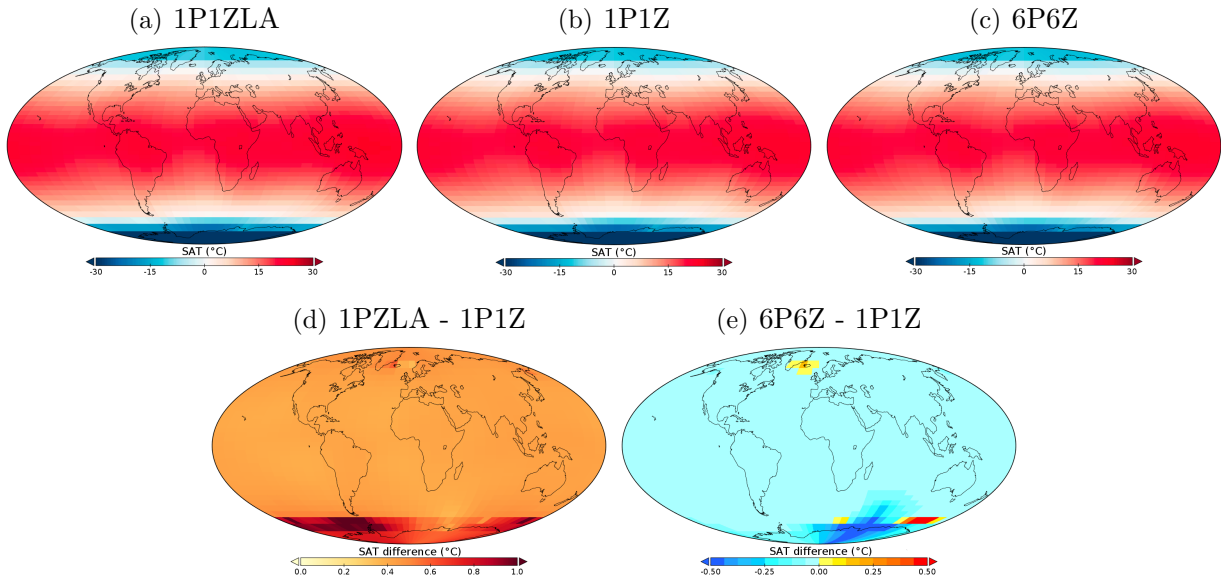
Figure 3.7: Surface air temperature (°C) for the model runs (a) 1P1ZLA, (b) 1P1Z and (c) 6P6Z. Surface air temperature difference for the biogeophysical scenario: (d) Difference between 1P1ZLA and 1P1Z. Dark/brown colors indicate large while white/yellow colors represent small differences. Note that the differences between these two simulations are always positive. Surface air temperature difference for the biogeochemical scenario: (e) Difference between 6P6Z and 1P1Z. Blue colors indicate a higher surface air temperature for the model run 1P1Z while red/yellow colors indicate a higher surface air temperature for the model run 6P6Z.

The general pattern of differences in SST between *1P1ZLA-1P1Z* is similar to SAT (Figure 3.7d and 3.8c) and we also find the same features in *6P6ZLA-6P6Z* although the magnitude is lower in the latter (Appendix 3.15 and 3.16). Here the SST is strictly speaking not SST but the mean temperature in the upper surface layer, from the surface to 29.38 m depth, which for practical purposes is called SST. The global average heating of the ocean surface is 0.33°C between *1P1ZLA* and *1P1Z*, which is in accordance with previous modeling studies [Manizza et al., 2005; Wetzel et al., 2006; Lengaigne et al., 2009; Patara et al., 2012]. We find a higher SST even in the regions where differences in chlorophyll are small (Figure 3.4). This missing spatial coincidence between the chlorophyll and SST patterns can be explained by the model setup. Chlorophyll biomass is not subject to physical transport but heat is transported by ocean currents, explaining why the patterns of the physical quantities are more smooth. Regional differences in SST are hardly visible. Both polar regions are characterized by a minor increase in SST because the sea-ice dynamics limit the redistribution of heat. The maximum local increase in SST is 0.47°C and is close to reported values in previous modeling studies [Wetzel et al., 2006; Lengaigne et al., 2007; Patara et al., 2012]. On the other hand, observations show a local heating effect of 1.5-4°C caused by the absorption of light by phytoplankton surface blooms [Sathyendranath et al., 1991; Kahru et al., 1993]; thus our model underestimates the local heating effect due to phytoplankton light absorption.
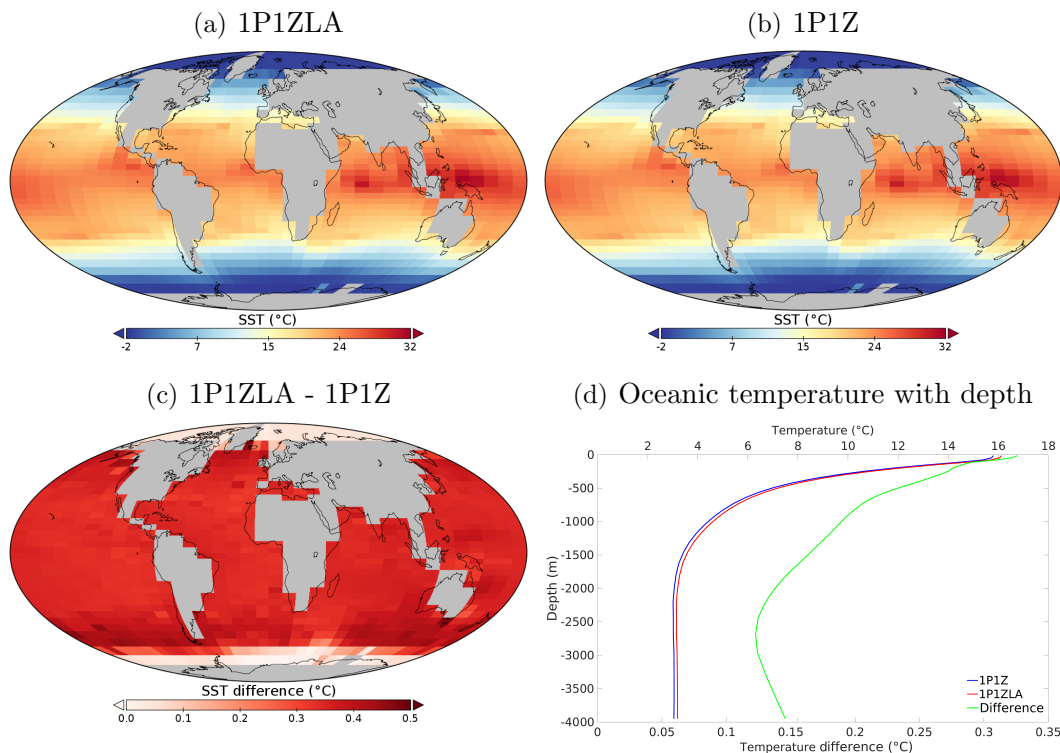
Figure 3.8: Sea surface temperature (°C) for the simulations (a) 1P1ZLA and (b) 1P1Z. Blue colors indicate low while red colors represent high ocean temperatures. (c) Differences of SST between the two simulations. White color indicates small and orange/brown colors represent large differences. Note that the differences between the model simulations are always positives. (d) Variation of the oceanic temperature with depth. The red line corresponds to the model run with phytoplankton light absorption. The blue line represents the model run without. The green line represents the difference between the model simulation with and without phytoplankton light absorption.

Increasing ecosystem complexity

An increase in ecosystem complexity (*6P6Z-1P1Z*) results in a global SAT decrease by 0.034°C (Figure 3.7e). This slight change is driven by the small decrease in atmospheric CO_2 concentration. The changes in SAT are less pronounced than the changes in SAT in the simulation with phytoplankton light absorption. The Southern Ocean is characterized by the largest SAT fluctuations with a local cooling of 1.64°C when ecosystem complexity increases (Figure 3.7e). The other world regions show a less pronounced cooling effect with a higher ecosystem complexity. Only a few grid cells in the Southern Ocean and in the North Atlantic show an increase in SAT. The global and regional changes in SST between *6P6Z-1P1Z* follow the SAT patterns but are almost negligible (Appendix 3.17).

Summary and conclusions

To study the relative importance of biogeophysical and biogeochemical climate-relevant mechanisms, we implemented phytoplankton light absorption in the EcoGENIE model [Ward et al., 2018] and varied the complexity of the ecosystem by increasing the number of phytoplankton and zooplankton groups. In our simulations the atmospheric CO_2 can evolve freely,

affecting therefore, the global heat budget. To obtain comparable primary productivity in all model runs, it was necessary to adjust the partitioning between the labile and refractory organic matter. We show that the climate system responds differently to our modifications in adding phytoplankton light absorption or increasing ecosystem complexity (Table 3.6).

Table 3.6: Summary of the impact of phytoplankton light absorption and increasing ecosystem complexity on the different climate variables described previously. The values represent the average differences between the biogeophysical and biogeochemical scenarios.

	Increasing ecosystem complexity (6P6Z-1P1Z)	Phytoplankton light absorption (1P1ZLA-1P1Z)
Biomass (mgChl/m^3)	-0.004	0.014
SST (°C)	-0.014	0.33
Atm. CO_2 (ppm)	-0.44	18
SAT (°C)	-0.034	0.45

A higher ecosystem complexity affects the plankton community, influencing the partitioning of organic matter going into the dissolved and particulate phase. Changes in the surface-to-volume ratio reduce the part of organic matter going into the dissolved phase and increase the part going into the particulate phase. As a result, the export production of POC increases while DOC decreases in *6P6Z*. The deeper downward flux of organic matter slightly affects the carbon cycle and with it the air-sea CO_2 flux. Hence, the atmospheric CO_2 concentration slightly decreases and the atmosphere cools down by 0.034°C when the ecosystem complexity increases. These small changes in atmospheric temperature and carbon cycle slightly reduce the sea surface temperature and slightly decrease the chlorophyll biomass.

Phytoplankton light absorption affects the climate system in various ways. Most notably, we find enhanced stratification, a higher SST and a reduced solubility of CO_2 that increases the air-sea CO_2 flux during the spin-up phase leading to higher atmospheric CO_2 concentration in steady state. In addition, the downward carbon flux is shallower with a stronger "microbial loop", contributing to higher atmospheric CO_2 concentration. Reduced sea-ice cover and enhanced upwelling only slightly affect the climate system. The sensitivity analysis indicates that by far the changes in CO_2 solubility have the largest effect on the climate system. All these changes lead to an increase by 0.45°C of the surface atmospheric temperature with phytoplankton light absorption.

This study shows clearly that phytoplankton light absorption has a higher impact on the climate system than a higher ecosystem complexity. Therefore we conclude that Earth system models should include phytoplankton light absorption by default for climate change scenarios.

Appendices

Coarse (old) versus fine (new) vertical resolution

The changes in the vertical resolution affect also biogeochemical quantities. The distribution patterns of chlorophyll are different between the model runs with the coarse (hereafter called "16z") and increased (hereafter called "32z") vertical resolution. On a global scale, the chlorophyll biomass is overestimated in "16z" (by 0.10044 mg/m^3 compared to observations) and underestimated in "32z" (by 0.06572 mg/m^3 compared to observations). Compared to SeaWiFS observations [O'Reilly et al., 1998], the chlorophyll concentrations is closer to observations in "32z". In contrast, chlorophyll patterns in the Arctic Ocean seem to be more realistic in "16z". Since we are more interested in the relative differences in chlorophyll between a climate state with and without phytoplankton light absorption and more or less complex food webs, the absolute values are less important.

(a) 1P1ZLA - old configuration   (b) 1P1ZLA - new configuration

(c) SeaWiFS observations
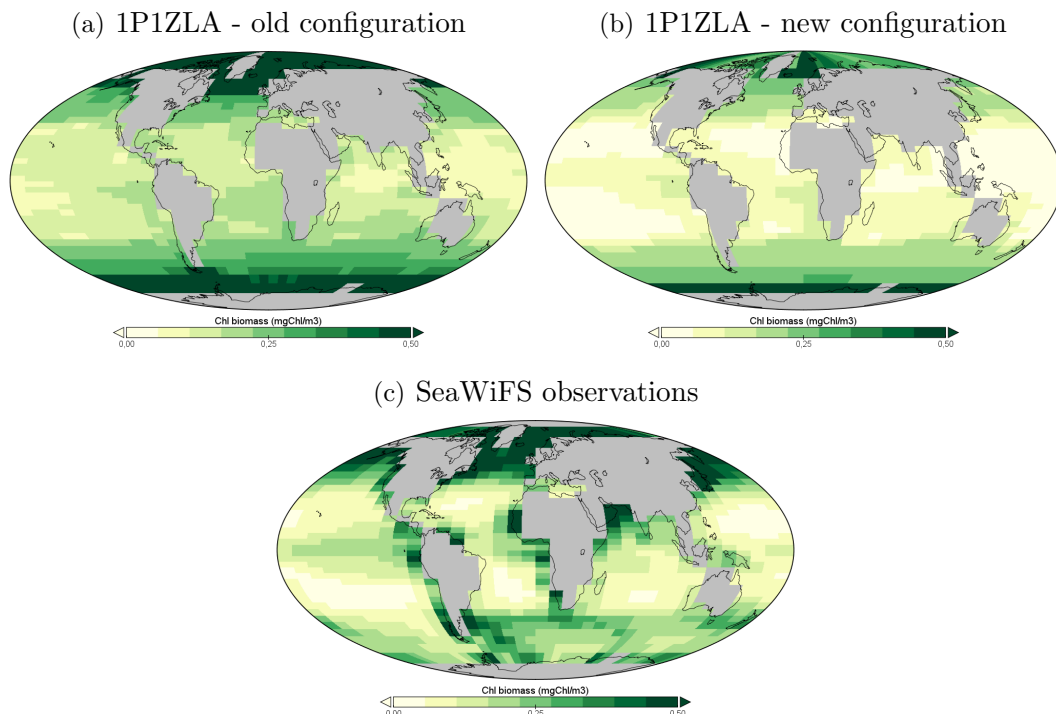
Appendix 3.1:   Chlorophyll biomass (mgChl/m^3) for the simulation 1P1ZLA (a) with the old configuration (b) with the new configuration. (c) Satellite-based chlorophyll observations from the Sea-Viewing Wide Field-of-View Sensor (SeaWIFS) [O'Reilly et al., 1998].

We also compared primary production between "16z" (the model run with the coarse resolution) and "32z" (the model run with increased vertical resolution). Primary production in "32z" is very similar to "16z" and comparable to reported values determined from observations.

Appendix 3.2: Simulated and observed primary production (Gt/yr).

Reference	Values (Gt/yr)
Falkowski et al. [1998]	45-50
Yool et al. [2013]	46.3-60.4
"16z" configuration	37.17
"32z" configuration	35.51

To compare the export production of POC with observations, we use the results of the model runs *1P1Z* between "32z" and "16z". In "32z" the export production is significantly reduced due to reduced nutrients concentrations, such as phosphate (Appendix 3.4) and a reduced surface chlorophyll biomass (Appendix 3.1). Nevertheless, the export production is in the range of estimated values based on observations. Again, the relative differences in export production between the different model experiments are more relevant in our study than the absolute values.

Appendix 3.3: Simulated and observed export production of particulate organic carbon (Gt/yr).

Reference	Values (Gt/yr)
Oschlies [2001]	3-16
Eppley [1972]; Behrenfeld and Falkowski [1997]	10.2-12.3
Louanchi and Najjar [2000] (WOA1998)	5.3
"16z" configuration	10.77
"32z" configuration	4.02

The high export production in "16z" explains the very high nutrient concentrations which eventually in turn result to increase export of organic matter. Appendix 3.4 shows the vertical profile of globally averaged phosphate concentrations. Compared to WOA2009 [Garcia et al., 2010], the magnitude in the concentrations is much better in "32z" compared to "16z". Only the surface concentrations are slightly too low and too high below 2500m compared to observations. The differences of the PO_4 vertical-profiles between the coarse (16 vertical oceanic layers) and fine (32 vertical oceanic layers) model configuration are the result of the partitioning between the labile and refractory DOP. Since we strive for the same primary productivity between the coarse and high-resolution model runs, the refractory part of DOP is larger in the model run with a higher resolution. In contrast, in the model run with the lower resolution more phosphorus is transferred into the labile DOP pool, where it is rapidly remineralized, increasing the PO_4 concentrations.
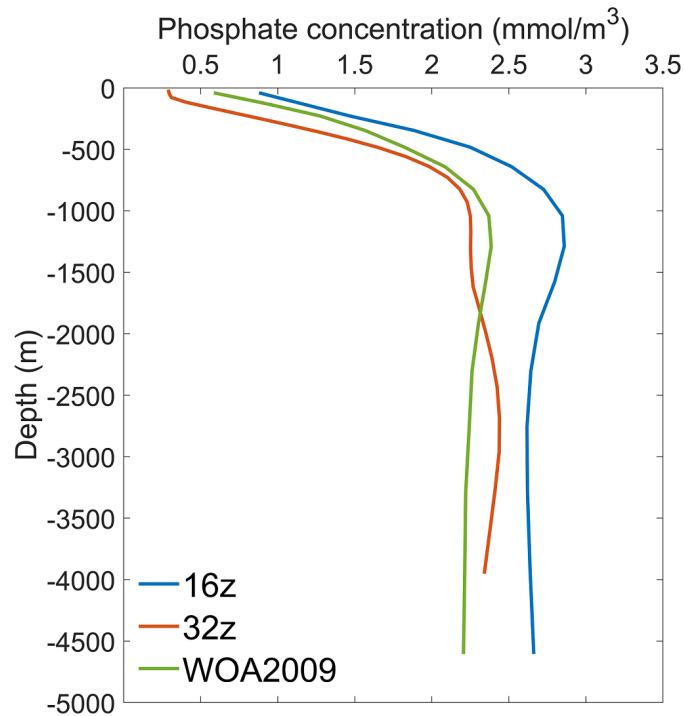
Appendix 3.4: Vertical profiles of observed and simulated phosphate concentrations (mmol/m^3). The red curve represents the model configuration with 32 oceanic layers. This curve is shorter than the other ones because the bathymetry is shallower in "32z". The blue curve represents the model configuration with 16 oceanic layers. The simulated phosphate concentrations are taken from the simulation 1P1ZLA. The green curve represents the WOA2009 observations [Garcia et al., 2010].

Plankton functional types

We use as the basis the model setup by Ward et al. [2018]. However instead of 8 phyto- and 8 zooplankton we take 6 phyto- and 6 zooplankton groups into account as it turned out that the smallest and biggest zooplankton groups and the two biggest phytoplankton groups have negligible biomass ($< 10^{-4}$ mmolC/m^3 on average). To be consistent in the model runs with low and high ecosystem complexity, we take the average of the pooled size classes for the model runs *1P1Z* and *1P1ZLA*.

Appendix 3.5: Size of the different phytoplankton and zooplankton species (μm) used during the experiments.

	1P1Z/1P1ZLA	6P6Z/6P6ZLA
Phytoplankton	46.25	0.60
Phytoplankton		1.90
Phytoplankton		6.0
Phytoplankton		19.0
Phytoplankton		60.0
Phytoplankton		190.0
Zooplankton	146.15	1.90
Zooplankton		6.0
Zooplankton		19.0
Zooplankton		60.0
Zooplankton		190.0
Zooplankton		600.0

Tuning of the model

To tune the model and obtain comparable primary production, we adjust the maximum fraction to DOM when ESD approaches zero (β_a in Eq. 3.1). To make sure that the changes we see in the climate system are not due to changes in this parameter, we conduct a couple of sensitivity experiments. First, we run a new experiment named *1P1ZLAbeta* which is identical to *1P1ZLA* but uses β_a from the model run *1P1Z*. Second, we run an experiment named *6P6Zbeta* which is identical to *6P6Z* but considers the value β_a from *1P1Z*. The results show that even with identical β_a, the export production of POC between *1P1ZLAbeta* and *1P1Z* and between *6P6Zbeta* and *1P1Z* are different. These sensitivity experiments indicate that β_a indeed is not responsible for the changes in the carbon cycling in our experiments.

Appendix 3.6: β_a, the fraction to DOM (%) and export production of POC (Gt/yr) for the sensitivity analyses.

Simulation	β_a	Fraction to DOM (%)	Export prod. POC (Gt/yr)
1P1Z	0.95	63.3	4.02
1P1ZLA	0.86	63.2	3.97
6P6Z	0.62	62.6	4.50
6P6ZLA	0.51	62.5	4.44
1P1ZLAbeta	0.95	63.3	3.98
6P6Zbeta	0.95	62.8	4.49

Chlorophyll biomass

The patterns of the chlorophyll biomass differences between *1P1ZLA-1P1Z* and *6P6ZLA-6P6Z* show differences in the equatorial regions. For *6P6ZLA-6P6Z* the nutrient fields vary in the equatorial regions, driving these changes in chlorophyll biomass. Moreover, the differences are larger for *1P1ZLA-1P1Z* in the polar regions due to the sea-ice dynamics.
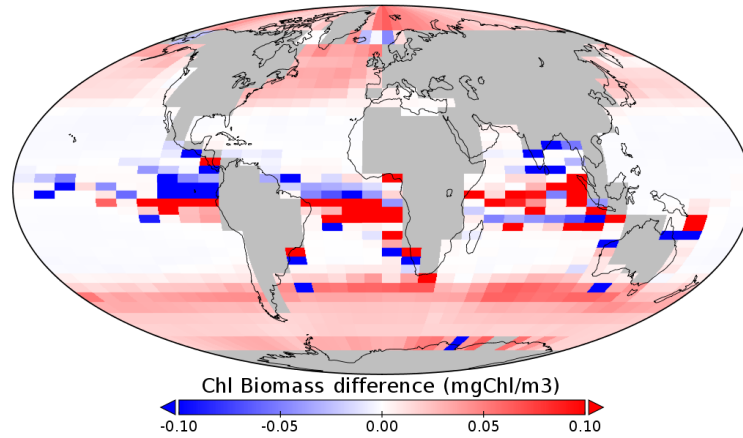
Appendix 3.7: Chlorophyll biomass difference (mgChl/m^3) between 6P6ZLA and 6P6Z. Blue color indicates a higher chlorophyll biomass in the simulations without phytoplankton light absorption while red color indicates a higher chlorophyll biomass in the simulations with phytoplankton light absorption.

Oceanic vertical velocity field

The oceanic vertical velocities between the simulations with and without phytoplankton light absorption are relatively similar. The upward vertical velocity is slightly higher in the upwelling regions along the African and South American coasts (Appendix 3.8). In these coastal regions, the upward velocity is enhanced by 0.11 m/yr and 0.54 m/yr, respectively.

(a) African upwelling region

(b) South American upwelling region
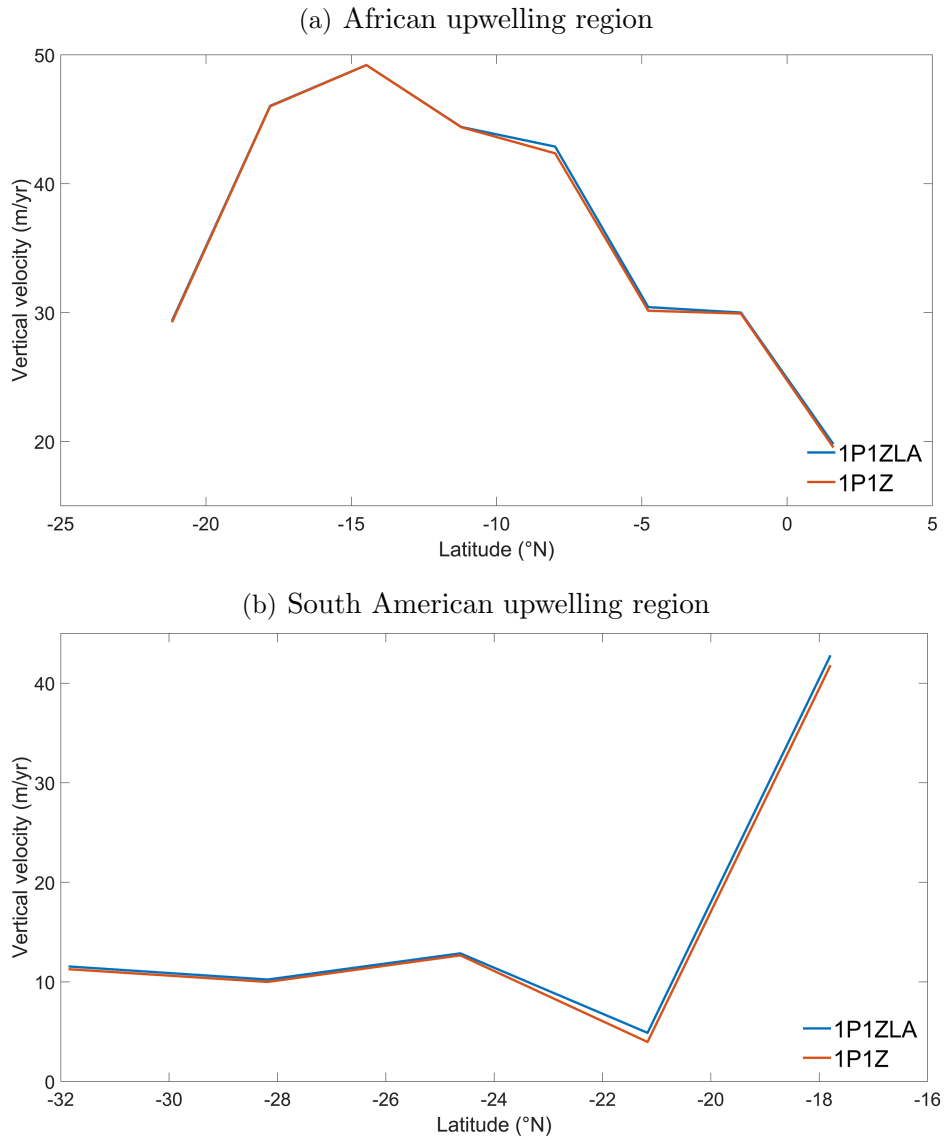
Appendix 3.8: Vertical velocity (m/yr) in the (a) African upwelling region and (b) South American upwelling region. Positive values indicate an upward vertical velocity. The blue curve represents the simulation 1P1ZLA while the red curve represents the simulation 1P1Z.

Phosphate limitation

For the simulation with phytoplankton light absorption, the phosphate limitation is lower all around the globe except in the subtropical gyres with negligible higher values. The regions with a lower phosphate limitation are characterized by higher surface phosphate concentrations and therefore enhanced phytoplankton growth and higher chlorophyll biomass. The maximum difference occurs along the Western African coast.
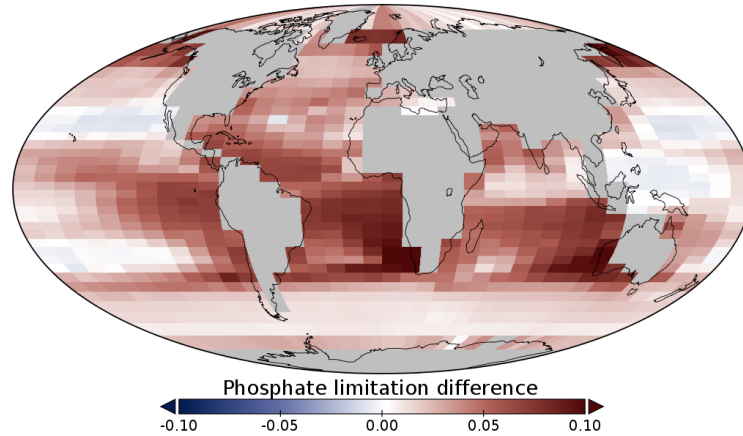
Appendix 3.9: Phosphate limitation difference between the simulations with and without phytoplankton light absorption. Blue color indicates a higher phosphate limitation in 1P1ZLA while red/brown colors indicate a lower phosphate limitation in 1P1ZLA.

Phosphate distribution

Phytoplankton light absorption slightly reduces the PO_4 inventory due to higher phytoplankton biomass and therefore a higher nutrient uptake. Increasing ecosystem complexity increases the vertically-integrated PO_4 concentration and can be explained by the deeper downward flux of organic matter. The vertically-integrated DOP decreases in *6P6Z* due to the plankton community, reducing the fraction of organic matter going into the dissolved pool.

Appendix 3.10: Vertically-integrated PO_4 and DOP concentrations (mol) for the four simulations

Simulation	PO_4 (mol)	DOP (mol)
1P1ZLA	$0.2917 \cdot 10^{16}$	$1.06 \cdot 10^{13}$
1P1Z	$0.2918 \cdot 10^{16}$	$1.04 \cdot 10^{13}$
6P6ZLA	$0.2968 \cdot 10^{16}$	$0.99 \cdot 10^{13}$
6P6Z	$0.2970 \cdot 10^{16}$	$0.98 \cdot 10^{13}$

The patterns of the vertical profiles of phosphate (PO_4) are similar but their magnitude differ. With a higher ecosystem complexity, the nutrients are lower in the surface and higher in the deep ocean. The former is the result of accounting for smaller phytoplankton with a higher surface to volume ratio enabling even the uptake at low nutrient concentrations. The higher nutrient concentrations in the deep ocean can be explained by a higher export production because of enhanced grazing and mortality.
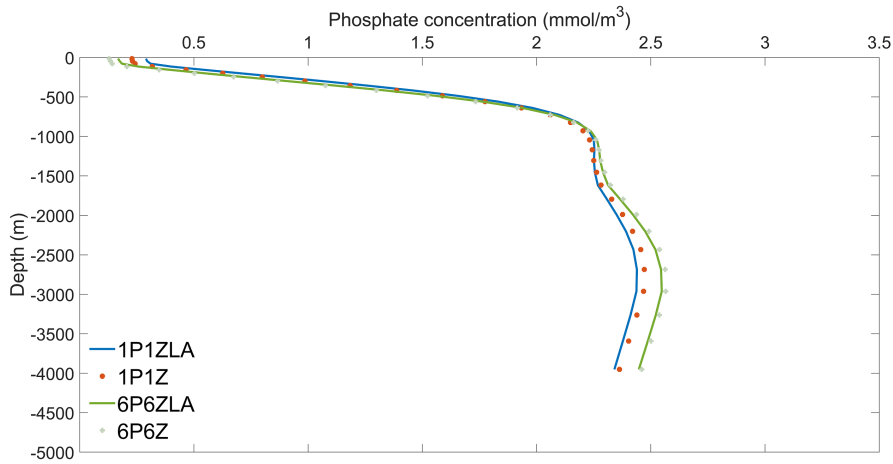
Appendix 3.11: Vertical phosphate profiles (mmol/m^3) along depth. The blue curve represents the vertical profile of the simulation 1P1ZLA. The red dots represent the vertical profile of the simulation 1P1Z. The green curve represents the vertical profile of the simulation 6P6ZLA. The grey dots represent the vertical profile of the simulation 6P6Z.

Preformed PO$_4$

Earlier studies showed that preformed nutrients positively correlate with atmospheric CO$_2$ concentration and can thus be used as an indicator of atmospheric CO$_2$ levels [Ito and Follows, 2005; Marinov et al., 2008]. Preformed nutrients refer to the nutrient concentrations of a water parcel since the last time it has been in contact with the atmosphere and are calculated from AOU. Following Duteil et al. [2012], we have calculated the preformed PO$_4$ for the different simulations. Specifically, we use the phosphate concentrations in the respective model layer minus the "regenerated" phosphorus that is determined by taking the AOU and assuming a phosphate to oxygen ratio of 1/138 [Ward et al., 2018]. As we have shown above, we find a deeper downward flux when we increase the ecosystem complexity. Thus preformed PO$_4$ concentrations in *6P6Z* are lower in the upper ∼500 m depth and higher below compared to *1P1Z* (Appendix 3.12); suggesting slightly reduced atmospheric CO$_2$ concentrations.
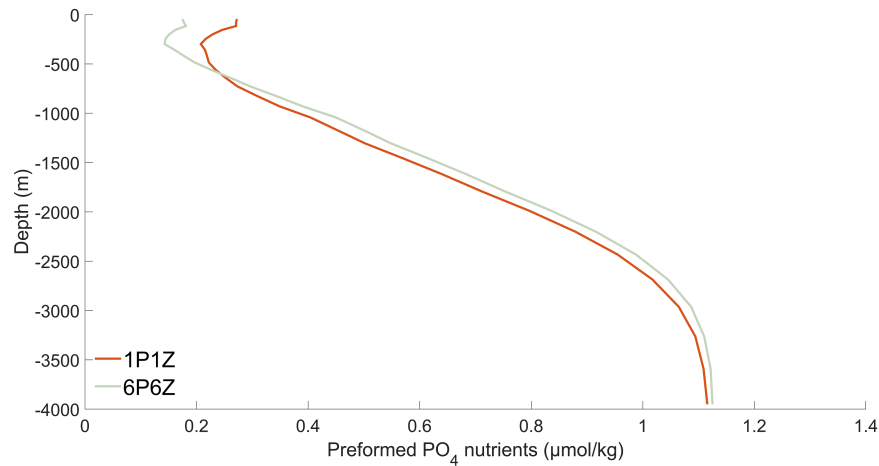
Appendix 3.12: Vertical distribution of the preformed PO_4 (μmol/kg) for the different simulations. The red curve represents the vertical profile of the simulation 1P1Z. The grey curve represents the vertical profile of the simulation 6P6Z. To smooth the profile, we applied a moving average function over a five-element sliding window for the entire water column.

Vertical oceanic temperature after 100 years

After only 100 years, in the deep part of the ocean, the temperature is lower in *1P1ZLA* compared to the reference simulation. This is due to the shading effect, where the heat is trapped in the surface of the ocean due to phytoplankton light absorption. This shading effect leads to a higher temperature in the upper and lower temperature in the deeper part of the ocean.
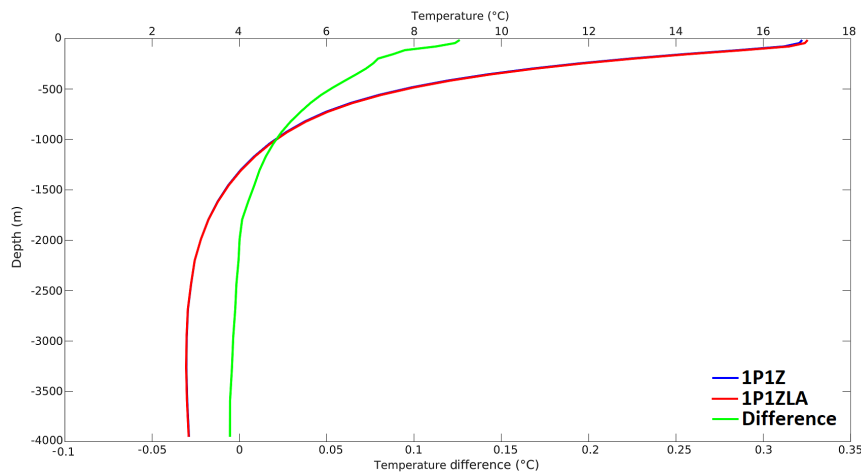
Appendix 3.13: Vertical oceanic temperature (°C) after only 100 years. The blue line represents the simulation without phytoplankton light absorption. The red line corresponds to the simulation with phytoplankton light absorption. The green line represents the difference between 1P1ZLA minus 1P1Z.

Heat fluxes in the atmosphere

The global heat fluxes in the atmosphere between *1P1ZLA* and *1P1Z* slightly differ. Most importantly, the longwave radiation in *1P1ZLA* is lower than in the reference simu-

lation because atmospheric CO_2 concentration is higher in *1P1ZLA*. As a consequence, the greenhouse gas effect increases, increasing the heat being trapped in the atmosphere and explaining the higher energy budget with phytoplankton light absorption.

Appendix 3.14: Global average of the different heat fluxes (W/m^2) in the atmosphere for the simulations with and without phytoplankton light absorption. The net longwave radiation flux is negative because this flux is leaving the atmosphere back to space.

Simulation	Net SW (W/m^2)	Net LW (W/m^2)	Sensible (W/m^2)	Latent (W/m^2)
1P1ZLA	115.34	-204.23	21.57	67.32
1P1Z	115.34	-204.44	21.34	67.76

Surface atmospheric temperature

The pattern of differences in SAT between the simulations *1P1ZLA-1P1Z* and *6P6ZLA-6P6Z* are nearly identical. Again the Southern Ocean is the most sensitive region. The maximum difference is 1.1°C between the model runs *1P1ZLA-1P1Z* while the maximum difference is 0.98°C between the model runs *6P6ZLA-6P6Z*. Everywhere else similar patterns with a lower magnitude of change for *6P6ZLA-6P6Z* occur. The average difference of SAT between *6P6ZLA-6P6Z* is 0.21°C.
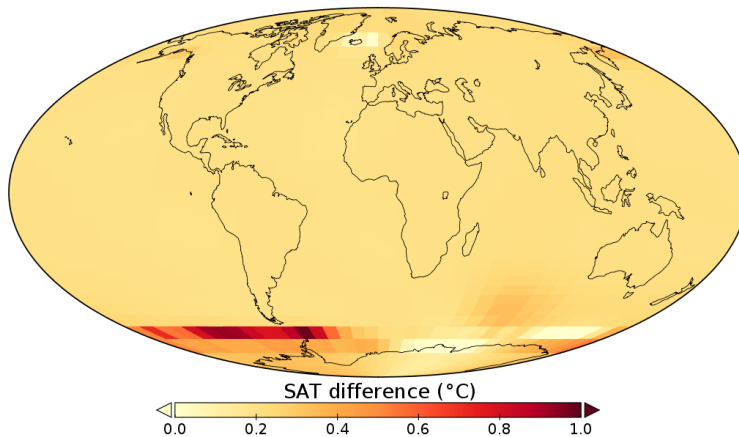
Appendix 3.15: Surface atmospheric temperature (°C) difference between 6P6ZLA and 6P6Z. White/yellow colors represent no or small differences while red/brown colors indicate a strong differences. Note the differences between the simulations are always positives.

Sea surface temperature

The pattern of differences in SST between the model runs *1P1ZLA-1P1Z* and *6P6ZLA-6P6Z* are almost identical. The averaged magnitude of changes is smaller in *6P6ZLA-6P6Z* (0.16°C) compared to *1P1ZLA-1P1Z* (0.33°C). Only local differences occur such as in the Southern Ocean.
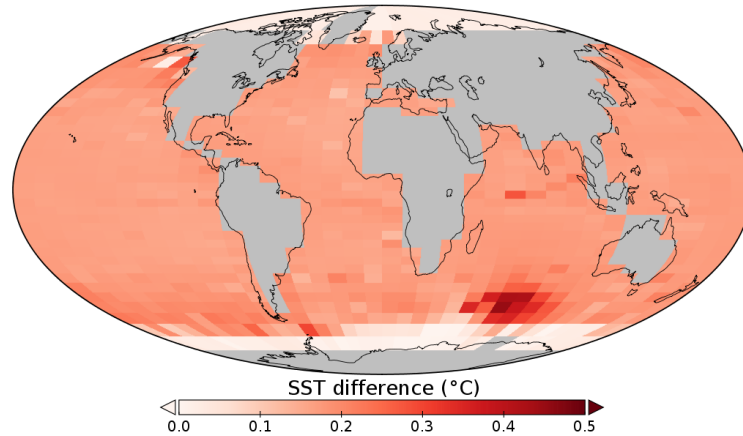
Appendix 3.16: Maps of sea surface temperature difference (°C) between 6P6ZLA and 6P6Z. The white color represents no or small differences while red/brown colors indicate large differences. Note that the differences between the simulations are always positives.

The regional patterns of difference in SST between *6P6Z-1P1Z* are similar to the regional patterns of difference in SAT. Only a few grids cells in the Southern Ocean and the North Atlantic show an increase in SST. The other world regions show a cooling effect when the ecosystem complexity increases.
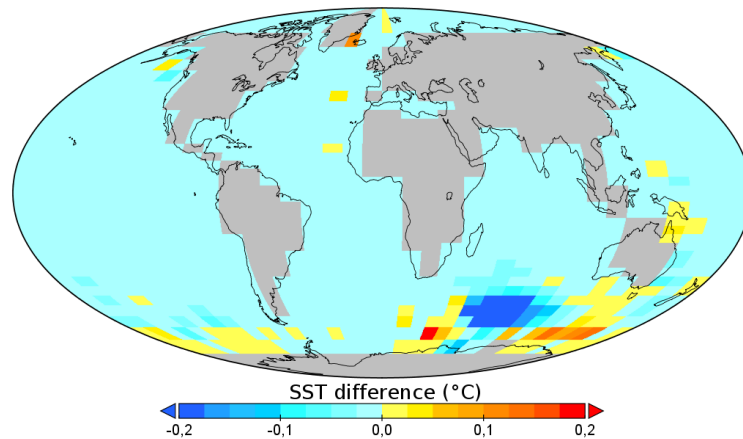
Appendix 3.17: Maps of sea surface temperature difference (°C) between 6P6Z and 1P1Z. Blue colors indicate a higher sea surface temperature for the model run 1P1Z while red/yellow colors indicate a higher sea surface temperature for the model run 6P6Z.

CLIMATE PATHWAYS BEHIND PHYTOPLANKTON-INDUCED ATMOSPHERIC WARMING

We investigate in which ways marine biologically-mediated heating increases the surface atmospheric temperature. While the effects of phytoplankton light absorption on the ocean have gained attention over the past years, the impact of this biogeophysical mechanism on the atmosphere is still unclear. Phytoplankton light absorption warms the surface of the ocean with consequences for the air-sea heat exchange and CO_2 flux. We focus on the ocean-atmosphere interface and study the importance of air-sea heat exchange versus air-sea CO_2 flux. To shed light on the role of phytoplankton light absorption on the surface atmospheric temperature, we performed different simulations with the EcoGENIE Earth system model. We configure the model without a seasonal cycle and, if not stated otherwise, the atmospheric CO_2 concentration is allowed to evolve freely. The climate pathways examined are: heat exchange, dissolved CO_2, solubility of CO_2, and sea-ice covered area. Overall we show that the air-sea CO_2 exchange has a larger effect on the biologically-induced atmospheric warming than the air-sea heat flux. Moreover, we notice that the freely evolving solubility of CO_2 has a cooling effect on the surface atmospheric temperature.

Introduction

Previous studies have shown that marine biota can modify the light penetration in the ocean with consequences on the atmospheric temperature and on the climate system [Shell et al., 2003; Wetzel et al., 2006; Gnanadesikan and Anderson, 2009]. Using an Earth system model (ESM) of intermediate complexity, we identify and compare the climate pathways behind the changes in atmospheric temperature due to phytoplankton light absorption.

Marine biota and phytoplankton play a major role in the absorption of light and therefore in the vertical distribution of heat in the upper layers of the ocean [Kowalczuk et al., 2019]. Indeed, observational evidence supports the hypothesis that chlorophyll increases the upper ocean heat uptake. For instance, satellite observations show that phytoplankton blooms can cause an increase of sea surface temperature (SST) of 1.5°C [Kahru et al., 1993]. Furthermore, previous remote sensing data indicate an increase in local SST of 4.5°C on a 4 day-timescale due to the presence of phytoplankton blooms [Capone et al., 1998]. Recent high-resolution in situ observations in the Indo-West Pacific Ocean indicate large anomalies of temperature of 0.95°C in the uppermost skin layer of the ocean when large phytoplankton blooms appear [Wurl et al., 2018]. However, all these observations are either on a short time scale or in a geographically limited area. To study the larger-scale impact of phytoplankton light absorption and its varying magnitude, Earth system models are employed.

Different models with different complexity are used to study the effect of phytoplankton light absorption. For instance, using ocean-only [Anderson et al., 2007] or general circulation models [Murtugudde et al., 2002; Lengaigne et al., 2007; Löptien et al., 2009], several studies focusing on the tropical Pacific Ocean report an increase of SST between 0.5-2°C. The same magnitude of ocean warming is reported with a general circulation model focusing on the Arctic Ocean [Lengaigne et al., 2009]. These changes in ocean temperature have an impact on the nutrient availability and the biogeochemical properties of the ocean [Manizza et al., 2008, and Chapter 3]. A warming of the surface of the ocean induced by marine biota also has consequences on the overall climate system. Patara et al. [2012] find that an increase of SST due to phytoplankton light absorption increases the atmospheric humidity content thereby increasing the greenhouse effect and the atmospheric temperature by up to 0.5°C. Furthermore, phytoplankton can amplify locally the seasonal cycle of the lowest atmospheric layer temperature by 1K [Shell et al., 2003]. Moreover, Shell et al. [2003] indicate that the climate effect of phytoplankton can even extend through the troposphere in mid-latitude regions, influencing the Walker and Hadley circulation.

It is therefore known that phytoplankton light absorption has a non-negligible role on the atmospheric temperature but which climate pathways are the most important behind this warming is still unclear. Phytoplankton light absorption affects the surface atmospheric temperature via two climate pathways. First, various modeling studies suggest that biologically-induced surface water heating can increase the air-sea heat exchange [Capone et al., 1998; Oschlies, 2004; Wetzel et al., 2006] with consequences on the formation of tropical storms and monsoons in the Arabian Sea [Sathyendranath et al., 1991]. Second, the solubility of gases and thus also the air-sea CO_2 exchange is affected by phytoplankton light absorption. For instance, Manizza et al. [2008] study the impact of this biogeophysical mechanism on the air-sea flux of CO_2 and find that phytoplankton light absorption has a small outgassing effect on a global scale with high regional fluctuations.

However, none of these studies have analyzed and compared the changes in air-sea heat and CO_2 exchange due to phytoplankton light absorption. To shed light on the biologically-induced atmospheric warming, we use a recent Earth system model of intermediate complexity [Claussen et al., 2002]. The model is called EcoGENIE [Ward et al., 2018] where we implemented phytoplankton light absorption in an earlier study (Chapter 3). We use the same model setup to determine now the importance of this biogeophysical mechanism on biologically-induced atmospheric warming. We conduct several simulations to determine the importance of the climate pathways behind the atmospheric warming. We consider two different biologically-induced changes: a change in air-sea heat and air-sea CO_2 exchange rates (Figure 4.1). The air-sea CO_2 exchange can be influenced by the dissolved CO_2 in the ocean in three different ways: through 1) the biological pump as a result of phytoplankton light absorption that affects the marine biogeochemical cycles [Manizza et al., 2008, and Chapter 3], 2) the solubility of CO_2 due fluctuations of SST and 3) sea-ice formation and resulting sea-ice extent altering the air-sea CO_2 flux.
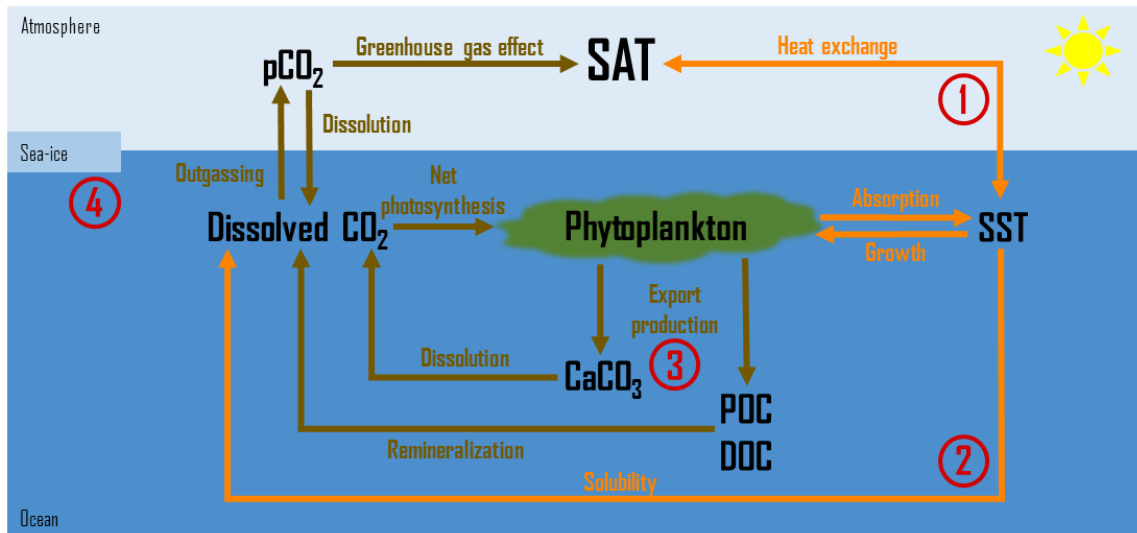
Figure 4.1: Representation of the four different biologically-induced pathways that affect the atmospheric temperature. (1) Marine biota via phytoplankton light absorption increases the SST, changing therefore the air-sea heat exchange and the atmospheric temperature. (2) Changes in SST also alter the solubility of CO_2 and its dissolved concentration. In turn, changes in dissolved CO_2 concentrations alter the air-sea CO_2 exchange and thus the greenhouse gas effect. (3) Phytoplankton light absorption modifies the marine biogeochemical cycles and particularly the export production of carbon. These changes in export production of carbon modify the dissolved CO_2 concentration and the greenhouse gas effect. (4) A warmer surface of the ocean can decrease the sea-ice extent. A reduction of sea-ice cover increases the air-sea CO_2 exchange area, changing the greenhouse gas concentrations. SAT = surface atmospheric temperature. SST = sea surface temperature. $CaCO_3$ = calcium carbonate. POC = particulate organic carbon. DOC = dissolved organic carbon.

The paper is organized as follow: In section 2, we describe the components of the model, the light absorption scheme and the air-sea exchanges. In section 3, we describe the simulations and the modeling strategy. In section 4, we report several sensitivity analyses of the climate system with EcoGENIE. In section 5, we present our results and detail the changes in both oceanic and atmospheric properties. In section 6, we conclude by commenting on the role of this biogeophysical mechanism in the atmospheric warming.

Model description

Our motivation is to study the interactions between the marine ecosystem, the biogeochemistry, the biogeophysics and the climate system. These interactions are computationally expensive in high-resolution models therefore we used an Earth system model of intermediate complexity [Claussen et al., 2002]. The Earth system model employed is the Grid-ENabled Integrated Earth system model (GENIE) [Lenton et al., 2007] composes of several modules describing the dynamics of the Earth system (Figure 4.2). This model has been previously calibrated and compared to observations several times [Edwards and Marsh, 2005; Lenton et al., 2006; Ridgwell et al., 2007; Marsh et al., 2011]. GENIE is widely used to study past climate and changes in the carbon cycle over geological times [Greene et al., 2019; Adloff et al., 2020]. Furthermore, GENIE has been used to demonstrate that the sensitivity of atmospheric CO_2 is mainly explained by the organic carbon pump [Cameron et al., 2005]. We use the carbon-centric version (cGENIE) that has been previously employed to study past mass extinction [Alvarez et al., 2019], the climate system [Ödalen et al., 2018] or biogeochemistry processes [Meyer et al., 2016]. GENIE is associated with the new ecosystem component (ECOGEM) to form the recent EcoGENIE model [Ward et al., 2018]. EcoGENIE has been used to determine the link between the marine plankton ecosystem and various past climate scenarios [Wilson et al., 2018] with a focus on phosphorus inventory [Reinhard et al., 2020b]. For our study, the model combines different components including ocean hydrodynamics, atmosphere, sea-ice, ocean biogeochemistry and marine ecosystem component. The efficient numerical terrestrial scheme [Williamson et al., 2006] is not used in this study, so the land surface is essentially passive. We use the same configuration as described in detail in Chapter 3 and thus only briefly explain the individual model components.
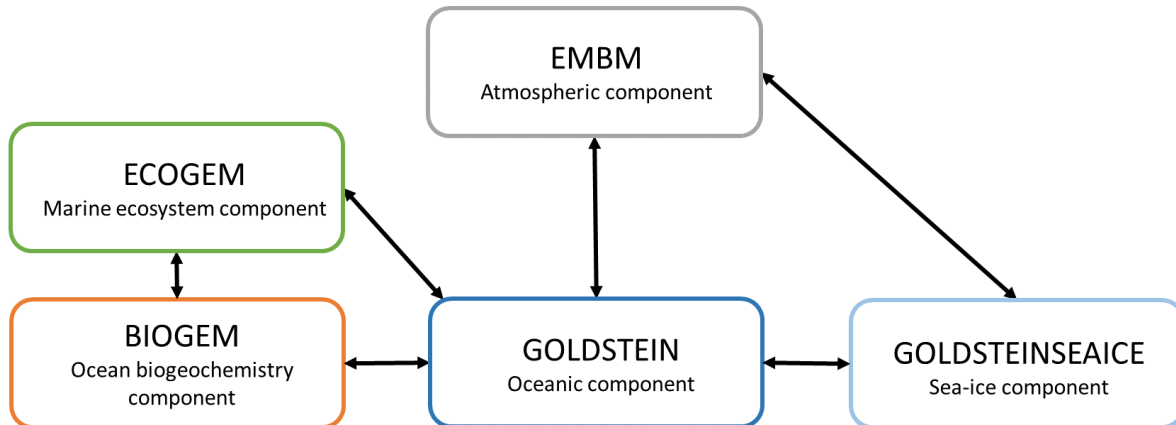
Figure 4.2: Representation of the components of the EcoGENIE model. The black arrows indicate the link between the different climatic components.

Modules

The physical components

The physics of the model contains a frictional-geostrophic ocean circulation (GOLDSTEIN), coupled to a 2D energy-moisture balance model of the atmosphere (EMBM) and a thermodynamic sea-ice model (GOLDSTEINSEAICE) [Edwards and Marsh, 2005; Marsh et al., 2011]. Heat and moisture are exchanged between the three components and act as a coupling strategy.

The oceanic component calculates the horizontal and vertical redistribution of heat, salinity and biogeochemical elements via advection, convection and mixing. The ocean module is configured on a 36×36 horizontal grid. The horizontal grid is uniform in longitude and uniform in sine latitude, giving $\sim 3.2°$ latitudinal increments at the equator increasing to $19.2°$ in the highest latitude. This horizontal grid has been used for previous biogeochemical simulations [Cameron et al., 2005; Colbourn, 2011]. We consider 32 vertical oceanic layers increasing logarithmically from 29.38 m for the surface layer to 456.56 m for the deepest layer. This vertical resolution has already been used to study the relative importance of biogeophysical and biogeochemical mechanisms on the climate system (Chapter 3).

The atmospheric component is based closely on the UVic Earth system model [Weaver et al., 2001]. The prognostic variables are atmospheric temperature and specific humidity. Precipitation removes instantaneously all moisture corresponding to an excess above a relative humidity threshold.

The sea-ice component solves the equation for part of the ocean covered by sea-ice. The prognostic variables are ice thickness and ice areal fraction. The transport of sea-ice includes sources and sinks of these variables. The growth or decay of sea ice depends on the net heat flux into the ice. The dynamics in this module consist of advection by currents and diffusion.

Ocean biogeochemistry component

The biogeochemical module (BIOGEM) represents the transformation and spatial redistribution of biogeochemical tracers [Ridgwell et al., 2007]. The state variables are inorganic resources and organic matter. The biological uptake is represented by an implicit biological community: nutrients are directly converted into organic matter via an uptake rate. The biological uptake is limited by light, temperature and nutrient availability. Organic matter is partitioned into dissolved and particulate phases (DOM and POM). The model includes iron (Fe) and phosphate (PO_4) as limiting nutrients. Similar to Chapter 3, we do not consider nitrate (NO_3^-) here. Furthermore, BIOGEM calculates the air-sea CO_2 and O_2 exchange. The value of atmospheric CO_2 predicted by BIOGEM is used as input for the radiative scheme of the atmospheric component, thus providing climate feedback.

Ecosystem component

The marine ecosystem component (ECOGEM) represents the marine plankton community and associated interactions in the ecosystem [Ward et al., 2018]. The biological uptake in ECOGEM replaces the BIOGEM uptake calculation and is limited by light, temperature and nutrient availability. Plankton biomass and organic matter are subject to processes such as resource competition and grazing before being passed to DOM and POM. The ecosystem is divided into different plankton functional types (PFTs) with specific traits. Furthermore, each PFT is sub-divided into size classes with specific size-dependent traits. We consider two classes of PFTs: phytoplankton and zooplankton. Phytoplankton is characterized by nutrient uptake and photosynthesis whereas zooplankton is characterized by predation traits. Zooplankton grazing depends on the concentration of prey biomass availability, with predominantly grazing on preys that are 10 times smaller than themselves. Each population is associated with biomass state variables for carbon, phosphate and chlorophyll. The production of dead organic matter is a function of mortality and messy feeding, with partitioning between non-sinking dissolved and sinking particulate organic matter. Finally, plankton mortality is reduced at very low biomass such that plankton cannot become extinct.

Light absorption in the ocean

The implementation of phytoplankton light absorption in EcoGENIE is the same as the scheme described in Chapter 3 and is a coupling between Eq. 4.1 and Eq. 4.2. For a simplification issue, in our model configuration, the incoming shortwave radiation does not vary seasonally. We look at long-term changes in the climate system therefore the absence of a seasonal cycle does not affect our results and main findings. The presence of organic, inorganic particles and dissolved molecules restrains the light penetration in the ocean [Ward et al., 2018]. The vertical light attenuation scheme is given by Eq.4.1:

$$I(z) = I_0 \cdot \exp(-k_w - k_{Chl} \cdot Chl_{tot}) \cdot z \qquad (4.1)$$

where $I(z)$ is the irradiation of the full solar spectrum at depth z, I_0 is the irradiation at the surface of the ocean, k_w is light absorption by clear water and inorganic particles (0.04 m^{-1}), k_{Chl} is the light absorption by chlorophyll (0.03 m^{-1}(mg Chl)$^{-1}$) and Chl_{tot} is the total chlorophyll concentration. The values for k_w and k_{Chl} are taken from Ward et al. [2018]. The parameter I_0 is negative in the model because it is a downward flux from the sun to the surface of the ocean. We allow primary production and light to penetrate until the sixth layer of the model (221.84 m deep), which is the lower limit of the euphotic zone [Tett, 1990]. In our model setup, maximum absorption occurs in the upper oceanic layer and minimum absorption occurs in the sixth layer.

Phytoplankton changes the optical properties of the ocean [Sonntag and Hense, 2011] through phytoplankton light absorption. Therefore it can cause a radiative heating and change the oceanic temperature. We implemented phytoplankton light absorption into the model following Hense [2007] and Patara et al. [2012] Eq.4.2:

$$\frac{\partial T}{\partial t} = \frac{1}{\rho \cdot c_p} \frac{\partial I}{\partial z} \qquad (4.2)$$

$\partial T / \partial t$ denotes the temperature changes, c_p is the specific heat capacity of water, ρ is the ocean density, I is the solar radiation incident at depth z. Part of the light absorbed is used by phytoplankton for photosynthesis and part is released in form of fluorescence and heat. However, the fluorescence form can be ignored, therefore it is assumed that the whole light absorption leads to heating of the water [Lewis et al., 1983].

Air-sea heat exchange

Heat is exchanged between the atmosphere, the ocean and the sea-ice components and acts as a coupling between these three modules. We detail here only the relevant fluxes for our study, the heat flux into the atmosphere. The vertically integrated atmospheric heat equation is given by Weaver et al. [2001] and Marsh et al. [2011] Eq. 4.3:

$$Q_{ta} = Q_{SW} \cdot C_A + Q_{LH} + Q_{LW} + Q_{SH} - Q_{PLW} \qquad (4.3)$$

Q_{ta} corresponds to the total heat flux into the atmosphere, Q_{SW} is the net shortwave radiation corresponding to the solar irradiance receives from the sun and reflected by the planet's albedo, C_A is a heat absorption coefficient (0.3 over the ocean, Marsh et al. [2011]), Q_{LH} is the latent heat flux corresponding to phase change of a thermodynamic system, Q_{SH} is the sensible heat flux corresponding to temperature change of a thermodynamic system, Q_{LW} is the net (upward minus downward) re-emitted longwave radiation corresponding to infrared energy coming from the planet and Q_{PLW} is the outgoing planetary longwave radiation.

The atmosphere loses heat through net longwave radiation, dominated by the outgoing longwave radiation, thus the total longwave heat flux ($Q_{LW} + Q_{PLW}$) is negative in the model. Furthermore, evaporative cooling of the ocean leads to a latent heat release in the atmosphere upon condensation and precipitation. Evaporated water vapour may be transported away from an oceanic source, to condense and precipitate elsewhere.

Air-sea CO_2 exchange

The atmospheric temperature depends on the atmospheric CO_2 concentration which is affected by the transfer of CO_2 between the ocean and the atmosphere. The flux of CO_2 across the atmosphere-ocean interface is given by Ridgwell et al. [2007] Eq. 4.4:

$$F_{CO_2} = k \cdot \rho \cdot (C_w - \alpha \cdot C_a) \cdot (1 - A) \qquad (4.4)$$

F_{CO_2} is the air-sea CO_2 flux, k corresponds to the gas transfer velocity, ρ is the ocean density, C_w is the concentration of dissolved gas in the surface ocean, α is the solubility coefficient calculated from Wanninkhof [1992] and depends on the sea surface temperature and salinity, C_a is the concentration of gas in the atmosphere and A is the fraction of the ocean covered by sea-ice.
Phytoplankton light absorption affects the flux of CO_2 via the parameters C_w, α and A. To study precisely the flux we either prescribe these parameters in the air-sea CO_2 exchange calculation or let them evolve freely. To prescribe these parameters we take the values from the reference run (see below).

Model setup and simulations

During this study, we are mainly interested in the relative differences between our selected simulations. We try to simulate a realistic mean climate system but the absolute value of the climate quantities are less relevant due to the limitations of such an intermediate complexity model.

For a realistic nutrient distribution in the ocean, we performed a BIOGEM spin-up for 10,000 years. During the spin-up the atmospheric CO_2 concentration is fixed to 278 ppm. The simulations restart for 1,000 years after the spin-up with ECOGEM, meaning that all simulations consider marine biota. The model setup, ecosystem community and grid resolution employed are the same as in Chapter 3 (Appendix 4.1) except that we run the model without any seasonal cycle. The seasonal cycle is removed for technical issues, we cannot prescribe the seasonal cycle of SST but only the annually-averaged SST. The absence of the seasonal cycle is not an issue for this study because we look at the importance of each climate pathway rather than focusing on the quantitative changes of the climate system.

The carbon cycle is closed in our simulations, meaning that there is no input of carbon through volcanic or anthropogenic activities. Only the size of the carbon reservoirs can vary. If not stated otherwise, the concentration of atmospheric CO_2 evolves freely in the simulations. Furthermore, all simulations are forced with the same constant flux of dissolved iron into the ocean surface [Mahowald et al., 2006].

Table 4.1: Description of the simulations conducted with EcoGENIE. All the simulations consider phytoplankton light absorption except the reference run Bio.

Name	Characteristics
Bio	Reference run
BioLA	Run with all pathways included
HEAT	Run with prescribed CO_2 pathway
CARB	Run with prescribed heat flux pathway
HCorg	Run with prescribed CO_2 solubility and sea-ice extent pathways
HCorgSI	Run with prescribed CO_2 solubility pathway
HCorgSol	Run with prescribed sea-ice extent pathway

To study the effect of phytoplankton light absorption on the atmospheric temperature we perform seven different simulations (Figure 4.3; Table 4.1):

- The first one, called "*Bio*" is the reference run and is the only simulation that does not include phytoplankton light absorption ($k_{Chl} = 0$ in Eq. 4.1). In this simulation, all the climate pathways evolve freely.

- The second one, called "*BioLA*" is the same as the reference run but with phytoplankton light absorption implemented. In this simulation, all the climate pathways evolve freely.

- The third simulation "*HEAT*" is the same as the second one except that we prescribe the atmospheric CO_2 concentration only for the atmospheric temperature calculation. For a comparison with the reference run, the prescribed atmospheric CO_2 concentration from *Bio* is used (169 ppm). The effect of CO_2 on atmospheric temperature is fixed but the air-sea heat fluxes evolve freely. This simulation determines the effect of air-sea heat flux on the energy budget.

- The fourth simulation is named "*CARB*" where we run the model with an uncoupled ocean-atmosphere setup. The atmospheric component is forced with the heat fluxes from the reference run and the atmospheric CO_2 concentration is prescribed with the value of *BioLA*. This simulation determines the effect of phytoplankton-induced changes of atmospheric CO_2 concentration on the atmospheric temperature. Please note that *CARB* is well suited for studying the atmosphere properties but not to examine ocean dynamics.

- The fifth simulation is named "*HCorg*" and we only allow the biological pump to affect the dissolved CO_2. The solubility of CO_2 (α in Eq. 4.4) and sea-ice extent (A in Eq. 4.4) parameters are prescribed using the respective values from *Bio*. The CO_2 solubility is fixed by prescribing the SST only for this calculation. In *HCorg* air-sea heat exchange and the biological pump parameter (C_w in Eq. 4.4) evolve freely.

- The sixth simulation is called "*HCorgSI*" where the biological pump and sea-ice extent affect dissolved CO_2. The solubility of the CO_2 parameter (α in Eq. 4.4) is prescribed using the value of *Bio*. In *HCorgSI* the air-sea heat exchange, the biological pump (C_w in Eq. 4.4) and sea-ice extent (A in Eq. 4.4) parameters evolve freely.

- The seventh and last simulation is called "*HCorgSol*" where the biological pump and the solubility pump affect dissolved CO_2 in the ocean. The sea-ice extent parameter (A in Eq. 4.4) is prescribed using the value of *Bio*. In *HCorgSol* the air-sea heat

exchange, the biological pump (C_w in Eq. 4.4) and the CO_2 solubility (α in Eq. 4.4) parameters evolve freely.
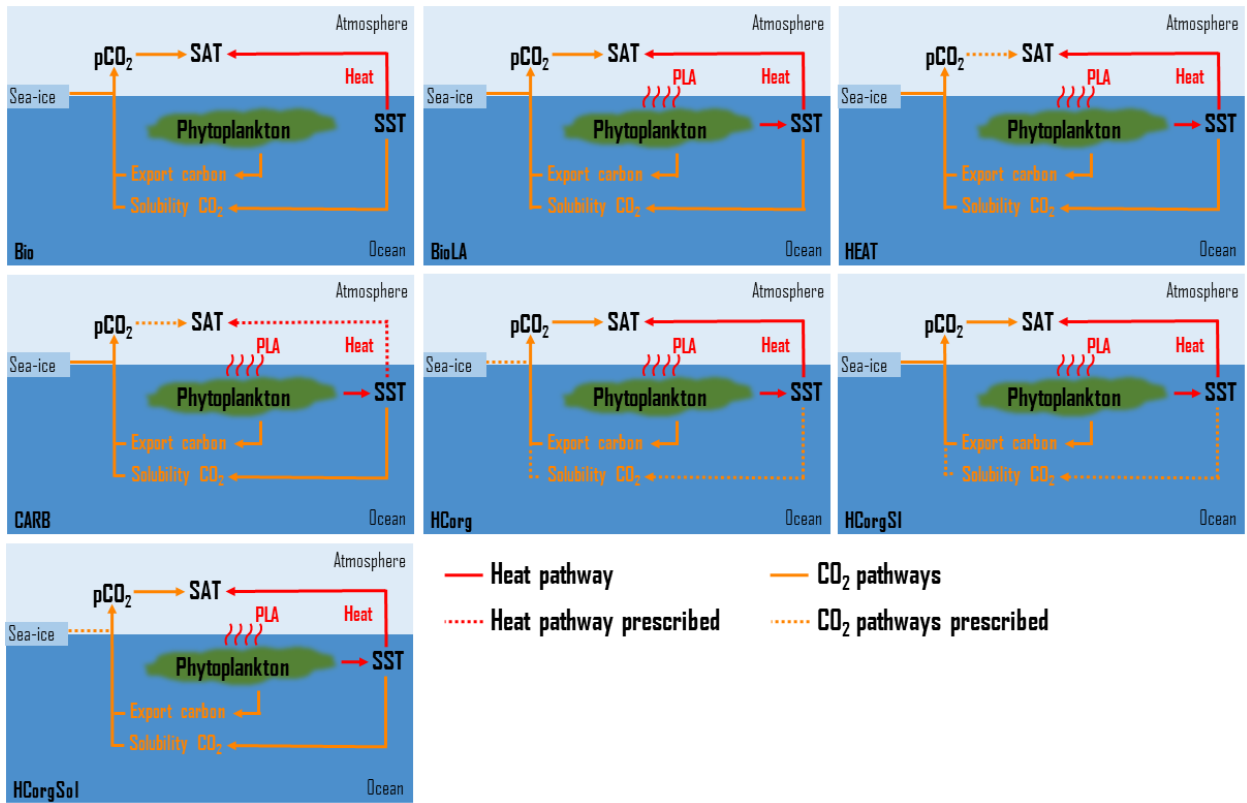
Figure 4.3: Sketch representing the climate pathways involved in the seven simulations conducted with EcoGENIE (PLA = Phytoplankton Light Absorption). Note that this figure is a simplification of Figure 4.1, only the relevant pathways are represented. The names of the simulations are on the bottom left of each panel. The dashed arrows indicate the climate pathways prescribed.

Sensitivity analysis

Climate variability

To analyze the climate variability of the model, we perform two sensitivity analyses (Table 4.2). Both simulations have the same model setup, restart from the spin-up described previously but their atmospheric CO_2 concentration differ. The first simulation (Sensi280) has an atmospheric CO_2 concentration of 280 ppm while the second one (Sensi320) has an atmospheric CO_2 concentration of 320 ppm. Furthermore, the simulations Sensi280 and Sensi320 consider phytoplankton light absorption.

Table 4.2: Chlorophyll concentration (mgChl/m^3), sea and atmospheric surface temperature (°C) for the sensitivity analysis of the climate. The difference represents the value of Sensi320 minus the value of Sensi280.

Simulation	Chloro. conc. (mgChl/m^3)	SST (°C)	SAT (°C)
Sensi280	0.1177	16.78	11.92
Sensi320	0.1175	17.17	12.44
Difference	-0.0002	0.39	0.52

An increase of 40 ppm in atmospheric CO_2 concentration slightly reduces the chlorophyll concentration but these changes are negligible. The oceanic and atmospheric heat budgets are affected by the changes in atmospheric CO_2 concentration. Increasing the greenhouse gas concentrations increases, in turn, the SAT and therefore the SST due to the exchange of heat between the ocean and the atmosphere.

Air-sea fluxes interactions

To estimate the unique effect of each climate pathway we ensure that the heat and CO_2 interaction is negligible. Due to the model setup, the flux of CO_2 across the air-sea interface (F_{CO_2}; Eq. 4.4) depends on the SST via the Schmidt number [Wanninkhof, 1992; Ridgwell et al., 2007]. We conduct two comparable sensitivity analysis and analyze the changes in F_{CO_2}. First, we artificially increase the SST by 1°C and do not exceed the maximum difference of SST between our simulation results (Table 4.3). This increase in SST only enhances F_{CO_2} by $4.26 \cdot 10^{-5}$ mol/m^2/yr, representing a raise of 2.58% of the total air-sea CO_2 exchange. Even large SST fluctuations negligibly affect the flux of CO_2 at the air-sea interface. Second, the mean wind speed affects the F_{CO_2} via the gas transfer velocity (k; Eq. 4.4). We increase the wind speed by 0.2 m/s, which is a comparable forcing of the artificial increase of 1°C of SST [Knutson and Tuleya, 2004]. This increase in mean wind speed enhances the F_{CO_2} by $1.44 \cdot 10^{-4}$ mol/m^2/yr, representing an increase of 8.69% of the total air-sea CO_2 flux. Clearly, the changes in wind speed are much larger than the changes in SST hence we consider that the effect of SST on the air-sea CO_2 exchange is small enough to be neglected.

Table 4.3: Changes in air-sea CO_2 exchange (mol/m^2/yr and %) regarding the sensitivity of the system towards the interplay between CO_2 and heat. For the first sensitivity analysis, the SST is increased by 1°C while for the second analysis, the annual mean wind speed is raised by 0.2 m/s. The third row corresponds to the maximum difference of SST between the simulations.

Sensitivity analysis	F_{CO_2} (mol/m^2/yr)	Changes (%)
+1°C	$+4.26 \cdot 10^{-5}$	2.58
+0.2 m/s	$+1.44 \cdot 10^{-4}$	8.69
+0.08°C	$+3.40 \cdot 10^{-6}$	0.21

Global response of the climate system

In this section we present the results of the simulations on a global scale, we do not consider local patterns because we removed any seasonal cycle in our model setup. As already mentioned, the absence of the seasonal cycle is not an issue for our study because we focus on the importance of each climate pathway rather than analyzing the quantitative

assessments of the climate pathways. First, we focus on the chlorophyll biomass and sea surface temperature because phytoplankton light absorption has a direct effect on these climate variables [Oschlies, 2004; Lengaigne et al., 2007; Paulsen et al., 2018]. Second, these changes in oceanic properties affect the carbon cycle [Manizza et al., 2008, and Chapter 3], therefore we study the changes in atmospheric CO_2 concentration between the simulations. Third, phytoplankton light absorption alters the atmospheric properties [Patara et al., 2012], thus we analyze the changes in radiative heat fluxes, humidity and evaporation between the simulations. Finally, due to changes in oceanic and atmospheric properties, the response of the surface atmospheric temperature is studied.

Chlorophyll biomass and sea surface temperature

Our results indicate differences of sea surface temperature (SST) and chlorophyll biomass, depending on the climate pathways included in our model setup (Table 4.4). The reference run *Bio* has the lowest chlorophyll biomass and a low SST while the simulation *BioLA* has the highest chlorophyll biomass and SST. As previously demonstrated, phytoplankton light absorption increases the chlorophyll biomass and therefore the SST via shallower downward flux of organic matter and higher surface nutrient concentrations [Manizza et al., 2008, and Chapter 3]. The chlorophyll biomass difference between *BioLA* and *Bio* is 0.012 mgChl/m^3 which is in agreement with previous estimates [Manizza et al., 2005, and Chapter 3]. However, the global difference of SST between *BioLA* and *Bio* of only 0.08°C is lower than previous estimates [Lengaigne et al., 2009; Löptien et al., 2009, and Chapter 3]. This under-estimation of the biologically-induced SST heating is due to non-seasonal radiative forcing of the model. The non-seasonal radiative forcing decreases the global heat budget (Appendix 4.2), explaining the lower response of the SST in our study.

The chlorophyll biomass is higher while the SST is lower in *HEAT* compared to the reference simulation (Table 4.4). This is rather counter-intuitive and is due to changes in oceanic circulation between these two simulations. For instance, the maximum Atlantic overturning circulation is 8.6 Sv in *HEAT* while it is 7.6 Sv in *Bio*. The stronger overturning circulation in *HEAT* increases the concentration of surface nutrients. Specifically the surface PO_4 concentration is about 0.21 μmol/kg in *HEAT* while it is about 0.19 μmol/kg in *Bio*. The higher surface PO_4 concentration in *HEAT* explains the higher chlorophyll biomass in this simulation compared to the reference simulation. The changes in the strength of the circulation explain as well the lower SST in *HEAT* compared *Bio*. The stronger oceanic circulation in *HEAT* leads to a more important redistribution of heat along the water column, explaining the surface cooling and the warming of the bottom water. Our results indicate that the bottom water temperature in *HEAT* is 3.57°C while it is 3.09°C in *Bio*.

The simulation *HCorg*, *HCorgSI* and *HCorgSol* have a higher chlorophyll biomass and SST than the reference run. Furthermore, the chlorophyll biomass and the SST are similar between the simulation *HCorg* and *HCorgSI* indicating that the changes in sea-ice extent due to phytoplankton light absorption do not affect these climate variables (Appendix 4.3). In addition, the chlorophyll biomass and SST are higher in *HCorg* than in *HCorgSol*, indicating that the solubility factor has a negative feedback on these climate variables. Between these two simulations, the only difference is the CO_2-solubility factor that can evolve freely in *HCorgSol*. In the simulation *HCorg*, the SST for the calculation of the solubility of CO_2 is prescribed using the values of the reference run. The SST in the reference run is lower than the SST in *HCorgSol*. Considering the physical and chemical properties of the ocean, a

low SST increases the solubility of CO_2 [Wanninkhof, 1992]. Therefore, the CO_2 solubility is reduced in *HCorgSol* compared to *HCorg*, due to the higher SST in *HCorgSol*. For instance, our results indicate that on a global scale, the oceanic CO_2 concentration is 27.200 μmol/kg in *HCorgSol* while it is 27.213 μmol/kg in *HCorg*. These changes in carbon cycle between the simulations affect the others biogeochemical cycles via the nutrient ratios [Ward et al., 2018]. As a consequence, the surface PO_4 concentration is about 0.216 μmol/kg in *HCorg* and about 0.214 μmol/kg in *HCorgSol*. The higher PO_4 concentration at the surface in *HCorg* leads to the higher chlorophyll biomass and higher SST due to phytoplankton light absorption compared to *HCorgSol*.

Table 4.4: Sea surface temperature (°C) and surface chlorophyll biomass (mgChl/m^3). There is no value for the simulation CARB because we run the model with an uncoupled ocean-atmosphere setup.

Simulation	SST (°C)	Chlorophyll biomass (mgChl/m^3)
Bio	15.26	0.09949
BioLA	15.34	0.11178
HEAT	15.25	0.10827
CARB	-	-
HCorg	15.30	0.10964
HCorgSI	15.30	0.10964
HCorgSol	15.28	0.10891

Atmospheric properties

The oceanic properties differ between the simulations, thus we expect differences between the atmospheric properties in each simulation. First, we compare the atmospheric CO_2 concentration, then the heat fluxes, the evaporation, the specific humidity and finally the surface atmospheric temperature.

Atmospheric CO_2 concentration

In all the simulations considering phytoplankton light absorption, the atmospheric CO_2 concentration is higher than in the reference run (Table 4.5). The atmospheric CO_2 concentration is the lowest in *Bio* while it is the highest in *BioLA*, with a difference of 9 ppm. The difference of CO_2 concentration between the simulations *BioLA* and *Bio* is lower than previous estimate (Chapter 3) and is due to the non-seasonal cycle forcing (Appendix 4.2). As already described in Chapter 3, the higher atmospheric CO_2 concentration in *BioLA* is mainly explained by lower CO_2 solubility due to a higher SST.

In *HEAT*, the atmospheric CO_2 concentration is prescribed only in the atmospheric temperature calculation, therefore the atmospheric CO_2 concentration can vary due to changes in dissolved oceanic CO_2, solubility and sea-ice extent, and therefore affect the other climate variables. The atmospheric CO_2 concentration in *HEAT* is slightly higher than in *Bio*. The chlorophyll biomass is more important in *HEAT* than in the reference simulation, indicating a higher amount of organic matter and therefore a more important remineralization rate in the ocean. During the remineralization process, CO_2 is produced [Sarmiento and Gruber, 2006], therefore the higher remineralization rate in *HEAT* increases the dissolved CO_2 concentration. On a global scale, our results indicate that the surface dissolved CO_2 is about 6.354 mol/kg in *HEAT* while it is 6.302 mol/kg in *BIO*. The more important dissolved CO_2

concentration in *HEAT* increases the air-sea CO_2 flux and therefore the atmospheric CO_2 concentration (see Eq. 4.4).

The atmospheric CO_2 concentration in *CARB* is similar to the one in *BioLA* because we prescribed the value against the one in *BioLA*.

The simulations *HCorg*, *HCorgSI* and *HCorgSol* have a higher atmospheric CO_2 concentration than the reference run. This is again not surprising because these simulations consider phytoplankton light absorption which increase the atmospheric CO_2 concentration (Chapter 3). The atmospheric CO_2 concentration between *HCorg* and *HCorgSI* is similar due to the similar sea-ice extent (Appendix 4.3) and sea-ice thickness, the sea-ice does not have an impact on the atmospheric CO_2 concentration. The slightly higher atmospheric CO_2 concentration in *HCorgSol* compared to *HCorg* is due to changes in CO_2 solubility between these two simulations. As described above, the CO_2 solubility is lower in *HCorgSol* compared to *HCorg*. As a consequence, the air-sea CO_2 flux is higher in *HCorgSol* compared to *HCorg*, leading to a slightly higher atmospheric CO_2 concentration in *HCorgSol* (Eq. 4.4).

Table 4.5: Comparison of the atmospheric CO_2 concentration (ppm) for the seven simulations.

Simulation	Atmospheric CO_2 (ppm)
Bio	169
BioLA	178
HEAT	171
CARB	178
HCorg	174
HCorgSI	174
HCorgSol	175

Heat fluxes

The air-sea heat flux is divided into the net shortwave radiation, the net re-emitted longwave radiation, the sensible heat flux and the latent heat flux (Figure 4.4). The simulations *HCorg* and *HCorgSI* have exactly the same heat fluxes because these simulations are identical in all points (Appendix 4.3). Furthermore, the simulations *BioLA* and *HCorgSol* also have the same heat fluxes. The only difference between these two simulations is the prescribed and different sea-ice extent for the calculation of the air-sea CO_2 flux. This change in air-sea CO_2 flux does not alter the air-sea heat flux explaining the identical radiative heat fluxes between *BioLA* and *HCorgSol*. Finally, the heat fluxes between *CARB* and *Bio* are identical because we prescribed the heat fluxes in *CARB* with the values of *Bio*.

The net shortwave heat flux is divided in two: the incoming shortwave radiation from the sun entering the atmosphere and the outgoing reflected shortwave radiation leaving the atmosphere. Figure 4.4a shows that the net shortwave heat flux is identical for all the simulations and is positive. The positive values indicate that net shortwave heat flux is dominated by the flux entering the system, the incoming radiation. The incoming shortwave radiation from the sun is always identical between simulations, therefore identical net shortwave heat flux implies that the outgoing reflected shortwave radiation is as well the same between simulations due to the treatment of shortwave radiation in the atmosphere given by Weaver et al. [2001].

The net longwave heat flux is negative for all simulations pointing out that this flux is dominated by the upward longwave radiation leaving the atmosphere (Figure 4.4b). A higher negative value of net longwave heat flux indicates a higher loss of heat in outer space. The simulations *Bio* and *CARB* have the highest net longwave heat flux while the simulation *HEAT* has the lowest heat flux, indicating that the simulation *HEAT* loses more heat than the others simulations. The higher heat loss in the simulation *HEAT* is due to a reduced amount of greenhouse gases, precisely a low specific humidity (Table 4.6) and atmospheric CO_2 concentration (Table 4.5). The lower amount of greenhouse gases in the atmosphere permits a higher loss of heat outside the atmosphere. All the simulations considering phytoplankton light absorption, except *CARB* where the heat fluxes are prescribed, have a higher net longwave heat flux compared to *Bio*, which is rather predictable because this biogeophysical mechanism is an additional heat source.

The sensible heat flux depends on the atmospheric and oceanic temperature [Fanning and Weaver, 1996; Weaver et al., 2001]. The sensible heat flux increases when the atmospheric temperature decreases and when the oceanic temperature increases. For the simulation *HEAT*, the sensible heat flux is the highest (Figure 4.4c) because the atmospheric temperature is the lowest (Table 4.7). In contrast, the sensible heat flux is the lowest for the simulation *BioLA* because the gradient of temperature between the ocean and the atmosphere is low. The sensible heat flux in *HCorg* and *HCorgSI* are close to the sensible heat flux of the reference run because their air-sea temperature gradients are almost similar.

The global mean latent heat flux (Figure 4.4d) depends mainly on the global mean precipitation rate [Weaver et al., 2001]. The precipitation rate between *BioLA*, *HCorg*, *HCorgSI* and *HCorgSol* are almost similar (Appendix 4.4) explaining the similar latent heat fluxes between these simulations. The precipitation rate in *HEAT* is higher than in *Bio*, explaining the higher latent heat flux in *HEAT*. Furthermore, the reference run and *CARB* have the smallest latent heat flux due to the small precipitation rate for these simulations.
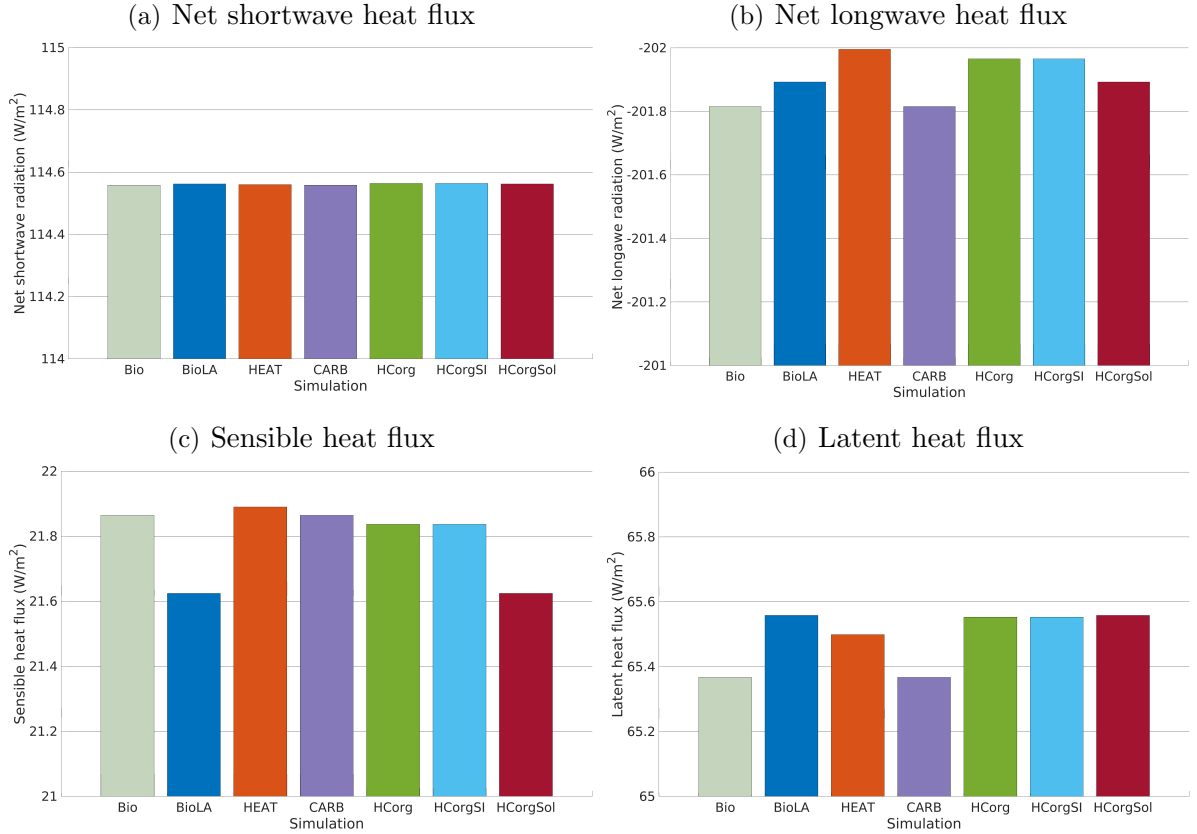
Figure 4.4: Global average of the different air-sea heat fluxes (W/m^2) for the seven simulations. (a) Net shortwave radiation at the top of the atmosphere. (b) Net re-emitted longwave radiation. The net longwave radiation is negative because it is dominated by the outgoing longwave radiation. (c) Sensible heat flux. (d) Latent heat flux. The color coding between the panels remains the same.

Specific humidity and evaporation

The specific humidity and the evaporation in *BioLA* and *HCorgSol* are similar and the same is true between the simulations *HCorg* and *HCorgSI* (Table 4.6). Furthermore, the specific humidity and evaporation are the lowest in the reference simulation due to the lowest latent heat flux in this simulation. Including phytoplankton light absorption changes the heat budget, specifically increasing the latent heat flux and therefore increasing the specific humidity and evaporation, which is consistent with Oschlies [2004]; Lengaigne et al. [2009]. In *BioLA* the specific humidity increases by 0.5% and the evaporation increases by 0.11% compared to the reference run, which is lower than previous values [Patara et al., 2012]. The different estimates between our results and Patara et al. [2012] may come from the non-seasonal cycle in our model setup, changing the heat budget and therefore the specific humidity and evaporation rate. Moreover, the specific humidity in *HEAT* is lower than in *BioLA* due to the lower latent heat flux in the simulation *HEAT*. The evaporation depends on several pathways and one of the most important is the humidity in the atmosphere [Peixoto and Oort, 1992], the lower is the humidity the higher is the evaporation rate. As a consequence, the evaporation is higher in *HEAT* than in the simulation *BioLA*. Furthermore, the specific humidity and the evaporation increase when the atmospheric temperature rises as well [Peixoto and Oort, 1992]. The specific humidity and evaporation is higher in the simulations *CARB* compared to *BioLA* because the surface atmospheric temperature is

higher in *CARB* (Table 4.7). The specific humidity and evaporation in *HCorg* and *HCorgSI* are slightly lower than in *BioLA* because the latent heat flux in *HCorg* and *HCorgSI* is slightly lower. Once the CO_2 solubility factor is considered (simulation *HCorgSol*), the values of the specific humidity and evaporation are similar to the values in *BioLA*. This is rather not surprising because the heat fluxes between *HCorgSol* and *BioLA* are identical.

Table 4.6: Comparison of important atmospheric properties: specific humidity (g/kg) and evaporation (mm/yr) for the seven simulations.

Simulation	Specific humidity (g/kg)	Evaporation (mm/yr)
Bio	11.762	834.70
BioLA	11.818	835.65
HEAT	11.794	836.28
CARB	11.845	835.96
HCorg	11.814	835.54
HCorgSI	11.814	835.54
HCorgSol	11.818	835.65

Surface atmospheric temperature

The difference of atmospheric properties between simulations lead indubitably to changes of the surface atmospheric temperature (Figure 4.5; Table 4.7). First of all, the reference simulation *Bio* has the lowest SAT because it doesn't include the additional heat source coming from the phytoplankton light absorption mechanism. The global difference of SAT between *BioLA* and *Bio* is 0.14°C which is lower than previous estimates [Shell et al., 2003; Patara et al., 2012, and Chapter 3]. The small difference of SAT compared to previous studies is clearly due to our model setup, with a non-seasonal solar radiation forcing.

Table 4.7: Global surface atmospheric temperature and changes compared to the reference simulation (°C). In the second column, a positive value indicates a higher while a negative value indicates a lower surface atmospheric temperature in the respective simulation compared to the reference simulation.

Simulation	SAT (°C)	Changes (°C)
Bio	9.31	-
BioLA	9.45	+0.14
HEAT	9.29	-0.02
CARB	10.02	+0.71
HCorg	9.34	+0.03
HCorgSI	9.34	+0.03
HCorgSol	9.30	-0.01

The lower SAT in *HEAT* compared to *Bio* is due to several reasons. Even if *HEAT* considers phytoplankton light absorption, we show that the SST in *HEAT* is lower than in the reference run. Furthermore, for the SAT computation, the atmospheric CO_2 concentration is identical between *Bio* and *HEAT* and the specific humidity is slightly higher in *HEAT*. Therefore the greenhouse gas effect between these two simulations is rather similar. However, the global net longwave heat flux decreases by ~ 0.2 W/m^2 in *HEAT*, leading to a cooling of the atmosphere. The combination of these different reasons explains the slightly lower SAT in *HEAT* compared to the reference simulation.

For the simulation *CARB*, the concentration of greenhouse gases (atmospheric CO_2 and specific humidity) is higher than in *Bio* while the air-sea heat fluxes are identical. As a consequence, more heat is trapped in the atmosphere and the SAT increases by 0.71°C compared to the reference run.

The sea-ice extent and thickness are identical between *HCorg* and *HCorgSI* (Appendix 4.3), resulting in identical response of the climate system and identical SAT. The specific humidity and the atmospheric CO_2 concentration are slightly higher in *HCorg* compared to *Bio*. This slightly higher greenhouse gas concentration leads to a small increase in SAT of *HCorg* compared to *Bio*.

In *HCorgSol* the atmospheric CO_2 concentration and the specific humidity are higher than in the reference simulation. However, the sensible heat flux and the net longwave heat flux are lower in *HCorgSol*. Even if the greenhouse gas concentrations are higher, the reduced air-sea heat fluxes lead to a slight decrease in SAT in the simulation *HCorgSol* compared to *Bio*.
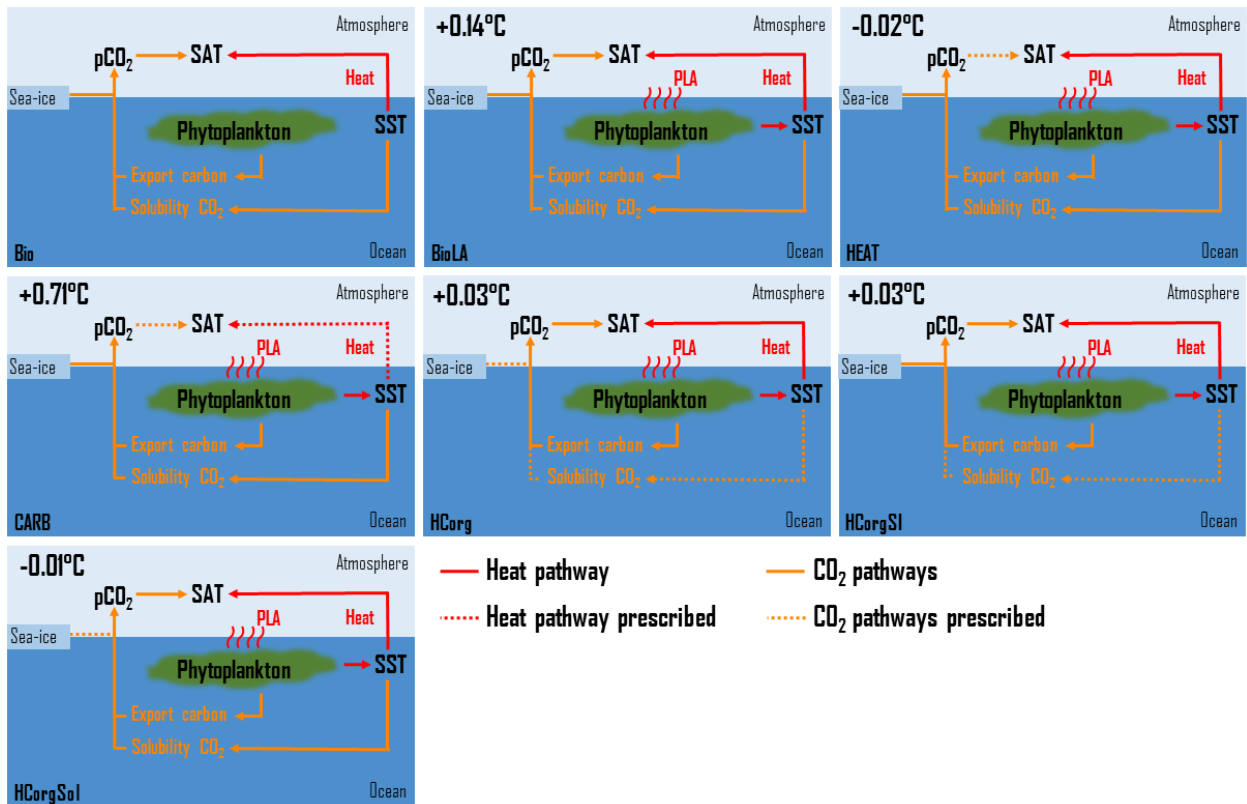
Figure 4.5: Sketch representing the surface atmospheric temperature (SAT) changes between the simulations and the reference run. On the top left corner is located the value of SAT change compared to *Bio*. The rest of the sketch is similar to Figure 4.3.

Summary and conclusion

To study how phytoplankton light absorption alters the surface atmospheric temperature via air-sea heat and CO_2 exchange, we use the EcoGENIE model [Ward et al., 2018]. For the first time, we compare the role of these individual fluxes and quantify their influence

on biologically-induced atmospheric warming. We show that without any seasonality and with all the climate pathways included, the surface atmospheric temperature increases by 0.14°C due to phytoplankton light absorption. As suggested by Capone et al. [1998]; Oschlies [2004]; Wetzel et al. [2006], phytoplankton light absorption changes the air-sea heat flux. Our results indicate that when only this air-sea interaction is considered, the atmosphere cools by 0.02°C compared to a simulation without the biogeophysical mechanism. Moreover, when only the air-sea CO_2 exchange is considered, the atmospheric temperature increases by 0.71°C. Clearly, our results indicate that the air-sea CO_2 exchange has a more important effect than the air-sea heat flux on the phytoplankton-induced warming of the atmosphere. With our model setup, the sea-ice extent and thickness slightly vary between simulations, therefore sea-ice processes hardly affect the air-sea CO_2 flux and thus the climate system. Moreover, including the solubility pathway changes the heat fluxes, specifically reducing the sensible heat flux and the net longwave heat flux compared to the reference simulation. As a consequence, this climate pathway has a negative effect on the atmospheric temperature. To conclude, phytoplankton light absorption influences the climate pathways at the ocean-atmosphere interface, particularly the air-sea CO_2 exchange that is important for the phytoplankton-induced atmospheric warming.

For future work, more studies with higher complexity models are necessary to make quantitative assessments rather than qualitative assessments as in our study. For instance, a model with a dynamic atmosphere such as PLASIM-GENIE [Holden et al., 2016] could be a good aspiration to complete our study. Observations and modeling studies indicate that positively buoyant phytoplankton groups, such as cyanobacteria, are important to study the climate system [Sonntag and Hense, 2011; Paulsen et al., 2018; Wurl et al., 2018]. Implementing these microorganisms to assess our research question could be a beneficial follow-up of our study. Moreover, similar simulations must be conducted with a seasonal variation of the shortwave radiation to better understand the role of phytoplankton in the climate system.

Appendices

Plankton functional types

We base our ecosystem community on the community described by Ward et al. [2018]. However, instead of using 16 plankton functional types (PFTs) we only use 2 PFTs: one phytoplankton group and one zooplankton group (Appendix 4.1). We show that the complexity of the ecosystem does not have an important impact on the climate system compared to the effect of phytoplankton light absorption (Chapter 3). Therefore we reduced the ecosystem complexity to increase the computational time of the model.

Appendix 4.1: Size of the different plankton functional types (μm) used during the simulations.

PFT	Size (μm)
Phytoplankton	46.25
Zooplankton	146.15

Seasonal and non-seasonal cycle

We compare two model simulations with phytoplankton light absorption. The model setups are similar except that we switched off the seasonal cycle in one simulation. Turning off the seasonal cycle decreases the SST by 0.77°C. Furthermore, the difference of atmospheric CO_2 concentration is 6 ppm. This difference is due to different SST and therefore CO_2 solubility between these simulations. These results indicate that switching off the seasonal cycle damps the response of the climate system to phytoplankton light absorption.

Appendix 4.2: Sea surface temperature (°C) and atmospheric CO_2 concentration (ppm) for simulations with and without a seasonal cycle.

Simulation	SST (°C)	Atm. CO_2 conc. (ppm)
Seasonal cycle	16.11	184
Non-seasonal cycle	15.34	178

Our results without seasonality indicate that the difference of SST between BioLA and Bio is 0.14°C. Similar simulations have been conducted with a seasonal cycle and the SST difference is 0.33°C (Chapter 3). The absence of a seasonal cycle reduces the difference of SST between the simulations with and without phytoplankton light absorption.

Sea-ice

The global sea-ice cover and the global sea-ice area between the simulations HCorg and HCorgSI are identical, explaining their identical climate state. Moreover, the variation of sea-ice between all simulations is small. The maximum global sea-ice cover of 1.42% occurs between the simulations CARB and HCorgSol.

Appendix 4.3: Global sea-ice cover (%) and global sea-ice area (km^2) for the different simulations.

Simulation	Sea-ice cover (%)	Sea-ice area (km^2)
Bio	9.79	$3.60 \cdot 10^7$
BioLA	9.76	$3.59 \cdot 10^7$
HEAT	9.91	$3.64 \cdot 10^7$
CARB	8.60	$3.16 \cdot 10^7$
HCorg	9.92	$3.65 \cdot 10^7$
HCorgSI	9.92	$3.65 \cdot 10^7$
HCorgSol	10.02	$3.68 \cdot 10^7$

Precipitation

Slight fluctuations in precipitation are visible in the Appendix 4.4. First of all, the precipitation between *BioLA* and *HCorgSol* are similar and the same is true for the precipitation between *HCorg* and *HCorgSI*. The precipitation rate is the highest in the simulation *BioLA* due to the important specific humidity. In contrast, *HEAT* has a low specific humidity explaining the lowest precipitation rate for this simulation.

Appendix 4.4: Precipitation (mm/yr) for the different simulations.

Simulation	Precipitation (mm/yr)
Bio	834.62
BioLA	837.07
HEAT	836.30
CARB	834.05
HCorg	837.00
HCorgSI	837.00
HCorgSol	837.07

EFFECT OF PHYTOPLANKTON LIGHT ABSORPTION UNDER WARMING SCENARIOS

Marine biota and its impact on the climate system has attracted increasing attention in recent climate studies. In particular, biogeophysical mechanisms such as phytoplankton light absorption have gained attention. Phytoplankton light absorption is a climate-relevant mechanism influencing the ocean heat budget and the whole climate system. Under global warming, the distribution of phytoplankton and its effects on the climate are expected to change. The role of phytoplankton light absorption in a warmer climate with prescribed atmospheric CO_2 concentration has been investigated. However, none of these studies take into account future socio-economic aspects. Additionally, previous studies evidence that phytoplankton light absorption mainly affects the climate system via increased atmospheric CO_2 concentration and the impact of a prescribed atmospheric CO_2 concentration to study this biogeophysical mechanism is unclear. To shed light on these research questions, we performed simulations under the Representative Concentration Pathways (RCPs) and their extensions with the EcoGENIE Earth system model. First, we compare simulations under the same RCP scenario with and without the biogeophysical mechanism. We show that phytoplankton light absorption increases the surface chlorophyll biomass and surface phosphate concentrations but rather minor changes occur in the atmospheric and oceanic temperature. Moreover, implementing phytoplankton light absorption leads to a similar response of the climate, independent of the RCP scenario considered. Second, we compare simulations under RCP and pre-industrial scenarios with and without phytoplankton light absorption. We show that phytoplankton light absorption increases the reduction of chlorophyll biomass driven by global warming via a lower concentration of surface nutrients. As a consequence, phytoplankton light absorption has the potential to slightly counteract the global warming of the planet. Third, we show that prescribing atmospheric CO_2 concentration blur the real effect of phytoplankton light absorption on the climate system. Overall, we show that phytoplankton light absorption has an important role in the long-term climate adjustment and can slightly counter-interact global warming.

Introduction

Under different predicted global warming scenarios, the distribution and abundance of phytoplankton are expected to change. How these changes in phytoplankton biomass and biogeography affect biogeophysical mechanisms such as phytoplankton light absorption remain poorly known. Using an Earth system model (ESM) of intermediate complexity, we study the effect of phytoplankton light absorption on the climate system under realistic future climate scenarios.

With global warming, phytoplankton abundance and distribution are predicted to decline. For instance, ocean transparency observations show that phytoplankton biomass decreases of $\sim 1\%$ per year since 1899 [Boyce et al., 2010]. However, these observations are under debate and temporal sampling bias might have occurred [Rykaczewski and Dunne, 2011]. Furthermore, remotely-sensed ocean color data shows that between 1998 and 2006 low surface chlorophyll areas have expanded by 15% on a global scale [Polovina et al., 2008]. This decline in chlorophyll concentration has also been observed on a regional scale [McClain et al., 2004] and is associated with an increase of sea surface temperature [Gregg et al., 2005]. Moreover, revised satellite data indicate a striking decline in chlorophyll biomass in the Indian Ocean between 1998 and 2015 [Gregg et al., 2017]. Supporting these observations, most Earth system models project a decline in net primary production in the future due to global warming. For instance, an inter-comparison study with four coupled climate models reports a decrease in net primary production of 2-20% by 2100 under a low greenhouse gas emissions scenario [Steinacher et al., 2010]. With a fully coupled climate model, Moore et al. [2018] indicate a primary production decrease of 24% by 2300 under a high fossil fuel emission scenario. Furthermore, a CMIP5 model intercomparison shows that primary production is predicted to decrease in the tropics and North Atlantic ocean under different global warming scenarios [Bopp et al., 2013]. This regional decline is also reported in the Indian Ocean, where an averaged reduction of total chlorophyll of 2.41% per year between 1998 and 2012 is revealed [Rousseaux and Gregg, 2015]. These changes in phytoplankton abundance, distribution and biogeography have an impact on biogeophysical mechanisms such as phytoplankton light absorption.

Different modeling studies investigate the effect of phytoplankton light absorption in a warmer world. It is speculated that increasing atmospheric temperature reduces phytoplankton abundance [Behrenfeld et al., 2006; Falkowski and Oliver, 2007], increasing therefore, ocean clarity and reducing the biological increase of sea surface temperature (SST), thus counteracting, in part the warming associated with climate change [Patara et al., 2012]. To study the effect of phytoplankton light absorption in a warmer climate system, Sonntag [2013] conducted simulations with a 3D general circulation model coupled to a biogeochemical model. The author ran simulations with present-day SST forcing and simulations with a homogeneous increase by 3°C of the previous SST forcing, in each case with and without phytoplankton light absorption. The author indicates a regional and seasonal shift in phytoplankton distribution between the present-day and warmer scenario when the absorption feedback is taken into account. Moreover, implementing phytoplankton light absorption in the warmer scenario leads to a local SST increase of 0.2°C compared to the simulation without the biogeophysical mechanism. This result indicates a positive feedback of phytoplankton light absorption on the climate system in a warmer ocean. Another approach is used by Paulsen [2018] to study the effect of phytoplankton light absorption under a warmer climate. Paulsen [2018] performed simulations with a fully coupled Earths system model

under a scenario with a transient increase of 1% of atmospheric CO_2 concentration per year. With phytoplankton light absorption, the author reports a decline of chlorophyll concentrations associated with weaker oceanic circulation, specifically in the upwelling regions. As a consequence, the local SST warming is up to 0.7K with the active feedback between light and phytoplankton. Moreover, using a coupled ocean-atmosphere model, Park et al. [2015] focus on the Arctic region to study phytoplankton light absorption under a warming scenario. They conduct simulations, with and without the biogeophysical feedback, where atmospheric CO_2 concentration increases by 1% per year from the level of 1990 to double its initial concentration. The authors claim that future phytoplankton changes amplify Arctic warming by 20% when phytoplankton light absorption is considered.

Several modeling studies report a contradictory effect of phytoplankton light absorption on the climate system under future global warming. It is speculated that the ocean surface would either cool down due to the decrease in phytoplankton concentration [Patara et al., 2012] or warm-up due to advective processes [Anderson et al., 2009; Jochum et al., 2010]. To investigate these diverging hypotheses, phytoplankton light absorption has been studied under a warmer ocean [Sonntag, 2013] and warming scenarios following a transient 1% rising of CO_2 per year [Park et al., 2015; Paulsen, 2018]. The transient scenario is of plausible magnitude for the twenty-first century but idealized, therefore to make a link with more realistic scenarios, some corrections must be applied [Gregory and Forster, 2008; Gregory et al., 2015]. Furthermore, the transient scenario doesn't take into account the future socio-economic aspects. We therefore conduct simulations following more realistic greenhouse gas concentration scenarios such as the Representative Concentration Pathways (RCPs). Besides, the effect of phytoplankton light absorption under global warming has been investigated with idealized [Sonntag, 2013; Park et al., 2015] or complex climate models [Paulsen, 2018] but never with climate models of intermediate complexity. Thus we wonder if climate models of intermediate complexity are sufficient to capture the patterns and magnitude of changes evidence with complex climate models. To address these questions we apply the EcoGENIE Earth system model [Ward et al., 2018] and force the atmospheric CO_2 concentration following the four RCP scenarios used by the fifth Intergovernmental Panel on Climate Change (IPCC) Assessment Report to make predictions. The aim is to study potential changes in the effect of phytoplankton light absorption in the future.

The Representative Concentration Pathway scenarios

The Representative Concentration Pathways (RCP) scenarios are potential greenhouse gas concentration trajectories adopted by the IPCC [Meinshausen et al., 2011; IPCC, 2014]. These scenarios describe different climate systems depending on the volume of greenhouse gases emitted in the next years (Figure 5.1). There are originally four RCPs scenarios, namely RCP2.6, RCP4.5, RCP6.0 and RCP8.5, labelled after a possible radiative forcing in the year 2100 (2.6, 4.5, 6.0 and 8.5 W/m^2 respectively). These scenarios are consistent with socio-economic assumptions and associated greenhouse gas emissions. They represent a strong mitigation scenario (RCP2.6), two intermediate scenarios (RCP4.5 and RCP6.0) and a high greenhouse gas emissions scenario (RCP8.5). The RCP scenarios only span the period from 2005 to 2100, thus conducting a study on multi-century climate analysis requires data beyond 2100. We therefore use the Extended Concentration Pathways (ECPs) designed by several stakeholders and scientific groups [Meinshausen et al., 2011]. The ECPs assume a constant atmospheric CO_2 concentration between 2250 and 2500, except for the ECP2.6 scenario. The strong mitigation scenarios (RCP2.6 and ECP2.6) include negative

CO_2 emissions, leading to a decrease in atmospheric CO_2 concentration between 2100 and 2500. For practical purposes, referring to the RCP scenarios indicate the period between 1765 and 2500.
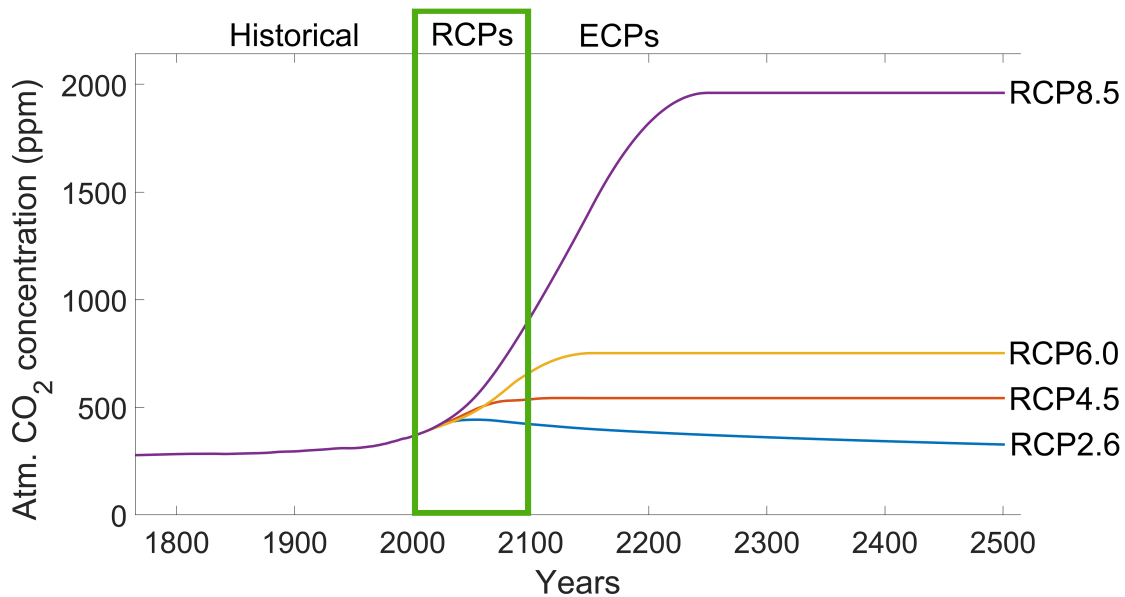
Figure 5.1: Atmospheric CO_2 concentration (ppm) over time for the RCP scenarios and their extensions. The four scenarios presented are the scenarios used by the fifth IPCC Assessment Report to model future climate projections. The database is divided into three periods: the period from 1765 to 2005 represents the historical records, the period from 2005 to 2100 represents the RCPs scenarios (green rectangle) and the period from 2100 to 2500 represents the ECPs scenarios. Data from Meinshausen et al. [2011].

Model description

The Earth system model used is called EcoGENIE [Ward et al., 2018] and is an association between a new ecosystem component and a previous model (GENIE; Lenton et al. [2007]). GENIE has been widely used to study past climate systems and the carbon cycle over geological times [Gibbs et al., 2016; Meyer et al., 2016; Greene et al., 2019]. EcoGENIE has already been used to analyze the role of marine phytoplankton in the warm early Eocene period [Wilson et al., 2018]. We used the same configuration as described in detail in Chapter 3 and therefore only briefly explain the climate modules here. For this study, we modify the ecosystem component and the oceanic component to implement phytoplankton light absorption.

Modules

Ocean, atmosphere and sea-ice

The oceanic component is a 3D frictional-geostrophic oceanic component (GOLDSTEIN) that calculates the horizontal and vertical redistribution of heat, salinity and biogeochemical elements. The horizontal grid (36×36) is uniform in longitude and uniform in sine latitude, giving ~$3.2°$ latitudinal increments at the equator increasing to $19.2°$ in the polar regions. This horizontal grid has been used to study the global carbon cycle [Cameron et al., 2005].

Furthermore, we consider 32 vertical oceanic layers, increasing logarithmically from 29.38 m for the surface layer to 456.56 m for the deepest layer (Chapter 3).

The atmospheric component (EMBM) is based closely on the UVic Earth system model [Weaver et al., 2001] and is a 2D model. Atmospheric temperature and specific humidity are the prognostic variables. Precipitation instantaneously removes all moisture corresponding to the excess above a relative humidity threshold.

The sea-ice component (GOLDSTEINSEAICE) considers ice thickness and ice areal fraction as prognostic variables. The transport of sea-ice includes the sources and sinks of these variables. The growth and decay of sea-ice depend on the net heat flux into the sea-ice. The sea-ice component acts as a coupling module between the ocean and the atmosphere, where heat and freshwater are exchanged and conserved between these three modules.

Ocean biogeochemistry

The biogeochemical module (BIOGEM) represents the transformation and spatial redistribution of biogeochemical tracers [Ridgwell et al., 2007]. The state variables are inorganic resources and organic matter. Organic matter is partitioned into dissolved and particulate organic matter (DOM and POM). The model includes iron (Fe) and phosphate (PO_4) as limiting nutrients but similar to Chapter 3, we do not consider nitrate (NO_3^-) here. Furthermore, BIOGEM calculates the air-sea CO_2 and O_2 exchange.

Ecosystem community

The marine ecosystem component (ECOGEM) represents the marine plankton community and associated interactions within the ecosystem [Ward et al., 2018]. The biological uptake in ECOGEM is limited by light, temperature and nutrient availability. Plankton biomass and organic matter are subject to processes such as resource competition and grazing before being passed to DOM and POM. The ecosystem is divided into different plankton functional types (PFTs) with specific traits. Furthermore, each PFT is sub-divided into size classes with specific size-dependent traits. We incorporate two classes of PFTs: phytoplankton and zooplankton. Phytoplankton is characterized by nutrient uptake and photosynthesis whereas zooplankton is characterized by predation traits. Zooplankton grazing depends on the concentration of prey biomass availability, predominantly grazing on preys that are 10 times smaller than themselves. Each population is associated with biomass state variables for carbon, phosphate and chlorophyll. The production of dead organic matter is a function of mortality and messy feeding, with partitioning between non-sinking DOM and sinking POM. Finally, plankton mortality is reduced at very low biomasses such that plankton cannot become extinct.

Phytoplankton light absorption

In the model configuration of this study, the incoming shortwave radiation varies seasonally. The presence of organic matter, inorganic matter and dissolved molecules limit the propagation of light within the ocean [Ward et al., 2018]. The vertical light attenuation scheme is given by Eq. 5.1

$$I(z) = I_0 \cdot \exp(-k_w - k_{Chl} \cdot Chl_{tot}) \cdot z \qquad (5.1)$$

where $I(z)$ is the radiation at depth z, I_0 is the radiation at the surface of the ocean, k_w is light absorption by clear water (0.04 m^{-1}), k_{Chl} is the light absorption by chlorophyll (0.03 $m^{-1}(mg\ Chl)^{-1}$) and Chl_{tot} is the total chlorophyll concentration. The values for k_w and

k_{Chl} are taken from Ward et al. [2018]. The parameter I_0 is negative in the model because it is a downward flux from the sun to the surface of the ocean. The light penetrates until the sixth oceanic layer of the model (221.84 m), where maximum absorption occurs in the surface layer and minimum light absorption happen in the sixth layer. As seen in Chapters 3 and 4, phytoplankton changes the optical properties of the ocean through phytoplankton light absorption. It can cause a radiative heating and change the heat distribution in the water column. We implemented phytoplankton light absorption into the model following Hense [2007] and Patara et al. [2012] Eq.5.2:

$$\frac{\partial T}{\partial t} = \frac{1}{\rho \cdot c_p} \frac{\partial I}{\partial z} \tag{5.2}$$

$\partial T / \partial t$ denotes the temperature changes, c_p is the specific heat capacity of water, ρ is the ocean density, I is the solar radiation incident at the ocean surface, and z is the depth. We assume that the whole light absorption leads to a heating of the water [Lewis et al., 1983].

Model setup and simulations

We use EcoGENIE [Ward et al., 2018] to study the effect of global warming and the resulting changes on phytoplankton light absorption. We use the same model setup and parametrization as described in Chapter 3, with a 32 layer vertical oceanic grid, primary production allowed until the sixth grid layer (221.84 m deep) and a seasonally variable incoming shortwave radiation. The ecosystem community is consistent with the community described in Chapters 3 and 4, with one phytoplankton species and one zooplankton species (Appendix 5.1). We first run a 10,000 years spin-up with only BIOGEM to have a realistic distribution of nutrients. The simulations restart after the spin-up for 737 years with ECOGEM. The simulations are 737 years long because it is the duration available for the atmospheric CO_2 concentration in the RCP dataset [Meinshausen et al., 2011]. We run the simulations with prescribed atmospheric CO_2 restoring forcings (Figure 5.1; Table 5.1) and not prescribed CO_2 emissions to ensure that the atmospheric CO_2 concentration between our simulations and the RCP scenarios are consistent. Moreover, all simulations are forced with the same constant flux of dissolved iron into the ocean surface [Mahowald et al., 2006].

Table 5.1: Name, description and atmospheric CO_2 concentration (ppm) at the end of the simulations (PLA = phytoplankton light absorption).

Simulation	Description	Atm. CO_2 (ppm)
PI	Pre-industrial run	280
PI-LA	Pre-industrial run with PLA	280
RCP2.6	RCP2.6 scenario	327
RCP2.6-LA	RCP2.6 scenario with PLA	327
RCP4.5	RCP4.5 scenario	543
RCP4.5-LA	RCP4.5 scenario with PLA	543
RCP6.0	RCP6.0 scenario	752
RCP6.0-LA	RCP6.0 scenario with PLA	752
RCP8.5	RCP8.5 scenario	1961
RCP8.5-LA	RCP8.5 scenario with PLA	1961

PI-LA and *PI* are the pre-industrial simulations, with and without phytoplankton light absorption, respectively. *RCP2.6-LA* and *RCP2.6* are the simulations following the RCP2.6

scenario, with and without phytoplankton light absorption, respectively. The simulations *RCP4.5-LA* and *RCP4.5* follow the RCP4.5 scenario, with and without phytoplankton light absorption, respectively. The simulations *RCP6.0-LA* and *RCP6.0* follow the RCP6.0 scenario, with and without phytoplankton light absorption, respectively. Finally, *RCP8.5-LA* and *RCP8.5* are the simulations following the RCP8.5 scenario, with and without phytoplankton light absorption, respectively.

Climate system with and without phytoplankton light absorption

This study is divided into two parts: (1) first we compare the effect of phytoplankton light absorption under the same scenario (e.g. comparing *RCP2.6-LA* and *RCP2.6*), and (2) second we compare the effect of phytoplankton light absorption on future climate' evolution (e.g. comparing *RCP2.6-LA* and *PI-LA*). In this section, we look at climate-relevant variables such as chlorophyll biomass, surface PO_4 concentration, sea surface temperature, and surface atmospheric temperature.

Pre-industrial scenario

To study the effect of phytoplankton light absorption on the climate system under a pre-industrial scenario, we compare the simulations *PI-LA* and *PI*. In these simulations, the atmospheric CO_2 is fixed to a pre-industrial concentration, i.e. 280 ppm.

Phytoplankton biomass and phosphate concentration at the surface

On a global scale, the chlorophyll concentration is higher by 0.0183 mgChl/m^3 in the simulation *PI-LA* (Figure 5.2a) which is a similar order of magnitude as the increase in phytoplankton biomass in Chapter 3 and 4. Furthermore, pronounced regional differences occur between the simulations *PI-LA* and *PI*. The largest chlorophyll biomass fluctuations are located in the polar regions where sea-ice thickness decreases by 1.66 mm in *PI-LA*, increasing the light availability and stimulating the growth of phytoplankton in high-latitude regions. Moreover, the upwelling and mid-latitude regions show a higher chlorophyll concentration in the simulation *PI-LA*. These local patterns are due to enhanced upward vertical velocity in *PI-LA*, increasing the surface phosphate (PO_4) concentration by 0.073 mmol/m^3 (Figure 5.2b), permitting a higher nutrient uptake and therefore a higher phytoplankton biomass (Chapter 3; Manizza et al. [2008]). The Southern Ocean is characterized by a large increase of PO_4 while the increase in chlorophyll biomass is smaller. The response of the phytoplankton biomass is not as large as expected because the phytoplankton in the Southern Ocean is limited by iron.
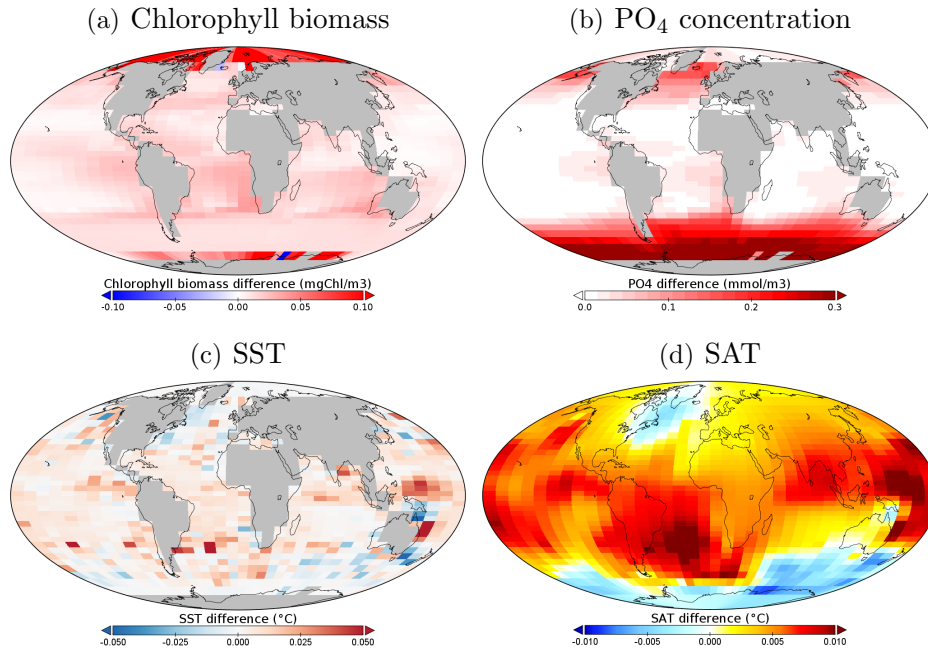
Figure 5.2: Comparison of the climate-relevant variables between the simulation PI-LA and PI. (a) Surface chlorophyll biomass difference (mgChl/m³). (b) Surface phosphate concentration difference (mmol/m³). (c) Sea surface temperature difference (°C). (d) Surface atmospheric temperature difference (°C). For the panels (a), (c) and (d) the color coding is similar. White color indicates no difference. Blue color represents a lower while red color indicates a higher chlorophyll biomass, SST or SAT in PI-LA. For the panel (b), white color indicates no changes while red color represents a higher PO_4 concentration in PI-LA. Note that for this panel, the difference is always positive.

Sea surface temperature

Due to higher chlorophyll biomass at the surface, we expect variations in SST (Figure 5.2c). In this instance, SST is defined as the mean temperature in the upper surface layer, from the surface to 29.38 m depth, which for practical purposes is called SST. Globally, the SSTs are nearly identical between *PI-LA* and *PI*, with a small increase of 0.00453°C in the simulation with phytoplankton light absorption. This result is in agreement with previous pre-industrial simulations that study this biogeophysical mechanism [Paulsen, 2018]. However, on a local scale, the maximum SST variation of 0.066°C located in the southern Atlantic Ocean is lower than previous estimates [Paulsen, 2018]. These lower local estimates are due to the coarse resolution of the grid and the local underestimation of the vertical velocity field of our model. Even if the local SST variations are rather small, Figure 5.2c indicates that the Southern Ocean and the northern Atlantic Ocean are characterized by a decrease of SST with phytoplankton light absorption. The patterns of chlorophyll biomass (Figure 5.2a) and SST (Figure 5.2c) are different and can be explained by the model setup. The state variables of the ecosystem component, such as chlorophyll biomass, are not subject to transport while physical quantities, such as heat, are transported by ocean currents. Heat is therefore redistributed all around the globe, explaining the missing spatial coincidence between chlorophyll biomass and SST.

Surface atmospheric temperature

Changes in oceanic heat budget and sea surface temperature affect the atmospheric radiative budget and the atmospheric temperature [Tokarska et al., 2016]. The small SST increase drives the small increase in surface atmospheric temperature (SAT) on a global scale (Figure 5.2d). Globally, the SATs are practically similar between *PI-LA* and *PI*, with a higher SAT of 0.004°C in the simulation *PI-LA*. This result is in agreement with the pre-industrial simulations of Paulsen [2018]. On a local scale, the maximum increase of SAT is 0.016°C, located in the southern Atlantic Ocean. The spatial patterns of SAT are similar to the spatial patterns of SST with a decrease of temperature in the Southern Ocean and the northern Atlantic Ocean in the simulation with phytoplankton light absorption.

RCP scenarios

In the following section, we describe the response of the climate system to phytoplankton light absorption under the different RCPs scenarios. We compare simulations with and without the biogeophysical mechanism under the same RCP scenario.

Chlorophyll biomass and phosphate concentration at the surface

On a global scale, under each RCP scenario, the simulations considering phytoplankton light absorption have higher chlorophyll biomass than the simulations without this biogeophysical mechanism (Figure 5.3; Table 5.2). The increase in surface chlorophyll biomass under the RCP scenarios is of similar order of magnitude as the increase in chlorophyll biomass under the pre-industrial scenario. On a local scale, differences are visible between each panel of Figure 5.3, particularly in the polar regions. Variations of sea-ice in high latitudes modify the light availability and therefore lead to important variations of phytoplankton biomass. Additionally, the strong fluctuations of chlorophyll biomass in the polar regions (Figure 5.3) are due to the rather coarse resolution of the grid in these regions. The local patterns in the upwelling and mid-latitude regions between pre-industrial (Figure 5.2a) and RCPs scenarios (Figure 5.3) are similar. In these regions, the chlorophyll biomass is higher in the simulations with phytoplankton light absorption, due to enhanced upward vertical velocity and nutrients distribution. Globally, the phosphate concentrations are higher in the simulations with phytoplankton light absorption (Figure 5.4; Table 5.2), allowing a higher nutrient uptake and an increase in phytoplankton growth in the upwelling and mid-latitude regions. As previously explained, the large increase of PO_4 in the Southern Ocean is not followed by a corresponding increase of chlorophyll biomass because the phytoplankton is limited by iron in the Southern Ocean.

(a) RCP2.6-LA - RCP2.6   (b) RCP4.5-LA - RCP4.5

(c) RCP6.0-LA - RCP6.0   (d) RCP8.5-LA - RCP8.5
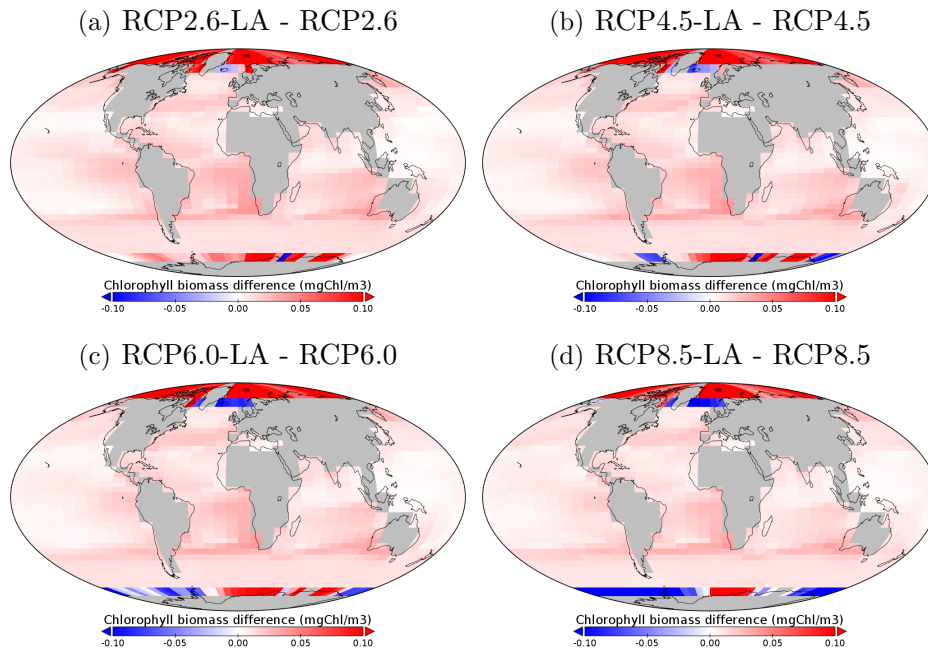
Figure 5.3:   Chlorophyll biomass difference (mgChl/m^3) between the simulations: (a) RCP2.6-LA - RCP2.6, (b) RCP4.5-LA - RCP4.5, (c) RCP6.0-LA - RCP6.0 and (d) RCP8.5-LA - RCP8.5. The color coding is identical for all panels. White color indicates no difference of chlorophyll biomass. Blue color represents a lower while red color indicates a higher chlorophyll biomass in the simulation with phytoplankton light absorption.

(a) RCP2.6-LA - RCP2.6   (b) RCP4.5-LA - RCP4.5

(c) RCP6.0-LA - RCP6.0   (d) RCP8.5-LA - RCP8.5
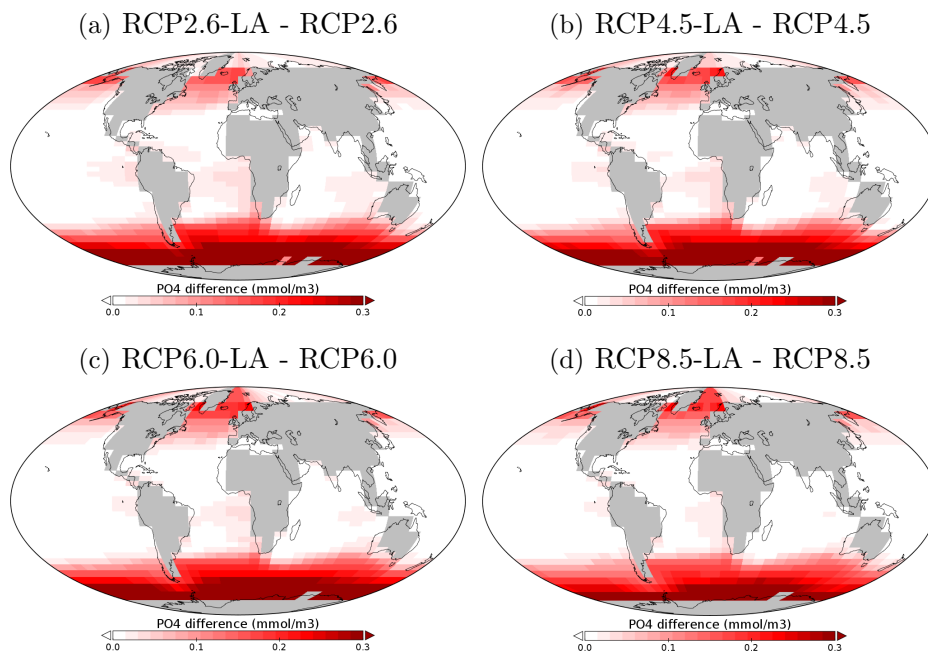
Figure 5.4:   Phosphate concentration difference (mmol/m^3) between the simulations: (a) RCP2.6-LA - RCP2.6, (b) RCP4.5-LA - RCP4.5, (c) RCP6.0-LA - RCP6.0 and (d) RCP8.5-LA - RCP8.5. The color coding is identical for all panels. White color represents no difference while red color indicates a higher PO_4 concentration in the simulation with phytoplankton light absorption. Note that the difference are always positive between simulations.

Sea surface temperature

Due to higher chlorophyll biomass with phytoplankton light absorption under the RCP scenarios, we also expect changes in sea surface temperature (Figure 5.5). On a global scale, the changes of SST under the RCP scenarios are low and slight variations occur between each scenario (Table 5.2). The global increase in phytoplankton biomass has a small global effect on the surface oceanic heat budget. These small global variations of SST between the simulations with and without phytoplankton light absorption are due to the prescribed atmospheric CO_2 concentrations. In Chapters 3 and 4, we show that phytoplankton light absorption increases the atmospheric CO_2 concentration. Moreover, we show in Chapter 4 that phytoplankton light absorption mainly affects the climate system via the air-sea CO_2 exchange. However, during this study and with our model setup, the atmospheric CO_2 concentration is prescribed therefore the biologically-driven air-sea CO_2 flux does not affect the climate system. Thus, simulations under the same RCP scenario have the same atmospheric CO_2 concentration and therefore small changes in heat budget and SST occur on a global scale. In contrast, on a local scale, large and sparse SST fluctuations are detected. For instance in Figure 5.5c, the maximum SST fluctuation is 0.18°C in the Southern Ocean, which is consistent with regional warming found elsewhere by Sonntag [2013] under his specific global warming scenarios. However, Paulsen [2018] find a more substantial regional SST warming, mainly in the upwelling regions, compared to our regional warming. Our lower estimates are due to the underestimation of the vertical velocity field in the upwelling regions. The spatial patterns of Figure 5.5 are similar to Figure 5.2c, with a decrease of SST in the Southern Ocean and the northern Atlantic Ocean. Once again, the missing spatial coincidence between the chlorophyll biomass patterns and the SST patterns is due to the model setup.
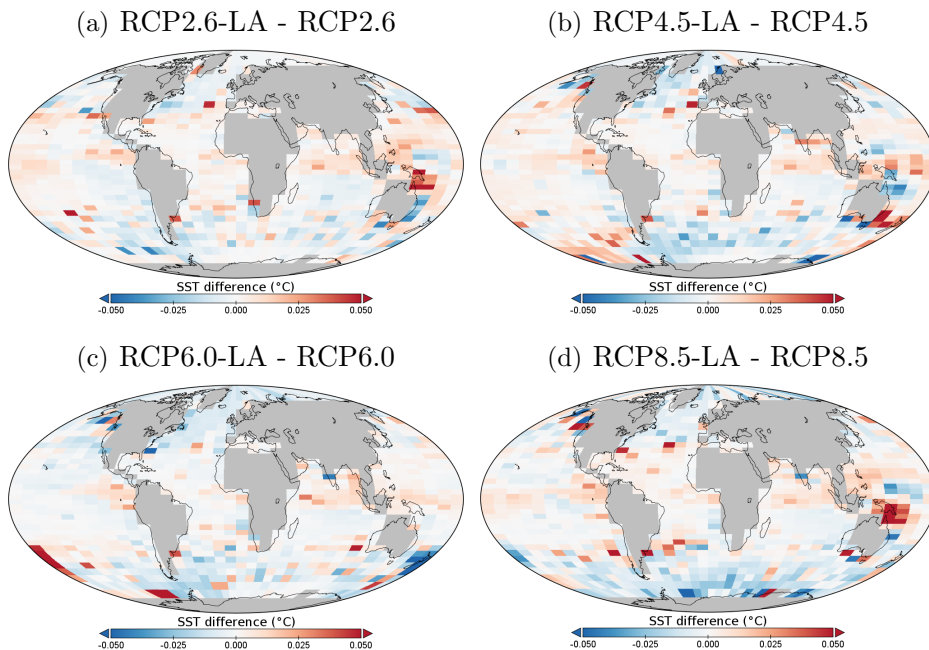
Figure 5.5: Sea surface temperature difference (°C) between the simulations: (a) RCP2.6-LA - RCP2.6, (b) RCP4.5-LA - RCP4.5, (c) RCP6.0-LA - RCP6.0 and (d) RCP8.5-LA - RCP8.5. The color coding is identical for all panels. White color indicates no difference of sea surface temperature. Blue color represents a lower while red color indicates a higher SST in the simulation with phytoplankton light absorption.

Surface atmospheric temperature

Due to the small variations in SST and prescribed atmospheric CO_2 concentration, the global difference of surface atmospheric temperature is small (Figure 5.6; Table 5.2). In Chapter 4, we show that the air-sea CO_2 flux is the most important climate pathway for the biologically-induced atmospheric warming. Due to the prescribed atmospheric CO_2 concentration this climate pathway does not affect the SAT. As a consequence, the difference of SAT between simulations under the same RCP scenario is pretty small, with temperature variations <0.02°C. In contrast on a local scale, large SAT fluctuations occur between simulations with and without phytoplankton light absorption. For instance, in Figure 5.6c the maximum SAT difference of 0.63°C is located in the Southern Ocean. This strong and local increase is consistent with the regional warming found by Paulsen [2018] under her specific global warming simulations. Moreover, the spatial patterns of change in SAT reflect the spatial patterns of change in SST. The SAT decreases in the Southern Ocean and the northern Atlantic Ocean, similar to the pattern of change under the pre-industrial scenario (Figure 5.2d).

(a) RCP2.6-LA - RCP2.6   (b) RCP4.5-LA - RCP4.5

(c) RCP6.0-LA - RCP6.0   (d) RCP8.5-LA - RCP8.5
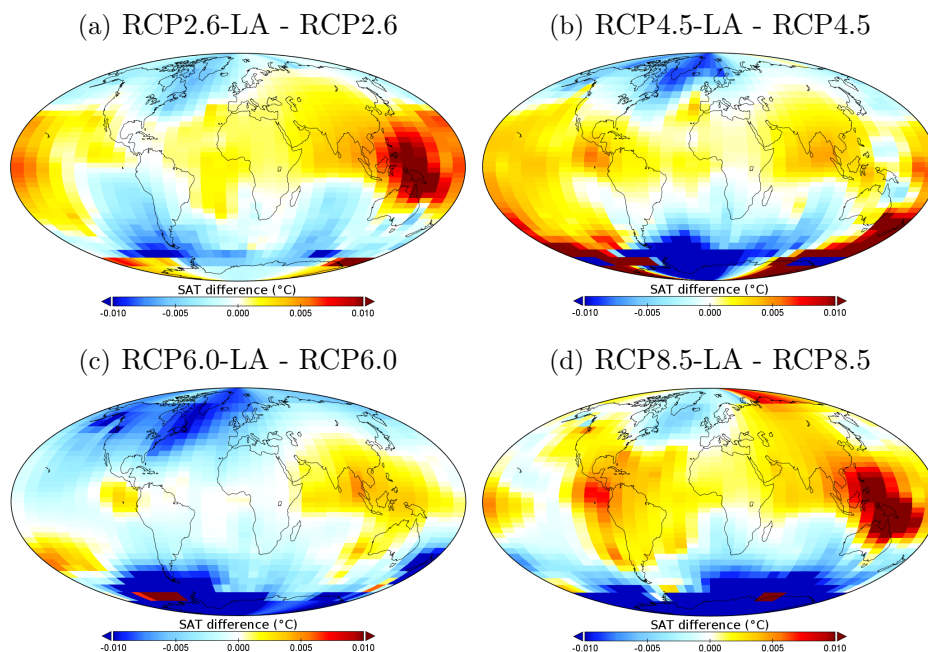
Figure 5.6: Surface atmospheric temperature difference (°C) between the simulations: (a) RCP2.6-LA - RCP2.6, (b) RCP4.5-LA - RCP4.5, (c) RCP6.0-LA - RCP6.0 and (d) RCP8.5-LA - RCP8.5. The color coding is identical for all panels. White color indicates no difference of surface atmospheric temperature. Blue color represents a lower while red color indicates a higher SAT in the simulation with phytoplankton light absorption.

Scenarios comparison

The response of the climate system to phytoplankton light absorption is, to some extent, similar between each scenario (Table 5.2). On a global scale, phytoplankton light absorption increases chlorophyll concentration and these values are in similar order of magnitude as previous estimates [Manizza et al., 2005, and Chapter 3]. Furthermore, the phosphate concentration increases in the simulations with the active biogeophysical mechanism. These changes in biogeochemical properties are due to a shallower downward flux of organic mat-

ter and an enhanced upward vertical velocity field (see Chapter 3). These global increases in surface nutrient field and phytoplankton biomass do not affect the oceanic and atmospheric energy budget, indeed the changes in SST and SAT are minor and trivial. These small changes are due to the prescribed and identical atmospheric CO_2 concentration for simulations under the same RCP scenario. With prescribed atmospheric CO_2 concentration, the biologically-driven air-sea CO_2 flux cannot affect the global response of the climate system when phytoplankton light absorption is considered. To capture the global effect of this biogeophysical mechanism, it is important to let the atmospheric CO_2 concentration evolve freely. In contrast, prescribing atmospheric CO_2 concentration is sufficient to capture the regional patterns in SST and SAT. On a local scale, the magnitude of change in SST and SAT are in agreement with previous studies under pre-industrial [Paulsen, 2018] and future climate scenarios [Sonntag, 2013; Paulsen, 2018].

Table 5.2: Global differences between the simulations with and without phytoplankton light absorption for the climate-relevant variables. The values for the chlorophyll biomass and PO_4 concentration represent the surface values.

Scenario	Chl. biomass (mgChl/m^3)	PO$_4$ (mmol/m^3)	SST (°C)	SAT (°C)
PI	0.01830	0.073	0.00453	0.004
RCP2.6	0.01833	0.074	0.00072	0.00033
RCP4.5	0.01748	0.073	0.00007	-0.00079
RCP6.0	0.01795	0.071	-0.00118	-0.00145
RCP8.5	0.01210	0.064	-0.00067	-0.00156

Phytoplankton light absorption on future climate' evolution

To address the effect of a changing phytoplankton distribution on future climate' evolution with phytoplankton light absorption, we compare the relative difference of RCP simulations (*RCP6.0-LA* and *RCP6.0*) to their respective pre-industrial climate states (*PI-LA* and *PI*). We only take into account the RCP6.0 scenario because the global climate response is identical between all RCP scenarios. We choose this RCP scenario because it is the closest scenario to previous studies, we can therefore compare our results with the estimates of Paulsen [2018]. We first elaborate on the effects on phytoplankton biomass, followed by the resulting impact on the sea surface temperature, and finally, we describe changes in the surface atmospheric temperature.

Surface chlorophyll biomass

On a global scale, phytoplankton biomass declines under global warming (Figure 5.7). The global decrease of chlorophyll biomass between *RCP6.0-LA* and *PI-LA* is about 0.00098 mgChl/m^3 while between *RCP6.0* and *PI*, it is about 0.00063 mgChl/m^3. These global differences represent a total decrease of ∼0.5% in phytoplankton biomass which is in agreement with previous modeling estimates [Boyce et al., 2010; Steinacher et al., 2010; Bopp et al., 2013]. These global decreases are due to changes in oceanic circulation and nutrient supply. The higher oceanic temperature in the simulations under the RCP scenario leads to enhanced ocean mixing and increases the ocean stratification (Appendix 5.2) which is consistent with Capotondi et al. [2012]. As a consequence, the nutrients at the surface are

reduced, especially the phosphate concentration, increasing nutrient stress for phytoplankton, in agreement with Bopp et al. [2001]. Our results indicate that phytoplankton light absorption increases the decline in chlorophyll biomass due to global warming (Figure 5.7c), and this is due to a stronger decrease in surface phosphate concentration when the biogeophysical mechanism is active. The surface PO_4 concentration decreases by 0.004 mmol/m^3 between *RCP6.0-LA* and *PI-LA* while it decreases by 0.0017 mmol/m^3 between *RCP6.0* and *PI*. This stronger decrease in surface PO_4 concentration between *RCP6.0-LA* and *PI-LA* is due to a smaller increased oceanic velocity between these simulations compared to the simulations between *RCP6.0* and *PI* (Appendix 5.2). The smaller increase in oceanic mixing between *RCP6.0-LA* and *PI-LA* lead to a higher decrease of phosphate at the surface and thus a stronger decrease of surface chlorophyll biomass between these simulations.

(a) RCP6.0LA - PI-LA (b) RCP6.0 - PI (c) (RCP6.0LA - PI-LA) - (RCP6.0 - PI)
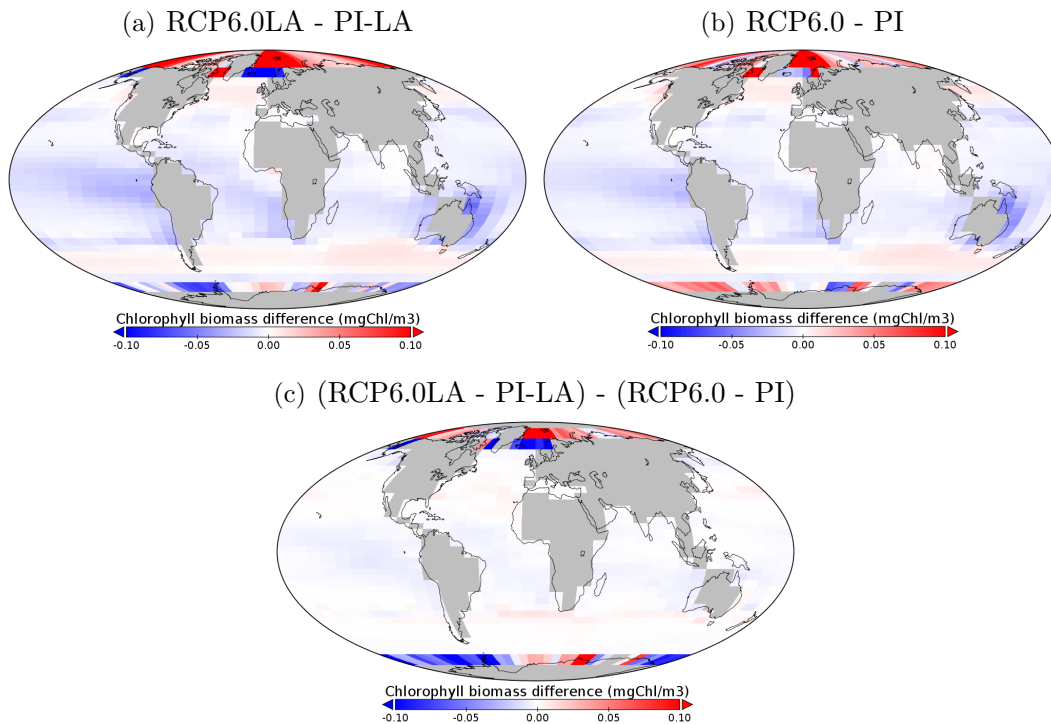
Figure 5.7: Changes in chlorophyll biomass (mgChl/m^3) between the simulations (a) RCP6.0LA - PI-LA, (b) RCP6.0 - PI. White color indicates no difference of chlorophyll biomass. Blue color represents a lower while red color indicates a higher chlorophyll biomass in the simulations under the global warming scenario. (c) (RCP6.0LA - PI-LA) - (RCP6.0 - PI). White color indicates no difference of chlorophyll biomass. Blue color represents a lower while red color indicates a higher chlorophyll biomass in the simulations with phytoplankton light absorption.

Sea surface temperature

Globally, the SST is higher in the simulations under the global warming scenario (Figure 5.8a-b). The SST increases by 3.454°C between the simulations *RCP6.0-LA* and *PI-LA* while it increases by 3.459°C between *RCP6.0* and *PI*. This large increase is of similar order of magnitude as the SST increase found by Paulsen [2018] with a transient increase of atmospheric CO_2 concentration. The higher SST under the RCP scenario is due to the higher atmospheric CO_2 concentrations under this scenario, increasing the overall heat budget and the SST. The global increase of SST is uniform around the globe, except in the polar regions

where changes in sea-ice and the relatively coarse resolution explain the weaker warming of the ocean surface. Furthermore, the regional patterns are consistent between Figure 5.8a and Figure 5.8b, indicating that phytoplankton light absorption does not alter the local increase of SST. On a global scale, phytoplankton light absorption reduces the warming of the ocean surface by 0.0057°C (Figure 5.8c). This lower increase of SST is related to the stronger decline in chlorophyll biomass in the simulations with the active biogeophysical mechanism. Less chlorophyll biomass absorbs less light and traps less heat in the ocean surface, explaining the reduced SST increase with phytoplankton light absorption. This result is in agreement with previous suggestions discussed by Patara et al. [2012].

(a) RCP6.0LA - PI-LA   (b) RCP6.0 - PI

(c) (RCP6.0LA - PI-LA) - (RCP6.0 - PI)
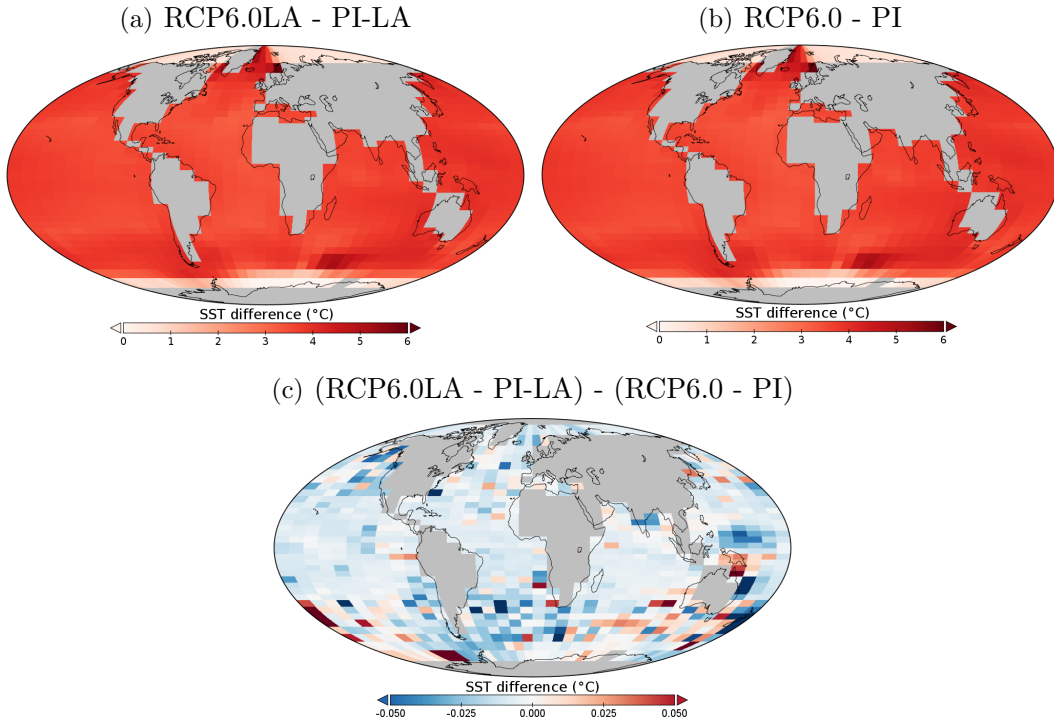
Figure 5.8:   Changes in sea surface temperature (°C) between the simulations (a) RCP6.0LA - PI-LA and (b) RCP6.0 - PI. White color represents no difference while red color indicates a higher SST in the simulations under the global warming scenario. (c) Difference between (RCP6.0LA - PI-LA) - (RCP6.0 - PI). White color indicates no difference of sea surface temperature. Blue color represents a lower while red color indicates a higher SST in the simulations with phytoplankton light absorption.

Surface atmospheric temperature

On a global scale, the SAT is higher in the simulations under the warming scenario (Figure 5.9a-b). The SAT increases by 4.43°C between *RCP6.0-LA* and *PI-LA* and increases by 4.44°C between *RCP6.0* and *PI*. These global increases of SAT between the RCP6.0 and pre-industrial scenarios are due to the higher atmospheric CO_2 concentration leading to a higher greenhouse gas effect in the simulations under the global warming scenario. Furthermore, the global increase of SAT is uniform around the globe, except above the polar regions. These regional patterns are due to rather coarse grid resolution in the high latitude regions. The local increase of SAT can be up to 6°C, which is in agreement with the local warming found by [Paulsen, 2018]. Globally, phytoplankton light absorption reduces the warming of the atmosphere by 0.0053°C (Figure 5.9c). This phenomenon is due to the

smaller increase of SST in the simulations with phytoplankton light absorption, leading to weaker sea-air heat exchange, decreasing therefore the warming of the atmosphere.

(a) RCP6.0LA - PI-LA (b) RCP6.0 - PI

(c) (RCP6.0LA - PI-LA) - (RCP6.0 - PI)
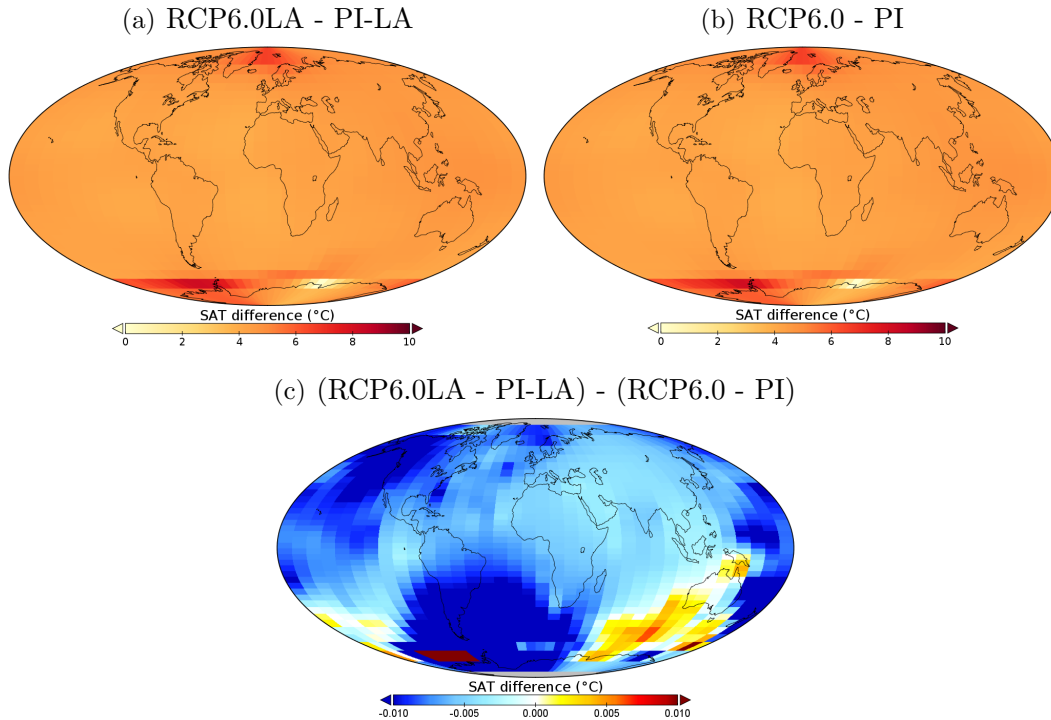
Figure 5.9: Changes in surface atmospheric temperature (°C) between the simulations (a) RCP6.0LA - PI-LA and (b) RCP6.0 - PI. White color represents no difference while red color indicates a higher SAT in the simulations under the global warming scenario. (c) Difference between (RCP6.0LA - PI-LA) - (RCP6.0 - PI). White color indicates no difference of surface atmospheric temperature. Blue color represents a lower while red color indicates a higher SAT with phytoplankton light absorption.

Summary and conclusions

The effect of phytoplankton light absorption on the climate system has been investigated by previous model studies under constant CO_2 forcing [Patara et al., 2012], under transient atmospheric CO_2 increase [Park et al., 2015; Paulsen, 2018] and under an artificial increase of SST [Sonntag, 2013]. As a logical extension, we conduct simulations under global warming scenarios taking into account future socio-economic aspects, with and without the biogeophysical mechanism to assess its impact on the future climate system. To study the role of phytoplankton light absorption under these scenarios, we implemented the biogeophysical mechanism into the EcoGENIE model [Ward et al., 2018]. We compare the effect of phytoplankton light absorption under RCPs and pre-industrial scenarios.

In the first part of the results section we show that, for all scenarios, the surface chlorophyll biomass and surface phosphate concentrations increase when phytoplankton light absorption is considered. However, these changes in biogeochemical properties slightly affect the oceanic and atmospheric budget on a global scale (Table 5.2). These slight global variations of temperature are due to the prescribed atmospheric CO_2 concentration between simulations under the same RCP scenario. Previous studies find that phytoplankton light

absorption has a significant effect on the climate system (Chapter 3) and alters the air-sea CO_2 flux (Chapter 4). Therefore prescribing the atmospheric CO_2 concentration for climate studies will blur the real effect of phytoplankton light absorption on the climate system. To capture the global effect of phytoplankton light absorption under global warming, we suggest to prescribe the CO_2 emissions rather than the atmospheric CO_2 concentration. In contrast, prescribing atmospheric CO_2 concentration is sufficient to capture the regional patterns in SST and SAT. Moreover, the effect of phytoplankton light absorption is similar between the different RCP scenarios. For each scenario, the changes in heat budget associated with the active biogeophysical mechanism are smaller than the changes in heat budget due to the increased atmospheric CO_2 concentration.

In the second part of the results section, our simulations indicate that global warming leads to a decrease in chlorophyll biomass and this result is supported by previous modeling studies [Steinacher et al., 2010; Bopp et al., 2013] and observations [Polovina et al., 2008; Boyce et al., 2010]. Furthermore, our results indicate a reduced increase in SST and SAT when phytoplankton light absorption is implemented in the simulations. Global warming reduces the phytoplankton abundance, increasing ocean clarity and reducing the biologically-induced increase of SST and atmospheric temperature. The predicted damping in phytoplankton biomass can therefore counteract the global warming of the planet, as suggested by [Patara et al., 2012].

More observations and research are needed to understand and simulate the role of phytoplankton in a changing climate system. Specifically, microorganisms such as cyanobacteria are expected to expand with future climate change [O'Neil et al., 2012; Paerl and Paul, 2012; Ullah et al., 2018] and their impact on the climate system through phytoplankton light absorption is important [Anderson et al., 2007; Sonntag, 2013; Paulsen et al., 2018]. A logical follow-up would be to include cyanobacteria in a similar study. Our research indicates that phytoplankton should be considered as an internal constituent of the climate system and thus is interacting with other climate components through biogeophysical mechanisms such as phytoplankton light absorption.

Appendices

Plankton functional types

We base our ecosystem community on the community described by Ward et al. [2018]. However, instead of using 16 plankton functional types (PFTs) we only use 2 PFTs: one phytoplankton group and one zooplankton group (Appendix 5.1). We show that the complexity of the ecosystem does not have an important impact on the climate system compared to the effect of phytoplankton light absorption (Chapter3). Therefore we reduced the ecosystem complexity to increase the computational time of the model.

Appendix 5.1: Size of the different plankton functional types (μm) used during the simulations.

PFT	Size (μm)
Phytoplankton	46.25
Zooplankton	146.15

Surface phosphate concentration and oceanic mixing

Global warming increases the overturning circulation and therefore decreases the mixed layer depth (MLD). As a consequence, the surface phosphate concentration decreases in the global warming scenario compared to the pre-industrial scenario. For instance, the phosphate concentration decreases by 0.0040 mmol/m^3 between *RCP6.0-LA* and *PI-LA*, and decreases by 0.0017 mmol/m^3 between *RCP6.0* and *PI*. These results indicate that phytoplankton light absorption leads to a stronger decrease in nutrient supply due to smaller increased oceanic velocity.

Appendix 5.2: Simulated phosphate concentration at the surface (mmol/m^3), maximum AMOC (Sv) and mixed layer depth (m).

Simulation	PO$_4$ conc. (mmol/m^3)	AMOC max. (Sv)	MLD (m)
RCP6.0-LA	0.2734	18.184	122.1
RCP6.0	0.2024	18.212	121.9
PI-LA	0.2774	15.226	123.1
PI	0.2041	15.237	123.3

SUMMARY AND CONCLUSIONS

In this thesis, I investigated the role of phytoplankton in the climate system and how it can affect its environment. I focus on one particular biogeophysical mechanism: phytoplankton light absorption. For this purpose, I implemented this mechanism in EcoGENIE, an Earth system model on intermediate complexity. More specifically, I analyzed the relative importance of phytoplankton light absorption in the representation of the climate system. I also studied what are the climate pathways behind the biologically-induced atmospheric warming. Finally, in a set of global warming scenarios, I investigated the role of phytoplankton light absorption in a warmer world.

Research findings

Considering the work presented in the previous chapters, I can now answer the research questions raised in the introduction. In recent years, the scientific community has rather put its attention on increasing the complexity of Earth system models with respect to marine biota. But several observational [Smith and Baker, 1978; Wurl et al., 2018] and modeling studies [Wetzel et al., 2006; Lengaigne et al., 2007] have shown that phytoplankton light absorption affects significantly the climate system. One remaining question concerns the importance of phytoplankton light absorption on the climate system compared to a higher ecosystem complexity. Therefore my first research question is:

1. **Does phytoplankton light absorption have a higher impact on the climate system than an increase in marine ecosystem complexity?**

To answer this question, I compared the effect of phytoplankton light absorption on the climate system versus the effect of increasing ecosystem complexity. Phytoplankton light absorption affects the climate in various ways. This biogeophysical mechanism immediately affects the stratification and increases SST. The global increase in SST is in agreement with previous modeling studies [Manizza et al., 2005; Wetzel et al., 2006; Patara et al., 2012]. The higher SST with phytoplankton light absorption leads to a reduction of CO_2 solubility in the ocean. As a consequence, the air-sea CO_2 flux increases leading to higher atmospheric CO_2 concentration. My results evidence that by far changes in CO_2 solubility have the largest effect on the climate system but second-order effects occur. The downward carbon flux is shallower with phytoplankton light absorption, contributing to increase the atmospheric CO_2 concentration as well. Reduced sea-ice cover and enhanced upwelling only slightly affect the climate system. Overall, phytoplankton light absorption increases the surface atmospheric temperature by 0.45°C. This value is higher than previous estimates [Shell et al., 2003; Patara et al., 2012] due to the different experimental strategies and model setups between these studies and my work. Shell et al. [2003] use an uncoupled ocean-atmosphere model while Patara et al. [2012] prescribe the atmospheric CO_2 concentration in their simulations.

The stronger SAT response in my work is due to the coupled ocean-atmosphere model and the closed carbon cycle in which atmospheric CO_2 is allowed to evolve freely.

A higher marine ecosystem complexity affects the plankton community, influencing the partitioning of organic matter going into the dissolved and particulate phases. As a result, the vertically-integrated export production of POC increases while vertically-integrated DOC concentration decreases. The deeper downward flux of organic matter hardly influences the carbon cycle and with it the air-sea CO_2 flux. Hence the atmospheric CO_2 concentration is slightly reduced and the atmosphere cools down by 0.034°C with a higher ecosystem complexity. Furthermore, these slight changes in carbon cycle and atmospheric temperature hardly reduce the SST and chlorophyll biomass.

Considering my model setup, globally phytoplankton light absorption has a higher impact on the climate system than an increase in ecosystem complexity. Phytoplankton light absorption should thus be considered as a climate-relevant mechanism.

While I answered this first research question, I showed that phytoplankton light absorption warms the atmosphere. Previous modeling studies suggest that phytoplankton light absorption could affect the atmospheric temperature via air-sea heat exchange but none of them studied in detail this question [Capone et al., 1998; Wetzel et al., 2006]. Furthermore, previous studies [Manizza et al., 2008, and Chapter 3] suggest that phytoplankton-induced atmospheric warming might be due to changes in biogeochemical properties of the ocean, and thus in air-sea CO_2 flux. As a logical extension, I raised and answered the second research question:

2. **How does phytoplankton light absorption increase the atmosphere temperature?**

To answer this question, I focus on the interface between the ocean and the atmosphere. I compared the importance of the changes in air-sea heat flux and air-sea CO_2 exchange due to phytoplankton light absorption. With my model setup, I was able to isolate the individual effect of these two fluxes. First, my results evidence that considering only the air-sea heat flux slightly decreases the surface atmospheric temperature by 0.02°C. This decrease is mainly explained by the reduced amount of greenhouse gases when the CO_2 effect is neglected, thus increasing the outgoing longwave radiation. Second, my results show that considering only the air-sea CO_2 flux increases the surface atmospheric temperature by 0.71°C. The higher SAT is justified by the higher atmospheric CO_2 concentration and specific humidity when the heat effect is ignored.

With my model setup, I show that the phytoplankton-induced warming of the atmosphere is mainly due to increase air-sea CO_2 flux and resulting increase in atmospheric CO_2 concentrations. Furthermore, with my model setup, I show that changes in sea-ice distribution due to phytoplankton light absorption are small and thus hardly affect the air-sea climate pathways. In contrast, the sensible and longwave heat fluxes are reduced in the CO_2-solubility pathway, thus surface atmospheric temperature decreases.

Answering the second research question, I show that phytoplankton light absorption mainly increases the atmospheric temperature via increased air-sea CO_2 flux, resulting in higher atmospheric CO_2 concentration. With ongoing global warming, the atmospheric CO_2 concentration increases and the effect of phytoplankton light absorption is thus expected to change. This biogeophysical mechanism has been investigated under warmer ocean scenario [Sonntag, 2013] or transient increase in atmospheric CO_2 concentration [Park et al., 2015; Paulsen et al., 2018]. However, no studies investigate the effect of phytoplankton light

absorption under global warming scenarios taking into account future socio-economics aspects. In addition, the effect of phytoplankton light absorption under global warming has been investigated with idealized [Sonntag, 2013; Park et al., 2015] or complex climate models [Paulsen, 2018] but never with climate models of intermediate complexity. As a logical extension, I raised and answered the third research question:

3. **How does phytoplankton light absorption alter the climate system under global warming scenarios?**

First, I compared the effect of phytoplankton light absorption on the climate system under pre-industrial and RCPs scenarios. Considering this biogeophysical mechanism evokes similar responses of the climate system for the different scenarios. Independent of the scenario considered, phytoplankton light absorption increases the vertical velocity field and the phosphate concentration at the surface. These changes, in turn, increase the surface concentration of chlorophyll biomass but the overall planetary heat budget is slightly affected. The slight changes in atmospheric and sea surface temperature are due to the prescribed atmospheric CO_2 concentrations between the simulations. The prescribed atmospheric CO_2 concentrations blur the real effect of phytoplankton light absorption and the phytoplankton-driven increase in air-sea CO_2 flux cannot affect the climate system. To capture the effect of phytoplankton light absorption on a global scale, the atmospheric CO_2 concentration should thus be allowed to evolve freely. To study this biogeophysical mechanism under warming scenarios on a global scale, one option could be to prescribe the CO_2 emissions rather than the atmospheric CO_2 concentration. In contrast, prescribing atmospheric CO_2 concentration is sufficient to capture the regional effect of phytoplankton light absorption in the heat budget. The local magnitudes of changes in SST and SAT are in agreement with previous modeling estimates [Sonntag, 2013; Paulsen et al., 2018].

Second, I compare the effect of phytoplankton light absorption between a pre-industrial and an RCP scenario. My results evidence that global warming reduces the chlorophyll biomass, which is supported by previous modeling studies [Bopp et al., 2013] and observations [Boyce et al., 2010]. Furthermore, implementing phytoplankton light absorption leads to a stronger decline in chlorophyll biomass, further increasing ocean clarity. As a consequence, phytoplankton light absorption reduces oceanic and atmospheric heating due to global warming. My results demonstrate that the predicted damping in chlorophyll biomass can therefore slightly reduce the expected heating of the planet, slightly counteracting global warming, which is in agreement with Patara et al. [2012].

General conclusion

The results of this thesis suggest that rather than focusing on increasing ecosystem complexity, we should account for a larger number of marine biologically driven mechanisms in Earth system models to improve the quality of climate projections. I demonstrate that phytoplankton light absorption affects the climate system mainly via air-sea CO_2 exchange and is therefore important to let the atmospheric CO_2 concentrations evolve freely to study this biogeophysical mechanism in climate studies. My results evidence that prescribing atmospheric CO_2 concentration will blur the real effect of phytoplankton light absorption on the climate system under global warming scenarios. To study phytoplankton light absorption under climate change scenarios, it would be judicious to prescribe the CO_2 emissions rather than the atmospheric CO_2 concentration. Moreover, future changes in phytoplankton distribution and biogeography have the potential to affect the ongoing global warming via

this biogeophysical mechanism. My results conclude that phytoplankton light absorption influences the climate system on relevant scales and magnitude. As a comparison, the effect of this biogeophysical mechanism on the climate system is slightly smaller than the effect of the water-vapor feedback [Dessler et al., 2008] but higher than the wetland methane emissions feedback [Gedney et al., 2004]. Therefore, my work evidences that phytoplankton light absorption is a climate-relevant mechanism that should be considered by default in climate studies due to its large impact on long-term climate adjustment.

Extensions and perspectives of this work

This thesis is an important step to understand the role of marine biota in the climate system, however, further improvements are needed.

Model development

The ecophysiological parameters of EcoGENIE are well constrained by observations but switching from a parameterised biological pump (cGENIE; [Ridgwell et al., 2007]) to an explicit ecological model (EcoGENIE; [Ward et al., 2018]) slightly deteriorate the distributions of important biogeochemical tracers. For future work, EcoGENIE should be calibrated against biogeochemical observations with the EnKF methodology [Hargreaves et al., 2004; Annan et al., 2005].

The horizontal grid setup in this work gives valuable estimates in the low and mid-latitudes. However, in the high latitudes, where sea-ice is present, the grid resolution is coarse. To obtain better features and a more realistic sea-ice distribution, the horizontal grid resolution needs to be increased. For instance, Marsh et al. [2011] suggest using a 64 x 32 resolution which gives a better representation of the sea-ice dynamics in the polar regions.

In this thesis, I look at the importance of several climate mechanisms and focus on qualitative assessments. For quantitative comparisons between the climate mechanisms and processes, the model needs improvements. First, the single-layer atmospheric model introduces several weaknesses for the climate simulations. It could be replaced with the 3D reduced complexity Atmosphere General Circulation Model (AGCM) called PLASIM [Fraedrich et al., 2005; Lunkeit et al., 2007]. This model has already been coupled to the GENIE framework [Holden et al., 2016] and could upgrade the representation of the atmospheric properties. Second, to improve the global carbon cycle and the evaporation rate, the Efficient Numerical Land Scheme (ENTS; [Williamson et al., 2006]) could be coupled with EcoGENIE. This land surface model has already been coupled and calibrated with a different version of the GENIE framework [Holden et al., 2010; Kemppinen et al., 2019]. Third, the model could be extended by including a representation of the deep-sea sediments (SEDGEM; [Ridgwell and Hargreaves, 2007]), improving therefore the marine carbon cycle, specifically by sequestrating carbon compounds in the ocean floor on a millennial-scale.

Plankton functional types

During this work, I study phytoplankton light absorption with a phytoplankton community having the same traits: nutrient uptake and photosynthesis. However, several phytoplankton groups, such as cyanobacteria have traits that have the potential to alter relevant mechanisms: they are positively buoyant. In addition, cyanobacteria form surface blooms

extending over up to several million square meters [Capone et al., 1998]. The high concentration of positively buoyant cyanobacteria results in strong heat trapping at the surface of the ocean. Several observations [Kahru et al., 1993; Capone et al., 1998] and modeling studies [Hense, 2007; Paulsen et al., 2018] show that cyanobacteria affect the heat budget in the ocean via phytoplankton light absorption. However, none of the previous modeling studies considering cyanobacteria allow freely evolving atmospheric CO_2 concentrations. Implementing this particular phytoplankton group and trying to answer my research questions could be a logical extension of this work.

Further biogeophysical mechanisms

In this thesis, I only focus on the most considered biogeophysical mechanism in Earth system models: phytoplankton light absorption. However, phytoplankton blooms can affect ocean physics via two other biogeophysical mechanisms. Phytoplankton can first increase the surface and subsurface albedo [Balch et al., 1991], locally reducing the seasonal SST by 0.2°C [Jung and Moon, 2019]. Second phytoplankton can reduce the turbulent wind mixing [Deacon, 1979], locally changing the SST by ±1°C [Sonntag, 2013]. So far, only Sonntag and Hense [2011] with an idealized 1-D model and Sonntag [2013] with a 3D general circulation model coupled to a biogeochemical model compare the effect of the three biogeophysical mechanisms. Both studies evidence that the effects of phytoplankton light absorption and biologically-induced reduction of the wind drag are larger than the effects due to changes in the surface albedo. To assess, the importance of these mechanisms and how they affect the climate system, studies with Earth system models are necessary. Additionally, more observations and data are needed to correctly parameterize the albedo and turbulent wind mixing mechanisms in models.

Observations

In the different studies presented, the distribution of phytoplankton is plausible on a global scale. However, on a regional scale, more observations are needed to improve the local distribution and the effect of marine biota on the climate system. The distribution of phytoplankton should not only be investigated in a present-day climate but can also be analyzed under global warming. To study the future distribution of phytoplankton, more research should be done on the environmental control of phytoplankton [Boyd et al., 2010; Lewis et al., 2020; Van de Waal and Litchman, 2020].

In addition to improving the knowledge on phytoplankton light absorption, more studies about its parameterization are needed. In this thesis, I use an absorbing coefficient by chlorophyll of 0.03 m^{-1}(mg Chl)$^{-1}$ while others studies use a higher [Murtugudde et al., 2002; Oschlies, 2004; Paulsen et al., 2018] or lower [Olivieri and Chavez, 2000; Spitz et al., 2003] coefficient. Furthermore, I used a constant absorption coefficient by chlorophyll while this parameter depends on the wavelength of the light spectrum [Morel, 1988; Morel and Maritorena, 2001; Manizza et al., 2008]. Therefore, more observations are needed concerning the light absorption rate of chlorophyll and other pigments to constrain the role of this biogeophysical mechanism in the climate system.

Bibliography

Adloff, M., Greene, S. E., Parkinson, I. J., Naafs, B. D. A., Preston, W., Ridgwell, A., Lunt, D. J., Jiménez, J. M. C., and Monteiro, F. M. (2020). Unravelling the sources of carbon emissions at the onset of Oceanic Anoxic Event (OAE) 1a. *Earth and Planetary Science Letters*, 530:115947.

Alvarez, S. A., Gibbs, S. J., Bown, P. R., Kim, H., Sheward, R. M., and Ridgwell, A. (2019). Diversity decoupled from ecosystem function and resilience during mass extinction recovery. *Nature*, 574(7777):242–245.

Anderson, W., Gnanadesikan, A., Hallberg, R., Dunne, J., and Samuels, B. (2007). Impact of ocean color on the maintenance of the Pacific Cold Tongue. *Geophysical Research Letters*, 34(11).

Anderson, W., Gnanadesikan, A., and Wittenberg, A. (2009). Regional impacts of ocean color on tropical Pacific variability. *Ocean Science Discussions*, 6(3).

Annan, J., Hargreaves, J., Edwards, N., and Marsh, R. (2005). Parameter estimation in an intermediate complexity earth system model using an ensemble Kalman filter. *Ocean modelling*, 8(1-2):135–154.

Arrhenius, S. (1896). XXXI. On the influence of carbonic acid in the air upon the temperature of the ground. *The London, Edinburgh, and Dublin Philosophical Magazine and Journal of Science*, 41(251):237–276.

Arrhenius, S. (1908). *Worlds in the making: the evolution of the universe.* Harper & Brothers.

Balch, W. M., Holligan, P. M., Ackleson, S. G., and Voss, K. J. (1991). Biological and optical properties of mesoscale coccolithophore blooms in the Gulf of Maine. *Limnology and Oceanography*, 36(4):629–643.

Behrenfeld, M. J. and Falkowski, P. G. (1997). Photosynthetic rates derived from satellite-based chlorophyll concentration. *Limnology and oceanography*, 42(1):1–20.

Behrenfeld, M. J., O'Malley, R. T., Siegel, D. A., McClain, C. R., Sarmiento, J. L., Feldman, G. C., Milligan, A. J., Falkowski, P. G., Letelier, R. M., and Boss, E. S. (2006). Climate-driven trends in contemporary ocean productivity. *Nature*, 444(7120):752–755.

Benitez-Nelson, C. R. (2000). The biogeochemical cycling of phosphorus in marine systems. *Earth-Science Reviews*, 51(1-4):109–135.

Benner, R. and Herndl, G. (2011). Bacterially derived dissolved organic matter in the microbial carbon pump. *Microbial carbon pump in the ocean*, pages 46–48.

Bodeker, G., Shiona, H., and Eskes, H. (2005). Indicators of Antarctic ozone depletion. *Atmospheric Chemistry and Physics*, 5(10):2603–2615.

Bopp, L., Monfray, P., Aumont, O., Dufresne, J.-L., Le Treut, H., Madec, G., Terray, L., and Orr, J. C. (2001). Potential impact of climate change on marine export production. *Global Biogeochemical Cycles*, 15(1):81–99.

Bopp, L., Resplandy, L., Orr, J. C., Doney, S. C., Dunne, J. P., Gehlen, M., Halloran, P., Heinze, C., Ilyina, T., Seferian, R., et al. (2013). Multiple stressors of ocean ecosystems in the 21st century: projections with CMIP5 models. *Biogeosciences*, 10:6225–6245.

Boulton, C. A., Allison, L. C., and Lenton, T. M. (2014). Early warning signals of Atlantic Meridional Overturning Circulation collapse in a fully coupled climate model. *Nature Communications*, 5(1):5752.

Boyce, D. G., Lewis, M. R., and Worm, B. (2010). Global phytoplankton decline over the past century. *Nature*, 466(7306):591–596.

Boyd, P. W., Strzepek, R., Fu, F., and Hutchins, D. A. (2010). Environmental control of open-ocean phytoplankton groups: Now and in the future. *Limnology and Oceanography*, 55(3):1353–1376.

Buckley, M. W. and Marshall, J. (2016). Observations, inferences, and mechanisms of the Atlantic Meridional Overturning Circulation: A review. *Reviews of Geophysics*, 54(1):5–63.

Buesseler, K. O. and Boyd, P. W. (2009). Shedding light on processes that control particle export and flux attenuation in the twilight zone of the open ocean. *Limnology and Oceanography*, 54(4):1210–1232.

Burrows, S. M., Hoose, C., Pöschl, U., and Lawrence, M. (2013). Ice nuclei in marine air: Biogenic particles or dust? *Atmospheric Chemistry and Physics*, 13(1):245–267.

Caldwell, P. M., Zelinka, M. D., and Klein, S. A. (2018). Evaluating emergent constraints on equilibrium climate sensitivity. *Journal of Climate*, 31(10):3921–3942.

Cameron, D. R., Lenton, T. M., Ridgwell, A. J., Shepherd, J. G., Marsh, R., and Yool, A. (2005). A factorial analysis of the marine carbon cycle and ocean circulation controls on atmospheric CO_2. *Global Biogeochemical Cycles*, 19(4).

Cao, L., Eby, M., Ridgwell, A., Caldeira, K., Archer, D., Ishida, A., Joos, F., Matsumoto, K., Mikolajewicz, U., Mouchet, A., et al. (2009). The role of ocean transport in the uptake of anthropogenic CO_2. *Biogeosciences*, 6(3):375–390.

Capone, D. G., Subramaniam, A., Montoya, J. P., Voss, M., Humborg, C., Johansen, A. M., Siefert, R. L., and Carpenter, E. J. (1998). An extensive bloom of the N_2-fixing cyanobacterium Trichodesmium erythraeum in the central Arabian Sea. *Marine Ecology Progress Series*, 172:281–292.

Capotondi, A., Alexander, M. A., Bond, N. A., Curchitser, E. N., and Scott, J. D. (2012). Enhanced upper ocean stratification with climate change in the CMIP3 models. *Journal of Geophysical Research: Oceans*, 117(C4).

Chalikov, D. and Verbitsky, M. Y. (1984). A new Earth climate model. *Nature*, 308(5960):609.

Charney, J. G., Arakawa, A., Baker, D. J., Bolin, B., Dickinson, R. E., Goody, R. M., Leith, C. E., Stommel, H. M., and Wunsch, C. I. (1979). *Carbon dioxide and climate: a scientific assessment*. National Academy of Sciences, Washington, DC.

Claussen, M., Mysak, L., Weaver, A., Crucifix, M., Fichefet, T., Loutre, M.-F., Weber, S., Alcamo, J., Alexeev, V., Berger, A., Calov, R., Ganopolski, A., Goosse, H., Lohmann, G., Lunkeit, F., Mokhov, I., Petoukhov, V., Stone, P., and Wang, W. (2002). Earth system models of intermediate complexity: closing the gap in the spectrum of climate system models. *Climate dynamics*, 18(7):579–586.

Colbourn, G. (2011). *Weathering effects on the carbon cycle in an Earth System Model*. PhD thesis, University of East Anglia.

Collins, M., Knutti, R., Arblaster, J., Dufresne, J.-L., Fichefet, T., Friedlingstein, P., Gao, X., Gutowski, W. J., Johns, T., Krinner, G., et al. (2013). Long-term climate change: projections, commitments and irreversibility. In *Climate Change 2013-The Physical Science Basis: Contribution of Working Group I to the Fifth Assessment Report of the Intergovernmental Panel on Climate Change*, pages 1029–1136. Cambridge University Press.

Conkright, M. E., Antonov, J. I., Baranova, O. K., Boyer, T. P., Garcia, H. E., Gelfeld, R., Johnson, D., Locarnini, R. A., Murphy, P. P., O'Brien, T. D., Smolyar, I., and Stephens, C. (2002). World Ocean Database 2001, Volume 1: Introduction. edited by: Levitus, S., NOAA Atlas, NESDIS 42, U.S. Government Printing Office, Washington, D.C., 167 pp.

Crichton, K. A., Wilson, J. D., Ridgwell, A., and Pearson, P. N. (2021). Calibration of temperature-dependent ocean microbial processes in the cGENIE.muffin (v0.9.13) Earth system model. *Geoscientific Model Development*, 14(1):125–149.

Deacon, E. (1979). The role of coral mucus in reducing the wind drag over coral reefs. *Boundary-Layer Meteorology*, 17(4):517–521.

Dessler, A., Zhang, Z., and Yang, P. (2008). Water-vapor climate feedback inferred from climate fluctuations, 2003–2008. *Geophysical Research Letters*, 35(20).

Dubischar, C. D. and Bathmann, U. V. (2002). The occurrence of faecal material in relation to different pelagic systems in the Southern Ocean and its importance for vertical flux. *Deep Sea Research Part II: Topical Studies in Oceanography*, 49(16):3229–3242.

Ducklow, H. W., Steinberg, D. K., and Buesseler, K. O. (2001). Upper ocean carbon export and the biological pump. *Oceanography*, 14(4):50–58.

Duteil, O., Koeve, W., Oschlies, A., Aumont, O., Bianchi, D., Bopp, L., Galbraith, E., Matear, R., Moore, J., Sarmiento, J. L., et al. (2012). Preformed and regenerated phosphate in ocean general circulation models: can right total concentrations be wrong? *Biogeosciences*, 9(5):1797–1807.

Edwards, N. R. and Marsh, R. (2005). Uncertainties due to transport-parameter sensitivity in an efficient 3-D ocean-climate model. *Climate Dynamics*, 24(4):415–433.

Edwards, N. R., Willmott, A. J., and Killworth, P. D. (1998). On the role of topography and wind stress on the stability of the thermohaline circulation. *Journal of Physical Oceanography*, 28(5):756–778.

Eppley, R. W. (1972). Temperature and phytoplankton growth in the sea. *Fish. bull*, 70(4):1063–1085.

Falkowski, P. G., Barber, R. T., and Smetacek, V. (1998). Biogeochemical controls and feedbacks on ocean primary production. *Science*, 281(5374):200–206.

Falkowski, P. G. and Oliver, M. J. (2007). Mix and match: how climate selects phytoplankton. *Nature reviews microbiology*, 5(10):813–819.

Fanning, A. F. and Weaver, A. J. (1996). An atmospheric energy-moisture balance model: Climatology, interpentadal climate change, and coupling to an ocean general circulation model. *Journal of Geophysical Research: Atmospheres*, 101(D10):15111–15128.

Fantle, M. S. and Ridgwell, A. (2020). Towards an understanding of the Ca isotopic signal related to ocean acidification and alkalinity overshoots in the rock record. *Chemical Geology*, 547:119672.

Fernandez, R. P., Kinnison, D. E., Lamarque, J.-F., Tilmes, S., and Saiz-Lopez, A. (2017). Impact of biogenic very short-lived bromine on the antarctic ozone hole during the 21st century. *Atmospheric Chemistry and Physics*, 17(3):1673–1688.

Fleming-Lehtinen, V. and Laamanen, M. (2012). Long-term changes in Secchi depth and the role of phytoplankton in explaining light attenuation in the Baltic Sea. *Estuarine, Coastal and Shelf Science*, 102:1–10.

Fraedrich, K., Kirk, E., Luksch, U., and Lunkeit, F. (2005). The portable university model of the atmosphere (PUMA): Storm track dynamics and low-frequency variability. *Meteorologische Zeitschrift*, 14(6):735–745.

Franks, P. J. (2002). NPZ models of plankton dynamics: their construction, coupling to physics, and application. *Journal of Oceanography*, 58(2):379–387.

Gallée, H., Van Ypersele, J., Fichefet, T., Tricot, C., and Berger, A. (1991). Simulation of the Last Glacial Cycle by a Coupled, Sectorially Averaged Climate—Ice Sheet Model: 1. The Climate Model. *Journal of Geophysical Research: Atmospheres*, 96(D7):13139–13161.

Garcia, H., Locarnini, R., Boyer, T., Antonov, J., Zweng, M., Baranova, O., and Johnson, D. (2010). World Ocean Atlas 2009, Volume 4: Nutrients (phosphate, nitrate, silicate). NOAA Atlas NESDIS 71, U.S. Government Printing Office, Washington, DC.

Gedney, N., Cox, P., and Huntingford, C. (2004). Climate feedback from wetland methane emissions. *Geophysical Research Letters*, 31(20).

Gibbs, S. J., Bown, P. R., Ridgwell, A., Young, J. R., Poulton, A. J., and O'Dea, S. A. (2016). Ocean warming, not acidification, controlled coccolithophore response during past greenhouse climate change. *Geology*, 44(1):59–62.

Gnanadesikan, A. and Anderson, W. G. (2009). Ocean water clarity and the ocean general circulation in a coupled climate model. *Journal of Physical Oceanography*, 39(2):314–332.

Goes, M., Murphy, L. N., and Clement, A. C. (2019). The stability of the AMOC during Heinrich events is not dependent on the AMOC strength in an Intermediate Complexity Earth System model ensemble. *Paleoceanography and Paleoclimatology*, 34(8):1359–1374.

Gondwe, M., Klaassen, W., Gieskes, W., and de Baar, H. (2001). Negligible direct radiative forcing of basin-scale climate by coccolithophore blooms. *Geophysical research letters*, 28(20):3911–3914.

Greene, S., Ridgwell, A., Kirtland Turner, S., Schmidt, D. N., Pälike, H., Thomas, E., Greene, L., and Hoogakker, B. (2019). Early Cenozoic decoupling of climate and carbonate compensation depth trends. *Paleoceanography and paleoclimatology*, 34(6):930–945.

Gregg, W. W., Casey, N. W., and McClain, C. R. (2005). Recent trends in global ocean chlorophyll. *Geophysical Research Letters*, 32(3).

Gregg, W. W., Rousseaux, C. S., and Franz, B. A. (2017). Global trends in ocean phytoplankton: a new assessment using revised ocean colour data. *Remote Sensing Letters*, 8(12):1102–1111.

Gregory, J. and Forster, P. (2008). Transient climate response estimated from radiative forcing and observed temperature change. *Journal of Geophysical Research: Atmospheres*, 113(D23).

Gregory, J. M., Andrews, T., and Good, P. (2015). The inconstancy of the transient climate response parameter under increasing CO_2. *Philosophical Transactions of the Royal Society A: Mathematical, Physical and Engineering Sciences*, 373(2054):20140417.

Griffies, S. M. (1998). The Gent–McWilliams skew flux. *Journal of Physical Oceanography*, 28(5):831–841.

Gutjahr, M., Ridgwell, A., Sexton, P. F., Anagnostou, E., Pearson, P. N., Pälike, H., Norris, R. D., Thomas, E., and Foster, G. L. (2017). Very large release of mostly volcanic carbon during the Palaeocene–Eocene Thermal Maximum. *Nature*, 548(7669):573.

Hargreaves, J., Annan, J., Edwards, N., and Marsh, R. (2004). An efficient climate forecasting method using an intermediate complexity Earth System Model and the ensemble Kalman filter. *Climate Dynamics*, 23(7-8):745–760.

Hense, I. (2007). Regulative feedback mechanisms in cyanobacteria-driven systems: a model study. *Marine Ecology Progress Series*, 339:41–47.

Hense, I., Meier, H. M., and Sonntag, S. (2013). Projected climate change impact on Baltic Sea cyanobacteria. *Climatic Change*, 119(2):391–406.

Hense, I., Stemmler, I., and Sonntag, S. (2017). Ideas and perspectives: climate-relevant marine biologically driven mechanisms in Earth system models. *Biogeosciences*, 14:403–413.

Holden, P., Edwards, N., Müller, S., Oliver, K., Death, R., and Ridgwell, A. (2013). Controls on the spatial distribution of oceanic $\delta^{13}C_{DIC}$. *Biogeosciences*, 10(3):1815–1833.

Holden, P. B., Edwards, N., Oliver, K., Lenton, T., and Wilkinson, R. (2010). A probabilistic calibration of climate sensitivity and terrestrial carbon change in GENIE-1. *Climate Dynamics*, 35(5):785–806.

Holden, P. B., Edwards, N. R., Fraedrich, K., Kirk, E., Lunkeit, F., and Zhu, X. (2016). PLASIM–GENIE v1.0: a new intermediate complexity AOGCM. *Geoscientific Model Development*, 9:3347–3361.

Holden, P. B., Edwards, N. R., Ridgwell, A., Wilkinson, R., Fraedrich, K., Lunkeit, F., Pollitt, H., Mercure, J.-F., Salas, P., Lam, A., et al. (2018). Climate–carbon cycle uncertainties and the Paris Agreement. *Nature Climate Change*, 8(7):609.

Hopkins, F. E., Suntharalingam, P., Gehlen, M., Andrews, O., Archer, S. D., Bopp, L., Buitenhuis, E., Dadou, I., Duce, R., Goris, N., et al. (2020). The impacts of ocean acidification on marine trace gases and the implications for atmospheric chemistry and climate. *Proceedings of the Royal Society A*, 476(2237):20190769.

Hossaini, R., Chipperfield, M., Montzka, S., Rap, A., Dhomse, S., and Feng, W. (2015). Efficiency of short-lived halogens at influencing climate through depletion of stratospheric ozone. *Nature Geoscience*, 8(3):186.

Hutchinson, P. A. and Webster, I. T. (1994). On the distribution of blue-green algae in lakes: Wind-tunnel tank experiments. *Limnology and oceanography*, 39(2):374–382.

Ilyina, T., Six, K. D., Segschneider, J., Maier-Reimer, E., Li, H., and Núñez-Riboni, I. (2013). Global ocean biogeochemistry model HAMOCC: Model architecture and performance as component of the MPI-Earth system model in different CMIP5 experimental realizations. *Journal of Advances in Modeling Earth Systems*, 5(2):287–315.

IPCC (2014). Synthesis report. contribution of working groups I, II and III to the fifth assessment report of the intergovernmental panel on climate change. *[Core Writing Team, R.K. Pachauri and L.A. Meyer (eds.)]*, IPCC, Geneva, Switzerland.

Ito, T. and Follows, M. J. (2005). Preformed phosphate, soft tissue pump and atmospheric CO_2. *Journal of Marine Research*, 63(4):813–839.

Jang, H.-Y., Yeh, S.-W., Chang, E.-C., and Kim, B.-M. (2016). Evidence of the observed change in the atmosphere–ocean interactions over the South China Sea during summer in a regional climate model. *Meteorology and Atmospheric Physics*, 128(5):639–648.

Jin, Z., Charlock, T. P., Smith Jr, W. L., and Rutledge, K. (2004). A parameterization of ocean surface albedo. *Geophysical research letters*, 31(22).

Jochum, M., Yeager, S., Lindsay, K., Moore, K., and Murtugudde, R. (2010). Quantification of the feedback between phytoplankton and ENSO in the Community Climate System Model. *Journal of Climate*, 23(11):2916–2925.

Jung, H.-C. and Moon, B.-K. (2019). Impacts of albedo and wind stress changes due to phytoplankton on ocean temperature in a coupled global ocean-biogeochemistry model. *Journal of the Korean Earth Science Society*, 40(4):392–405.

Kahru, M., Leppanen, J.-M., and Rud, O. (1993). Cyanobacterial blooms cause heating of the sea surface. *Marine Ecology Progress Series*, 101(1-2):1–7.

Käse, L. and Geuer, J. K. (2018). Phytoplankton Responses to Marine Climate Change – An Introduction. In *YOUMARES 8–Oceans Across Boundaries: Learning from each other*, pages 55–71. Springer, Cham.

Kemppinen, K., Holden, P. B., Edwards, N. R., Ridgwell, A., and Friend, A. D. (2019). Coupled climate–carbon cycle simulation of the Last Glacial Maximum atmospheric CO_2 decrease using a large ensemble of modern plausible parameter sets. *Climate of the Past*, 15:1039–1062.

Key, R. M., Kozyr, A., Sabine, C. L., Lee, K., Wanninkhof, R., Bullister, J. L., Feely, R. A., Millero, F. J., Mordy, C., and Peng, T.-H. (2004). A global ocean carbon climatology: Results from Global Data Analysis Project (GLODAP). *Global biogeochemical cycles*, 18(4).

Knutson, T. R. and Tuleya, R. E. (2004). Impact of CO_2-induced warming on simulated hurricane intensity and precipitation: Sensitivity to the choice of climate model and convective parameterization. *Journal of climate*, 17(18):3477–3495.

Knutti, R., Rugenstein, M. A., and Hegerl, G. C. (2017). Beyond equilibrium climate sensitivity. *Nature Geoscience*, 10(10):727.

Kowalczuk, P., Sagan, S., Makarewicz, A., Meler, J., Borzycka, K., Zabłocka, M., Zdun, A., Konik, M., Darecki, M., Granskog, M. A., and Pavlov, A. K. (2019). Bio-optical properties of surface waters in the Atlantic water inflow region off Spitsbergen (Arctic Ocean). *Journal of Geophysical Research: Oceans*, 124(3):1964–1987.

Kraus, E. and Turner, J. (1967). A one-dimensional model of the seasonal thermocline II. The general theory and its consequences. *Tellus*, 19(1):98–106.

Lalli, C. and Parsons, T. R. (1997). *Biological oceanography: an introduction*. Elsevier.

Lapenis, A. G. (1998). Arrhenius and the Intergovernmental Panel on Climate Change. *Eos, Transactions American Geophysical Union*, 79(23):271–271.

Laufkötter, C., Vogt, M., Gruber, N., Aita-Noguchi, M., Aumont, O., Bopp, L., Buitenhuis, E. T., Doney, S. C., Dunne, J. P., Hashioka, T., Hauck, J., Hirata, T., John, J. G., Le Quere, C., Lima, I. D., Nakano, H., Seferian, R., Totterdell, I. J., Vichi, M., and Volker, C. (2015). Drivers and uncertainties of future global marine primary production in marine ecosystem models. *Biogeosciences*, 12:6955–6984.

Le Quéré, C., Harrison, S. P., Colin Prentice, I., Buitenhuis, E. T., Aumont, O., Bopp, L., Claustre, H., Cotrim Da Cunha, L., Geider, R., Giraud, X., Klaas, C., Kohfeld, K. E., Legendre, L., Manizza, M., Platt, T., Rivkin, R. B., Sathyendranath, S., Uitz, J., Watson, A. J., and Wolf-Gladrow, D. (2005). Ecosystem dynamics based on plankton functional types for global ocean biogeochemistry models. *Global Change Biology*, 11(11):2016–2040.

LeGrand, P. and Alverson, K. (2001). Variations in atmospheric CO_2 during glacial cycles from an inverse ocean modeling perspective. *Paleoceanography*, 16(6):604–616.

Lengaigne, M., Madec, G., Bopp, L., Menkes, C., Aumont, O., and Cadule, P. (2009). Biophysical feedbacks in the Arctic Ocean using an Earth system model. *Geophysical Research Letters*, 36(21).

Lengaigne, M., Menkes, C., Aumont, O., Gorgues, T., Bopp, L., André, J.-M., and Madec, G. (2007). Influence of the oceanic biology on the tropical Pacific climate in a coupled general circulation model. *Climate Dynamics*, 28(5):503–516.

Lenton, T., Marsh, R., Price, A., Lunt, D., Aksenov, Y., Annan, J., Cooper-Chadwick, T., Cox, S., Edwards, N., Goswami, S., Hargreaves, J., Harris, P., Jiao, Z., Livina, V., Payne, A., Rutt, I., Shepherd, J., Valdes, P., Williams, G., Williamson, M., and Yool, A. (2007). Effects of atmospheric dynamics and ocean resolution on bi-stability of the thermohaline circulation examined using the Grid ENabled Integrated Earth system modelling (GENIE) framework. *Climate Dynamics*, 29(6):591–613.

Lenton, T., Williamson, M., Edwards, N., Marsh, R., Price, A., Ridgwell, A., Shepherd, J., Cox, S., et al. (2006). Millennial timescale carbon cycle and climate change in an efficient Earth system model. *Climate Dynamics*, 26(7-8):687.

Lewis, K., Van Dijken, G., and Arrigo, K. (2020). Changes in phytoplankton concentration now drive increased Arctic Ocean primary production. *Science*, 369(6500):198–202.

Lewis, M. R., Carr, M.-E., Feldman, G. C., Esaias, W., and McClain, C. (1990). Influence of penetrating solar radiation on the heat budget of the equatorial Pacific Ocean. *Nature*, 347(6293):543.

Lewis, M. R., Cullen, J. J., and Platt, T. (1983). Phytoplankton and thermal structure in the upper ocean: consequences of nonuniformity in chlorophyll profile. *Journal of Geophysical Research: Oceans*, 88(C4):2565–2570.

Lim, E.-P., Hendon, H. H., Arblaster, J. M., Chung, C., Moise, A. F., Hope, P., Young, G., and Zhao, M. (2016). Interaction of the recent 50 year SST trend and La Niña 2010: amplification of the Southern Annular Mode and Australian springtime rainfall. *Climate dynamics*, 47(7-8):2273–2291.

Lim, Y., Phang, S., Rahman, N. A., Sturges, W., and Malin, G. (2017). Halocarbon emissions from marine phytoplankton and climate change. *International journal of environmental science and technology*, 14(6):1355–1370.

Liss, P. S., Hatton, A. D., Malin, G., Nightingale, P. D., and Turner, S. M. (1997). Marine sulphur emissions. *Philosophical Transactions of the Royal Society of London. Series B: Biological Sciences*, 352(1350):159–169.

Löptien, U., Eden, C., Timmermann, A., and Dietze, H. (2009). Effects of biologically induced differential heating in an eddy-permitting coupled ocean-ecosystem model. *Journal of Geophysical Research: Oceans*, 114(C6).

Louanchi, F. and Najjar, R. G. (2000). A global monthly climatology of phosphate, nitrate, and silicate in the upper ocean: Spring-summer export production and shallow remineralization. *Global Biogeochemical Cycles*, 14(3):957–977.

Lumpkin, R. and Speer, K. (2007). Global ocean meridional overturning. *Journal of Physical Oceanography*, 37(10):2550–2562.

Lunkeit, F., Böttinger, M., Fraedrich, K., Heiko, J., Kirk, E., Kleidon, A., and Luksch, U. (2007). Planet Simulator Reference Manual Version 15.0. `http://epic.awi.de/29588/1/Lun2007d.pdf`, last access: 14th January 2021.

MacDougall, A. H., Frölicher, T. L., Jones, C. D., Rogel, J., Matthews, H. D., Zickfeld, K., Arora, V. K., Barrett, N. J., Brovkin, V., Burger, F. A., Eby, M., Eliseev, A. V., Hajima, T., Holden, P. B., Jeltsch-Thömmes, A., Koven, C., Mengis, N., Menviel, L., Michou, M.,

Mokhov, I. I., Oka, A., Schwinger, J., Séférian, R., Schaffer, G., Sokolov, A., Tachiir, K., Tjiputra, J., Wiltshire, A., and Ziehn, T. (2020). Is there warming in the pipeline? A multi-model analysis of the zero emission commitment from CO_2. *Biogeosciences*, 17:2987–3016.

Mahowald, N. M., Yoshioka, M., Collins, W. D., Conley, A. J., Fillmore, D. W., and Coleman, D. B. (2006). Climate response and radiative forcing from mineral aerosols during the last glacial maximum, pre-industrial, current and doubled-carbon dioxide climates. *Geophysical Research Letters*, 33(20).

Manizza, M., Le Quéré, C., Watson, A. J., and Buitenhuis, E. T. (2005). Bio-optical feedbacks among phytoplankton, upper ocean physics and sea-ice in a global model. *Geophysical Research Letters*, 32(5).

Manizza, M., Le Quéré, C., Watson, A. J., and Buitenhuis, E. T. (2008). Ocean biogeochemical response to phytoplankton-light feedback in a global model. *Journal of Geophysical Research: Oceans*, 113(C10).

Marinov, I., Gnanadesikan, A., Sarmiento, J. L., Toggweiler, J., Follows, M., and Mignone, B. (2008). Impact of oceanic circulation on biological carbon storage in the ocean and atmospheric pCO_2. *Global Biogeochemical Cycles*, 22(3).

Marsh, R., Müller, S., Yool, A., and Edwards, N. (2011). Incorporation of the C-GOLDSTEIN efficient climate model into the GENIE framework: "eb_go_gs" configurations of GENIE. *Geoscientific Model Development*, 4:957–992.

Marsh, R., Yool, A., Lenton, T., Gulamali, M., Edwards, N., Shepherd, J., Krznaric, M., Newhouse, S., and Cox, S. (2004). Bistability of the thermohaline circulation identified through comprehensive 2-parameter sweeps of an efficient climate model. *Climate Dynamics*, 23(7-8):761–777.

Marzeion, B., Timmermann, A., Murtugudde, R., and Jin, F.-F. (2005). Biophysical feedbacks in the tropical Pacific. *Journal of Climate*, 18(1):58–70.

McClain, C. R., Signorini, S. R., and Christian, J. R. (2004). Subtropical gyre variability observed by ocean-color satellites. *Deep Sea Research Part II: Topical Studies in Oceanography*, 51(1-3):281–301.

McCoy, D. T., Burrows, S. M., Wood, R., Grosvenor, D. P., Elliott, S. M., Ma, P.-L., Rasch, P. J., and Hartmann, D. L. (2015). Natural aerosols explain seasonal and spatial patterns of Southern Ocean cloud albedo. *Science advances*, 1(6):e1500157.

Meinshausen, M., Smith, S. J., Calvin, K., Daniel, J. S., Kainuma, M., Lamarque, J.-F., Matsumoto, K., Montzka, S., Raper, S., Riahi, K., Thomson, A., Velders, G., and van Vuuren, D. (2011). The RCP greenhouse gas concentrations and their extensions from 1765 to 2300. *Climatic change*, 109(1-2):213.

Menon, S., Denman, K. L., Brasseur, G., Chidthaisong, A., Ciais, P., Cox, P. M., Dickinson, R. E., Hauglustaine, D., Heinze, C., Holland, E., Jacob, D., Lohmann, U., Ramachandran, S., Wofsy, S. C., and Zhang, X. (2007). Couplings between changes in the climate system and biogeochemistry. Technical report, Lawrence Berkeley National Lab.(LBNL), Berkeley, CA (United States).

Meyer, K., Ridgwell, A., and Payne, J. (2016). The influence of the biological pump on ocean chemistry: implications for long-term trends in marine redox chemistry, the global carbon cycle, and marine animal ecosystems. *Geobiology*, 14(3):207–219.

Moore, J. K., Fu, W., Primeau, F., Britten, G. L., Lindsay, K., Long, M., Doney, S. C., Mahowald, N., Hoffman, F., and Randerson, J. T. (2018). Sustained climate warming drives declining marine biological productivity. *Science*, 359(6380):1139–1143.

Morel, A. (1988). Optical modeling of the upper ocean in relation to its biogenous matter content (case I waters). *Journal of geophysical research: oceans*, 93(C9):10749–10768.

Morel, A. and Maritorena, S. (2001). Bio-optical properties of oceanic waters: A reappraisal. *Journal of Geophysical Research: Oceans*, 106(C4):7163–7180.

Murtugudde, R., Beauchamp, J., McClain, C. R., Lewis, M., and Busalacchi, A. J. (2002). Effects of penetrative radiation on the upper tropical ocean circulation. *Journal of Climate*, 15(5):470–486.

Naafs, B. D. A., Monteiro, F. M., Pearson, A., Higgins, M. B., Pancost, R. D., and Ridgwell, A. (2019). Fundamentally different global marine nitrogen cycling in response to severe ocean deoxygenation. *Proceedings of the National Academy of Sciences*, 116(50):24979–24984.

Nielsen, E. S. (1975). *Marine photosynthesis with special emphasis on the ecological aspects.* Elsevier.

Ödalen, M., Nycander, J., Oliver, K. I., Brodeau, L., and Ridgwell, A. (2018). The influence of the ocean circulation state on ocean carbon storage and CO_2 drawdown potential in an Earth system model. *Biogeosciences*, 15(5):1367–1393.

Olivieri, R. A. and Chavez, F. P. (2000). A model of plankton dynamics for the coastal upwelling system of Monterey Bay, California. *Deep Sea Research Part II: Topical Studies in Oceanography*, 47(5-6):1077–1106.

Olsen, A., Key, R. M., Heuven, S. v., Lauvset, S. K., Velo, A., Lin, X., Schirnick, C., Kozyr, A., Tanhua, T., Hoppema, M., Jutterström, S., Steinfeldt, R., Jeansson, E., Ishii, M., Pérez, F. F., and Suzuki, T. (2016). The Global Ocean Data Analysis Project version 2 (GLODAPv2)–an internally consistent data product for the world ocean. *Earth System Science Data*, 8(2):297–323.

O'Reilly, J. E., Maritorena, S., Mitchell, B. G., Siegel, D. A., Carder, K. L., Garver, S. A., Kahru, M., and McClain, C. (1998). Ocean color chlorophyll algorithms for SeaWiFS. *Journal of Geophysical Research: Oceans*, 103(C11):24937–24953.

Oschlies, A. (2001). Model-derived estimates of new production: New results point towards lower values. *Deep Sea Research Part II: Topical Studies in Oceanography*, 48(10):2173–2197.

Oschlies, A. (2004). Feedbacks of biotically induced radiative heating on upper-ocean heat budget, circulation, and biological production in a coupled ecosystem-circulation model. *Journal of Geophysical Research: Oceans*, 109(C12).

O'Neil, J., Davis, T., Burford, M., and Gobler, C. (2012). The rise of harmful cyanobacteria blooms: The potential roles of eutrophication and climate change. *Harmful algae*, 14:313–334.

Paerl, H. W. and Paul, V. J. (2012). Climate change: Links to global expansion of harmful cyanobacteria. *Water research*, 46(5):1349–1363.

Park, J.-Y., Kug, J.-S., Bader, J., Rolph, R., and Kwon, M. (2015). Amplified Arctic warming by phytoplankton under greenhouse warming. *Proceedings of the National Academy of Sciences*, 112(19):5921–5926.

Patara, L., Vichi, M., Masina, S., Fogli, P. G., and Manzini, E. (2012). Global response to solar radiation absorbed by phytoplankton in a coupled climate model. *Climate dynamics*, 39(7-8):1951–1968.

Paulsen, H. (2018). *The effects of marine nitrogen-fixing cyanobacteria on ocean biogeochemistry and climate–an Earth system model perspective*. PhD thesis, Universität Hamburg, Hamburg.

Paulsen, H., Ilyina, T., Jungclaus, J. H., Six, K. D., and Stemmler, I. (2018). Light absorption by marine cyanobacteria affects tropical climate mean state and variability. *Earth System Dynamics*, 9(4):1283–1300.

Peixoto, J. P. and Oort, A. H. (1992). Physics of climate.

Petoukhov, V. (1980). A zonal climate model of heat and moisture exchange in the atmosphere over the underlying layers of ocean and land In: Golitsyn GS, Yaglom AM (eds) Physics of the atmosphere and the problem of climate.

Petoukhov, V., Claussen, M., Berger, A., Crucifix, M., Eby, M., Eliseev, A., Fichefet, T., Ganopolski, A., Goosse, H., Kamenkovich, I., Mokhov, I., Montoya, M., Mysak, L., Sokolov, A., Stone, P., Wang, Z., and Weaver, A. (2005). EMIC Intercomparison Project (EMIP–CO$_2$): comparative analysis of EMIC simulations of climate, and of equilibrium and transient responses to atmospheric CO$_2$ doubling. *Climate Dynamics*, 25(4):363–385.

Polimene, L., Sailley, S., Clark, D., Mitra, A., and Allen, J. I. (2017). Biological or microbial carbon pump? The role of phytoplankton stoichiometry in ocean carbon sequestration. *Journal of Plankton Research*, 39(2):180–186.

Polovina, J. J., Howell, E. A., and Abecassis, M. (2008). Ocean's least productive waters are expanding. *Geophysical Research Letters*, 35(3).

Ramp, S. R., Garwood, R. W., Davis, C. O., and Snow, R. L. (1991). Surface heating and patchiness in the coastal ocean off central California during a wind relaxation event. *Journal of Geophysical Research: Oceans*, 96(C8):14947–14957.

Rap, A., Scott, C. E., Spracklen, D. V., Bellouin, N., Forster, P. M., Carslaw, K. S., Schmidt, A., and Mann, G. (2013). Natural aerosol direct and indirect radiative effects. *Geophysical Research Letters*, 40(12):3297–3301.

Reinhard, C. T., Olson, S., Kirtland Turner, S., Pälike, C., Kanzaki, Y., and Ridgwell, A. (2020a). Oceanic and atmospheric methane cycling in the cGENIE Earth system model. *Geoscientific Model Development*, 13(11):5687–5706.

Reinhard, C. T., Planavsky, N. J., Ward, B. A., Love, G. D., Le Hir, G., and Ridgwell, A. (2020b). The impact of marine nutrient abundance on early eukaryotic ecosystems. *Geobiology*, 18(2):139–151.

Ridgwell, A. and Hargreaves, J. (2007). Regulation of atmospheric CO_2 by deep-sea sediments in an Earth system model. *Global Biogeochemical Cycles*, 21(2).

Ridgwell, A., Hargreaves, J., Edwards, N. R., Annan, J., Lenton, T. M., Marsh, R., Yool, A., and Watson, A. (2007). Marine geochemical data assimilation in an efficient Earth System Model of global biogeochemical cycling. *Biogeosciences*, 4(1):87–104.

Robinson, C., Wallace, D., Hyun, J.-H., Polimene, L., Benner, R., Zhang, Y., Cai, R., Zhang, R., and Jiao, N. (2018). An implementation strategy to quantify the marine microbial carbon pump and its sensitivity to global change. *National Science Review*, 5(4):474–480.

Rousseaux, C. S. and Gregg, W. W. (2015). Recent decadal trends in global phytoplankton composition. *Global Biogeochemical Cycles*, 29(10):1674–1688.

Rykaczewski, R. R. and Dunne, J. P. (2011). A measured look at ocean chlorophyll trends. *Nature*, 472(7342):E5–E6.

Sarmiento, J. L. and Gruber, N. (2006). *Ocean biogeochemical dynamics*. Princeton University Press.

Sarmiento, J. L. and Toggweiler, J. (1984). A new model for the role of the oceans in determining atmospheric pCO_2. *Nature*, 308(5960):621.

Sathyendranath, S., Gouveia, A. D., Shetye, S. R., Ravindran, P., and Platt, T. (1991). Biological control of surface temperature in the Arabian Sea. *Nature*, 349(6304):54.

Shaw, G. E. (1983). On the aerosol particle size distribution spectrum in Alaskan air mass systems: Arctic haze and non-haze episodes. *Journal of the Atmospheric Sciences*, 40(5):1313–1320.

Shell, K., Frouin, R., Nakamoto, S., and Somerville, R. (2003). Atmospheric response to solar radiation absorbed by phytoplankton. *Journal of Geophysical Research: Atmospheres*, 108(D15).

Shi, Y., Gong, W., Duan, Q., Charles, J., Xiao, C., and Wang, H. (2019). How parameter specification of an Earth system model of intermediate complexity influences its climate simulations. *Progress in Earth and Planetary Science*, 6(1):46.

Siegel, D. A., Ohlmann, J. C., Washburn, L., Bidigare, R. R., Nosse, C. T., Fields, E., and Zhou, Y. (1995). Solar radiation, phytoplankton pigments and the radiant heating of the equatorial Pacific warm pool. *Journal of Geophysical Research: Oceans*, 100(C3):4885–4891.

Sigman, D. M. and Boyle, E. A. (2000). Glacial/interglacial variations in atmospheric carbon dioxide. *Nature*, 407(6806):859.

Smith, R. C. and Baker, K. S. (1978). The bio-optical state of ocean waters and remote sensing. *Limnology and Oceanography*, 23(2):247–259.

Sonntag, S. (2013). *Modeling biological-physical feedback mechanisms in marine systems*. PhD thesis, Universität Hamburg, Hamburg.

Sonntag, S. and Hense, I. (2011). Phytoplankton behavior affects ocean mixed layer dynamics through biological-physical feedback mechanisms. *Geophysical Research Letters*, 38(15).

Spitz, Y., Newberger, P. A., and Allen, J. S. (2003). Ecosystem response to upwelling off the Oregon coast: Behavior of three nitrogen-based models. *Journal of Geophysical Research: Oceans*, 108(C3).

Steinacher, M., Joos, F., Frölicher, T., Bopp, L., Cadule, P., Cocco, V., Doney, S. C., Gehlen, M., Lindsay, K., Moore, J. K., et al. (2010). Projected 21st century decrease in marine productivity: a multi-model analysis. *Biogeosciences*, 7(3):979–1005.

Stevenson, A. (2010). *Oxford Dictionary of English.* Oxford University Press, USA.

Tagliabue, A., Aumont, O., DeAth, R., Dunne, J. P., Dutkiewicz, S., Galbraith, E., Misumi, K., Moore, J. K., Ridgwell, A., Sherman, E., et al. (2016). How well do global ocean biogeochemistry models simulate dissolved iron distributions? *Global Biogeochemical Cycles*, 30(2):149–174.

Tait, V. and Moore, R. (1995). Methyl chloride (CH_3Cl) production in phytoplankton cultures. *Limnology and oceanography*, 40(1):189–195.

Tett, P. (1990). The photic zone. *Light and Life in the Sea*, pages 59–87.

Timmermann, A. and Jin, F.-f. (2002). Phytoplankton influences on tropical climate. *Geophysical Research Letters*, 29(23):19–1–19–4.

Toggweiler, J., Murnane, R., Carson, S., Gnanadesikan, A., and Sarmiento, J. L. (2003). Representation of the carbon cycle in box models and GCMs, 2, Organic pump. *Global biogeochemical cycles*, 17(1).

Tokarska, K. B., Gillett, N. P., Weaver, A. J., Arora, V. K., and Eby, M. (2016). The climate response to five trillion tonnes of carbon. *Nature Climate Change*, 6(9):851–855.

Tréguer, P. J. and De La Rocha, C. L. (2013). The world ocean silica cycle. *Annual review of marine science*, 5:477–501.

Turner, J. T. (2015). Zooplankton fecal pellets, marine snow, phytodetritus and the ocean's biological pump. *Progress in Oceanography*, 130:205–248.

Tyrrell, T., Holligan, P., and Mobley, C. (1999). Optical impacts of oceanic coccolithophore blooms. *Journal of Geophysical Research: Oceans*, 104(C2):3223–3241.

Ullah, H., Nagelkerken, I., Goldenberg, S. U., and Fordham, D. A. (2018). Climate change could drive marine food web collapse through altered trophic flows and cyanobacterial proliferation. *PLoS biology*, 16(1):e2003446.

Van de Velde, S., Hülse, D., Reinhard, C., and Ridgwell, A. (2020). Anoxic iron and sulphur cycling in the cGENIE.muffin Earth system model (v0.9.16). *Geoscientific Model Development Discussions*, pages 1–44.

Van de Waal, D. B. and Litchman, E. (2020). Multiple global change stressor effects on phytoplankton nutrient acquisition in a future ocean. *Philosophical Transactions of the Royal Society B*, 375(1798):20190706.

Wanninkhof, R. (1992). Relationship between wind speed and gas exchange over the ocean. *Journal of Geophysical Research: Oceans*, 97(C5):7373–7382.

Ward, B. A. and Follows, M. J. (2016). Marine mixotrophy increases trophic transfer efficiency, mean organism size, and vertical carbon flux. *Proceedings of the National Academy of Sciences*, 113(11):2958–2963.

Ward, B. A., Wilson, J. D., Death, R., Monteiro, F. M., Yool, A., and Ridgwell, A. (2018). EcoGEnIE 1.0: plankton ecology in the cGEnIE Earth system model. *Geoscientific Model Development*, 11(10):4241–4267.

Watson, A. J. and Liss, P. S. (1998). Marine biological controls on climate via the carbon and sulphur geochemical cycles. *Philosophical Transactions of the Royal Society of London. Series B: Biological Sciences*, 353:41–51.

Weaver, A. J., Eby, M., Wiebe, E. C., Bitz, C. M., Duffy, P. B., Ewen, T. L., Fanning, A. F., Holland, M. M., MacFadyen, A., Damon Matthews, H., Meissner, K. J., Saenko, O., Schmittner, A., Wang, H., and Yoshimori, M. (2001). The UVic Earth System Climate Model: Model description, climatology, and applications to past, present and future climates. *Atmosphere-Ocean*, 39(4):361–428.

Weiss, R. F. (1970). The solubility of nitrogen, oxygen and argon in water and seawater. *Deep Sea Research and Oceanographic Abstracts*, 17(4):721–735.

Wetzel, P., Maier-Reimer, E., Botzet, M., Jungclaus, J., Keenlyside, N., and Latif, M. (2006). Effects of ocean biology on the penetrative radiation in a coupled climate model. *Journal of Climate*, 19(16):3973–3987.

Williamson, M., Lenton, T., Shepherd, J., and Edwards, N. (2006). An efficient numerical terrestrial scheme (ENTS) for Earth system modeling. *Ecological Modelling*, 198:362–374.

Wilson, J., Monteiro, F., Schmidt, D., Ward, B., and Ridgwell, A. (2018). Linking marine plankton ecosystems and climate: A new modeling approach to the warm early Eocene climate. *Paleoceanography and Paleoclimatology*, 33(12):1439–1452.

Wilson, T. W., Ladino, L. A., Alpert, P. A., Breckels, M. N., Brooks, I. M., Browse, J., Burrows, S. M., Carslaw, K. S., Huffman, J. A., Judd, C., et al. (2015). A marine biogenic source of atmospheric ice-nucleating particles. *Nature*, 525(7568):234.

Worden, A. Z., Follows, M. J., Giovannoni, S. J., Wilken, S., Zimmerman, A. E., and Keeling, P. J. (2015). Rethinking the marine carbon cycle: factoring in the multifarious lifestyles of microbes. *Science*, 347(6223).

Wurl, O., Bird, K., Cunliffe, M., Landing, W. M., Miller, U., Mustaffa, N. I. H., Ribas-Ribas, M., Witte, C., and Zappa, C. J. (2018). Warming and inhibition of salinization at the ocean's surface by cyanobacteria. *Geophysical research letters*, 45(9):4230–4237.

Yool, A., Popova, E., and Anderson, T. (2013). MEDUSA-2.0: an intermediate complexity biogeochemical model of the marine carbon cycle for climate change and ocean acidification studies. *Geoscientific Model Development*, 6(5):1767–1811.

Zeebe, R. E., Eicken, H., Robinson, D. H., Wolf-Gladrow, D., and Dieckmann, G. S. (1996). Modeling the heating and melting of sea ice through light absorption by microalgae. *Journal of Geophysical Research: Oceans*, 101(C1):1163–1181.

Zehr, J. P. and Kudela, R. M. (2011). Nitrogen cycle of the open ocean: from genes to ecosystems. *Annual Review of Marine Science*, 3:197–225.

Zhang, H. and Cao, L. (2016). Simulated effect of calcification feedback on atmospheric CO_2 and ocean acidification. *Scientific reports*, 6:20284.

Zhang, R.-H., Busalacchi, A. J., Wang, X., Ballabrera-Poy, J., Murtugudde, R. G., Hackert, E. C., and Chen, D. (2009). Role of ocean biology-induced climate feedback in the modulation of El Niño-Southern Oscillation. *Geophysical Research Letters*, 36(3).

Zickfeld, K., Eby, M., Weaver, A. J., Alexander, K., Crespin, E., Edwards, N. R., Eliseev, A. V., Feulner, G., Fichefet, T., Forest, C. E., Friedlingstein, P., Goosse, H., Holden, P. B., et al. (2013). Long-term climate change commitment and reversibility: an EMIC intercomparison. *Journal of Climate*, 26(16):5782–5809.

Versicherung an Eides statt

Hiermit versichere ich an Eides statt, dass ich die vorliegende Dissertation mit dem Titel: "The role of marine biota in the climate system - an Earth system model approach" selbstständig verfasst und keine anderen als die angegebenen Hilfsmittel – insbesondere keine im Quellenverzeichnis nicht benannten Internet-Quellen – benutzt habe. Alle Stellen, die wörtlich oder sinngemäß aus Veröffentlichungen entnommen wurden, sind als solche kenntlich gemacht. Ich versichere weiterhin, dass ich die Dissertation oder Teile davon vorher weder im In- noch im Ausland in einem anderen Prüfungsverfahren eingereicht habe und die eingereichte schriftliche Fassung der auf dem elektronischen Speichermedium entspricht.

Hamburg, den 5. April, 2021

Rémy Asselot
geboren am 27.01.1993
in Bordeaux, France